CHAPTER ONE

INTRODUCTION

1.1 Background to the study

Presently, silicon-based technology has gained a lot of importance in several electronics manufacturing industries. The bulk of electronics manufacturing is centered on silicon-based technology. Due to its narrow band gap, it is very easy for electrons in the valence band to be excited into the conduction band thus creating electron-hole pairs which of course triggers the flow of current. This fact has made silicon the best raw material in the semiconductor industry up till this present age. However, the silicon-based technology which gave us the transistor is fast approaching its hard physical limits, and is expected that future progress will require new nanoscale materials (Mathur, as cited in Jensen *et al*., 2007). Due to this fact, researchers and scientists are working tirelessly day and night to discover new and novel materials which will be based on the nanoscale. Scientists believe that this new set of materials will be able to replace silicon and even offer a better performance than silicon.

Silicon is a semiconductor having an indirect band gap of about 1.12 eV. This band gap (1.12 eV) corresponds to a wavelength of approximately 1100 nm which happens to be in the infrared region. Hence, silicon photovoltaics for instance, are not ideal for converting light based on shorter wavelength into electricity. Thus, for converting shorter wavelength of light to electricity, wide band gap semiconductors are promising materials in this aspect. The low band gap possessed by silicon limits devices fabricated by silicon to operate at relatively low temperatures less than 100 ^{o}C. Power transistors based on silicon material are quite approaching limits of operational frequency. This makes focus to be on other semiconductor

materials such as wide band gap materials because they can be used in high-temperature and power switching applications.

Wide band gap semiconductors (mostly II-VI and III-V) have relatively band gaps between 2.00 eV and 4.00 eV. This gives them the ability to operate at higher temperatures (as high as 300 ^{o}C) and voltages. The II-VI and III-V semiconductors have very unique optical properties which make them advantageous in fabricating high performance and optoelectronic devices. GaAs and ZnSe have direct band gaps and higher radiative recombination coefficients, and are thus, more useful for optoelectronics (Tsao, 2004). Although, today's most efficient and highest-power commercial semiconductor lasers are based on GaAs (Tsao, 2004), it is imperative to study other wide-band gap semiconductors for their optical and structural properties. Wide-band gap II–VI compounds are used to fabricate optoelectronic devices, especially light-emitting devices in the short-wavelength region of visible light, because of their direct gap and suitable band gap energies (Minoru and Jifeng, 2017). II–VI compounds are expected to be one of the most vital materials for high-performance optoelectronics devices such as light-emitting diodes (LEDs) and laser diodes (LDs) operating in the blue or ultraviolet spectral range. Additionally, the high ionicity of these compounds makes them good candidates for high electro-optical and electromechanical coupling (Minoru and Jifeng, 2017). However, it is pertinent to study these materials in the nanoscale category as they tend to present unique characteristics within this scale. The research area which is generally concerned with the study of nanoscale materials is referred to as nanotechnology.

In the last two decades, serious attention has been focused towards this interdisciplinary research area presently known as "nanotechnology." This technology makes use of knowledge from different academic disciplines such as Physics, Chemistry, Materials Science

and Engineering. With the aid of this technology, it is possible to reduce the dimensions of electronic devices down to the nanoscale range making them highly efficient. Based on this fact, devices can thus be manufactured through nanotechnology and such devices are termed "nano devices." A 'nano-device' can be manufactured using nanotechnology by controlling the structure of the materials either at the atomic or molecular scale. The recent development in the field of nanotechnology has opened new possibilities in processing information at a faster rate including the storage of data. Having observed that the components of electronic devices reduced from time to time, thus boosting their performance more at the reduced size, Gordon Moore, in 1965 made an observation which is presently regarded as Moore's law.

According to Moore's law, the number of transistors in a chip is doubled every eighteen to twenty two months (Abdolmadjid, 2010). This implies that very soon, the size of a transistor will become very small and as such, the speed of a processor will be limited by the size of the transistor.

One of the main reasons why semiconductors have found great applications in electronic devices is possibly due to the fact that their electronic properties can be greatly influenced in a controllable way by the addition of small quantity of impurities (otherwise known as doping) (Jeroh, 2012). The doped semiconductor which possesses high conductivity is called an extrinsic semiconductor, while the un-doped semiconductor is referred to as an intrinsic semiconductor. Doping of semiconductors is the process of locally manipulating their charge carrier density and conductivity, and it represents a key technology for semiconductor-based electronic devices (Sze and Kwok, 2007). Doping can also be described as the addition of very small quantity of foreign atoms (or impurity atoms otherwise known as dopants) to a pure semiconductor in order to improve its electrical characteristics. The doped

semiconductor can either be p-type consisting of more holes than electrons or n-type consisting of more electrons than holes. Conventional doping is usually achieved via the bombardment of semiconductors with energetic ions (the dopants) followed by thermal annealing; this is referred to as ion implantation (Wei *et al*., 2009). Depending on their number of valence electrons, the dopants (as donors) can either donate excess electrons as negative free charge carriers to the semiconductor conduction band at moderate temperature (n-type doping), or they (as acceptors) can accept additional electrons from surrounding atoms to complete the covalent chemical bonding, leaving positively charged holes as charge carriers in the semiconductor valence band (p-type doping) (Wei *et al*., 2009).

However, there have been only a few reports on the incorporation of rare-earth elements as dopants largely due to the low solubility limits of the rare earths in both III-V and II-VI semiconducting compounds as well as by their tendency to form clusters and to occupy other sites than the cation-substitutional ones (Dietl, 1994).

However, recent research (Paritosh *et al*., 2007; Luo *et al*., 2010) has been intensified towards the doping of semiconductors by rare-earth ions. Rare-earth (RE) doped semiconductors have been intensively studied for their potential use in integrated optoelectronic devices like visible (blue, green, and red) and infrared luminescent devices (Paritosh *et al*., 2007). In these materials, the excitation of the RE cations occur by the recombination of photo-generated carriers confined in the semiconductor and energy transfer from the semiconductor to the RE ions (Paritosh *et al*., 2007). Luo *et al*., (2010) suggested that rare-earth ions are unique doping centres, hence it is very important to study the effect of rare-earth ions doping on the improvement and modulation of optical properties of luminescence materials.

In this communication, the synthesis and characterization of zinc selenide (0% doping), europium-doped zinc selenide (ZnSe:Eu), europium-doped cadmium selenide (CdSe:Eu) and europium-doped magnesium selenide (MgSe:Eu) films by electrostatic spray pyrolysis (ESP) technique for the first time will be reported.

1.2 Statement of problem

The growth of ZnSe, ZnSe:Eu, CdSe:Eu and MgSe:Eu by electrostatic spray pyrolysis offers a fast and cost effective approach to studying their vast properties (optical, structural, morphological properties, etc) for various device fabrication.

There exists a number of studies on ZnSe films and limited study in the literature of ZnSe:Eu and CdSe:Eu films. As regards MgSe:Eu films, only studies on pure MgSe films are available in the literature. For ZnSe films, most literatures dwelt on air-blast (pressurized) spray pyrolysis, while for literature on ZnSe:Eu films, the use of close-spaced vacuum sublimation (CSVS), solvothermal and electrochemical deposition have been reported for deposition temperatures between 100 ^{o}C and 300 ^{o}C. However, in these studies, only temperature variation was considered in growing the films. For CdSe:Eu films, a study on CdSe:Eu nanocrystals exists, but a detailed analysis of its optical properties and applications is missing from the literature. In available literatures, electrostatic spray pyrolysis of ZnSe, ZnSe:Eu, CdSe:Eu and MgSe:Eu films in different variations have not been reported. Due to the fact that rare-earth ions have exceptional optical characteristics, it is therefore important to study the effect of rare-earth ions doping on the enhancement of the optical properties of semiconductor materials (in this case, II-VI semiconductors).

1.3 Aim and objectives of the study

This aim of this research is to synthesize and characterize rare-earth doped II-VI semiconductors using electrostatic spray pyrolysis.

The aim of the research can be achieved using the following objectives:

1. To obtain the optical properties of zinc selenide, Eu-doped zinc selenide, Eu-doped cadmium selenide and Eu-doped magnesium selenide films using the UV-VIS-NIR spectrophotometer.
2. To obtain the surface morphology of zinc selenide, Eu-doped zinc selenide, Eu-doped cadmium selenide and Eu-doped magnesium selenide films using scanning electron microscopy (SEM).
3. To obtain and confirm the elemental composition of zinc selenide, Eu-doped zinc selenide, Eu-doped cadmium selenide and Eu-doped magnesium selenide films using energy dispersive analysis x-ray spectroscopy (EDX).
4. To obtain and study the structural properties of zinc selenide, Eu-doped zinc selenide, Eu-doped cadmium selenide and Eu-doped magnesium selenide films using x-ray diffraction (XRD) technique.

1.4 Significance of study

Due to the importance of II-VI semiconductor materials and the luminescence property of europium, it is expected that doping these II-VI (ZnSe, CdSe and MgSe) semiconducting compounds with europium as dopant will produce new sets of rare-earth doped semiconductors with enhanced optical properties towards improving existing functions of optoelectronics and other semiconductor devices. Results obtained from this research will help manufacturers on the choice of materials to be considered for manufacturing

semiconductor-based devices. The results and discussions presented in this dissertation will serve as a guide towards understanding the properties of semiconductors at the nanoscale range.

To the academic audience and the general public, this research will add to the existing literatures on the growth and characterization of rare-earth doped semiconducting films.

1.5 Scope of study

This research is centered on the growth of ZnSe, ZnSe:Eu, MgSe:Eu and CdSe:Eu films using electrostatic spray pyrolysis technique. Parameters such as deposition temperature, flow-rate and dopant concentration were varied. The temperature was varied by a digital temperature controller connected to the spray pyrolysis unit, flow rate was varied by changing the volume of spray solution for each spray while dopant concentration was varied by changing the volume of dopant concentration per spray. After deposition, the films were characterized for their optical, morphological and structural properties with the aid of a UV-VIS spectrophotometer, scanning electron microscopy (SEM) and x-ray diffraction (XRD) techniques respectively. Elemental composition was determined by energy dispersive analysis x-ray (EDX) spectroscopy attached to the scanning electron microscope. The thickness of the all the films were obtained by a surface profilometer at room temperature. Discussions based on the obtained properties are presented.

1.6 Limitations of the study

A number of factors limited the scope of this research. Paramount amongst these is the non-availability of the dopant (europium trioxide) in Nigeria and even in the whole of West African region. A number of contacts were made and after a period of thirteen (13) months,

the dopant was finally obtained from Sigma Aldrich Company, Germany through a subsidiary-Bristol Scientific Company, Nigeria limited, Lagos. Another major factor that limited this study is the price of the dopant. The price of 5 g of the dopant (europium trioxide) used was sixty-four thousand, four hundred and fifty naira (#64,450). Hence a larger quantity could not be afforded and the 5 g available had to be managed for the entire deposition. Thus because of the small quantity of dopant purchased, the doping concentration in this study had to be limited. Also, because of the high cost of characterization in Nigeria, only some of the films were characterized structurally and were further used for the analysis of this research. Also, the lack of some characterization equipments in Nigeria limited this study to considering only optical, surface morphology, structural and elemental compositional characterizations respectively.

CHAPTER TWO

LITERATURE REVIEW

2.1 Conceptual framework

2.1.1 Classification of solids

Different classes of solids exist. Solids can be classified based on their structures. With reference to their structures, solids can be classified as either amorphous solid or crystalline solids. Amorphous solids belong to the category of solids that have a disordered structure at the microscopic level. In contrast, crystalline solids are solids which have a regular arrangement of atoms (or ordered atomic arrangement) in three dimensions. Crystalline solids can further be divided into the single crystalline solid and the polycrystalline solids.

Based on their electrical conductivities and band structures, solids can also be classified into three main categories. These are conductors, semiconductors and insulators. This shall bring us to the discussion of the band theory of solids.

2.1.2 Band theory of solids

Every solid contain electrons. The behaviour exhibited by these electrons when exposed to an applied electric field gives an insight on how materials can be classified as either a metal, an insulator or a semiconductor. According to the band theory, electrical conduction can take place in a solid only if a good number of free electrons are present and if vacant levels are available immediately above the occupied energy levels (Avadhanulu and Kshirsagar, 2008). The electrons in a crystal are arranged into different bands known as energy bands. These energy bands are referred to as either the conduction band (CB) or the valence band (VB). Both bands are separated by a region in which no electron state is allowed to exist. This forbidden region is called the energy gap or band gap and is denoted by E_g. The band gap can

be defined as the difference in energy between the top of the valence band and the bottom of the conduction band. The bottom of the conduction band is referred to as the conduction band edge (CBE) while the top of the valence band is known as the valence band edge (VBE).

2.1.2.1 Metals (conductors)

Metals are materials characterized by a large conductivity and they allow the unconditional flow of current through them. Metals have conductivities typically between 10^{-6} Ωcm^{-1} and 10^{4} Ωcm^{-1}. In metals, there is no energy gap as both the valence and conduction bands overlap. This overlap ensures the free flow of valence electrons within the crystal which make metals very good conductor of electricity. Examples of materials which are conducting in nature include copper, aluminum, etc. Figure 2.1 illustrates a simple energy band structure for a metal.

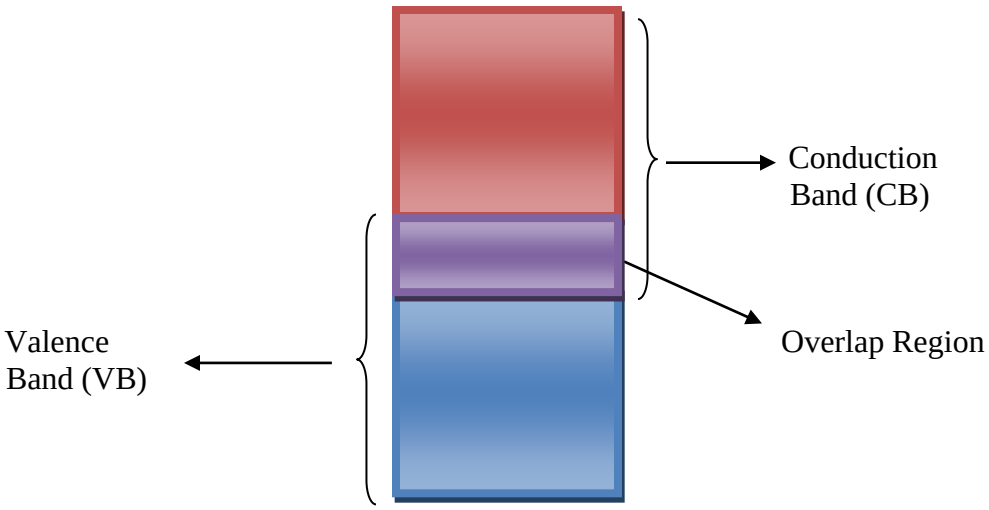

Figure 2.1: Band structure of a metal

2.1.2.2 Insulators

Insulators are materials that have very low or no conductivity. They are characterized by a large energy gap (or forbidden gap) which can be up to 6.00 eV. Due to this large energy gap,

it is often difficult for electrons to be thermally excited from the valence band to the conduction band. The implication of this is that conduction becomes impossible. Figure 2.2 illustrates a simple band structure of an insulator.

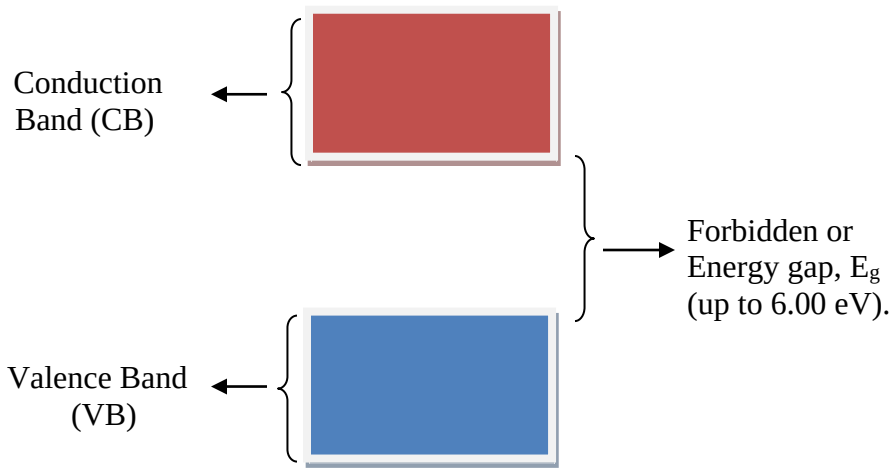

Figure 2.2: Energy band structure of a typical insulator. Forbidden band has value up to 6.00 eV which makes conduction impossible

2.1.2.3 Band theory of semiconductors

A semiconductor is a material whose conductivity and resistivity lies between that of a metal and an insulator. They are characterized by a conduction band (CB) and a valence band (VB) respectively. For a semiconductor at 0 K, the conduction band is completely empty while the valence band is filled with electrons. When the temperature of the semiconductor crystal is increased above 0 K, electrons from the valence band gain enough energy and are thermally excited to the conduction band thus creating an equal number of hole or vacancy in the valence band. When this happens, both the electrons which have been thermally excited into the conduction band and the holes or vacancies left behind in the valence band give rise to electron-hole pair which in turn triggers electrical conductivity. The semiconductor is

characterized by a small band gap which is actually less than 3.00 eV. For a typical semiconductor, the band gap lies between 0.50 eV and 1.50 eV. In the case of silicon which is a typical semiconductor, the band gap is about 1.12 eV. Due to the considerable small band gap exhibited by silicon, electrons in the valence band are easily excited to the conduction band. Once the electrons are excited into the conduction band, their response to external voltage (electric field) produces the flow of current. A schematic illustration of the band structure of a typical semiconductor at T > 0 K is presented in figure 2.3.

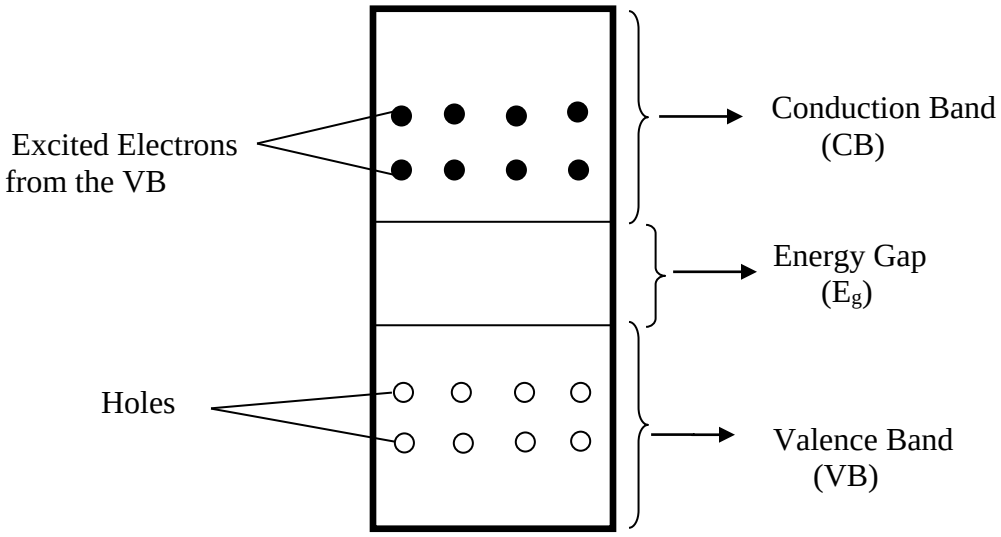

Figure 2.3: Band structure of a typical semiconductor at T > 0 K showing equal number of holes and electrons

2.2 Europium

Europium is an element represented by the chemical symbol; Eu. It was discovered in 1901 by Eugene Demarcay in Europe and named after the continent "Europe." Europium is a rare earth metal which belongs to the lanthanide series in period 6 of the periodic table. As a result of its being in the lanthanide series, europium assumes the oxidation state of +3, that is, Eu^{3+}.

However, europium can also exhibit the oxidation state of +2 (Eu^{2+}). All europium compounds having oxidation state of +2 are known to be slightly reducing. Its valence electrons are represented by the electronic configuration; [Xe] $4f^7 6s^2$.

In most applications, the phosphorescence of europium compounds is exploited for a number of purposes. Europium oxide has recorded a high feat as a dopant in phosphors in computer monitors and television sets. Eu^{3+} exhibits a red radiance while Eu^{2+} gives a blue radiance. The combination of both produces white light which is being exploited in the manufacture of fluorescent light bulbs.

2.3 Characteristic features of ZnSe, CdSe and MgSe

Zinc selenide is a binary semiconductor compound which consists of two chemical elements; zinc and selenide combined to form a single compound. ZnSe belongs to the class of semiconducting compounds which can be described by the general formula $A^{II}B^{VI}$ and is referred to as a II-VI semiconductor. Zinc selenide has a large band gap of about 2.70 eV, lattice spacing of about 5.65 Å and has eight (8) valence electrons. It crystallizes in the zinc blende and wurzite structure. Consequently, this compound offers a large variety of applications such as photo-detectors, thin-film solar cells, blue light-emitting devices, etc (Popa and Rusu, 2011). Among the II - VI compound semiconducting materials, ZnSe is used as a window layer for the fabrication of thin film solar cells (Kissinger *et al*., 2009).

Cadmium selenide is also a binary semiconducting compound described by the general formula $A^{II}B^{VI}$ and can be referred to as a II-VI semiconductor. It is a combination of cadmium and selenium compounds respectively. Cadmium selenide has a direct band gap of about 1.84 eV at 0 K and 1.74 eV at 300 K. CdSe nano particles are one of the most interesting semiconductors which a lot of current researches have focused on their

characteristics and applications (Amiri *et al*., 2013). CdSe is an important material for which can enhance the development of various modern technologies of solid state electronic devices such as high efficiency thin film transistors and light emitting diodes (Girija *et al*., 2009).

Magnesium selenide (MgSe) is a II-VI binary semiconductor with a band gap of about 2.10 eV. It is composed of magnesium and selenium. MgSe is a wide band gap semiconductor which may exist in various crystal structures such as zinc blende, wurtzite and rocksalt (Gnanamuthu *et al*., 2015).

2.4 Doping

The crystal lattice of a semiconductor can be modified by the introduction of foreign atoms. When this happens, the electrical properties of the semiconductor is altered and changes significantly. This process is referred to as doping. Expressed in another way, we may refer to doping as the addition of impurity atoms to a pure semiconductor. The impurity atoms or foreign atoms added to the pure semiconductor to improve its electrical characteristics are known as dopants. The semiconductor obtained after doping is called an extrinsic semiconductor while the un-doped semiconductor is referred to as an intrinsic semiconductor. In an extrinsic semiconductor, the equilibrium number of free electrons and holes are no longer equal since a tool other than electron-hole pair generation is used to create free carriers. Depending on the amount and type of impurity (or impurities) introduced, many electrical and optical properties of the semiconductor material may be modified or controlled to optimize desired behaviours or characteristics.

2.5 Nanoscience and nanotechnology

In the quest for the manufacture of very small and fast electronic systems such as the computer, mobile phones, televisions and other electronic gadgets, scientists have intensified

research in the area of solid state physics, chemistry, materials science, engineering and other disciplines to achieve this goal. Richard Feynman in 1959 (the birth of nanotechnology) proposed for the first time about the possibility of manipulating the atoms for its application in data storage down to the scale of a single atom (Singh *et al*., 2012). When the characteristic length of the microstructures is in the 1-100 nm range, it becomes comparable with the critical length scales, *i.e.* size and shape effects on physical phenomena offer their usefulness in the devices using nano-structured materials, nano-tools, and nano-devices (Singh *et al*., 2012). After the famous speech of Richard Feynman in 1959, Moore's law which focused on the possibility of developing small scale devices which can perform the same or even better functions than the already existing devices was later published in 1965. Moore's law implies that the fastest computer available in sales at any particular time doubles in speed every eighteen to twenty two months. The birth of nanotechnology could be traced to the speech delivered by the great physicist Prof. Richard P. Feynman on the 29th of December 1959 at the annual American Physical Society meeting at Caltech institute, with the title: "There is Plenty of Room at the Bottom." This speech was unique and held a defining place in the field now known as nanoscience and nanotechnology (Nai-Chang, 2008). In his speech, Feynman saw the future and projected a vision which is presently coming into reality. In his speech, Feynman asserted that nothing in the laws of physics prevented us from arranging atoms the way we want. Not only that Feynman's vision of manipulating and controlling things down to nano and even atomic scale becomes realizable, but novel nano-scale devices and characterization tools have also revolutionized means to exploring new science and developing new technology in a wide variety of research fields (Nai-Chang, 2008).

Nanoscience is not just the science of the small, but the science in which materials with small dimension show new physical phenomena, collectively called quantum effects, which are size-dependent and dramatically different from the properties of macroscale materials (Filipponi and Sutherland, 2013).

When nanoscience is applied in the development or manufacture of devices, the process is referred to as nanotechnology. Nanotechnology deals with the process of manipulating, controlling and the combination of atoms and molecules in order for materials, structures, components, devices and systems at the nanoscale level to be created. Nanotechnology provides us with the possibility of developing materials and devices which are characterized with improved functions and properties.

2.6 Nanofabrication

Nanofabrication involves the use of technologies in fabricating micro or very small devices. Nanofabrication can thus be defined as the process of manufacturing miniature structures whose sizes are in the nanoscale range. Microelectronics industries make use of nanofabrication in the process of manufacturing devices which are often made on silicon wafers. Nanofabrication can be broadly classified into two major areas. These are “top-down” approach and “bottom-up” approach. A schematic illustration of the methods used to prepare nanostructured materials is illustrated in figure 2.4.

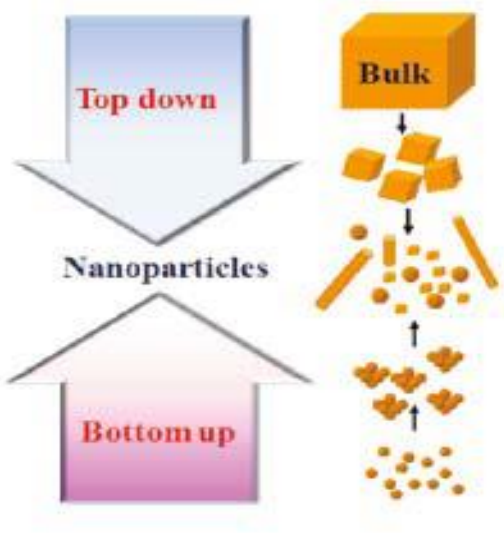

Figure 2.4: Preparative methods of nanoparticles (Alagarasi, 2011)

2.6.1 Top-down approach

This approach consists of disintegrating or decomposing the bulk material into smaller components until the desired dimension is attained. In the top down methods, the features are written directly onto a substrate, for example, by electron beams, and then by applying appropriate etching and deposition processes, the nanoscopic features are engraved (Minelli, 2004). The top-down approach often uses the traditional workshop or micro fabrication methods in which externally-controlled tools are used to cut, mill and shape materials into the desired shape and order (Ghosh, 2009). Examples of top-down approach include attrition and milling which are used for processing nanoparticles. Another example of the top-down approach is lithography. Lithography is the deposition of a computer generated pattern onto a substrate (e.g. glass). A number of disadvantages are synonymous with lithography. One of such disadvantages includes the significant introduction of crystallographic defects to the processed patterns. Other disadvantages are that their initial costs are very high, the requirements on the equipment and environment are harsh, and the most important set back is

that, it is nearly impossible to fabricate a single nanostructure or free the as-attained nanostructures from the substrates, hence, their applications are limited (Nweze, 2012). In spite of the defects, the top-down approach plays an important role in the synthesis and fabrication of nanomaterials in that the present state of nanoscience can be viewed as an amalgamation of bottom-up chemistry and top-down engineering techniques (Ghosh, 2009).

2.6.2 Bottom-up approach

Bottom-up approach of growing nanoparticles or nanomaterials involves the preparation of a bulk material by the assembling of a molecular structure atom-by-atom, molecule-by-molecule and cluster-by-cluster from the bottom until the desired bulk structure is achieved. This method is mainly applied in crystal growth processes. Using this method, nanostructures with fewer defects can be obtained when compared to the top-down approach. Bottom-up approach are mainly classified into gas phase processes such as chemical vapour deposition (CVD) and wet chemical processes such as chemical bath deposition (CBD), electro deposition, spray pyrolysis, successive ionic layer adsorption and reaction (SILAR), and so on.

In this research, we shall only be concerned with the bottom-up approach of growing semiconductor films. A few of these will be described in the next section that follows.

2.7 Bottom-up approaches for depositing semiconductor films

Various bottom-up techniques are available for the deposition of semiconductor films. Some of these techniques include spray pyrolysis, vacuum evaporation, chemical bath deposition, chemical vapour deposition, electrochemical deposition, sputter deposition, molecular beam

epitaxy, successive ionic layer adsorption and reaction (SILAR) deposition techniques and so on. Some of these techniques shall be briefly appraised in the subsections that follow.

2.7.1 Spray pyrolysis deposition technique

Spray pyrolysis has been widely used to produce fine powders because it is an inexpensive and continuous, ambient pressure process and is more economical than other processes (such as sol–gel and chemical vapor deposition) that involve multiple steps or that must be carried out under vacuum (Chen *et al*., 2006).

Spray pyrolysis deposition technique consists of a process whereby a precursor solution is transported from a reaction compartment via a diffusion tube (where nitrogen gas or compressed air serves as the carrier gas) to a spray nozzle and eventually deposited on a heated substrate. Basically, spray pyrolysis involves spraying a solution on a heated substrate where the constituents of the solution decompose to form the desired/required film. The spray pyrolysis system consists of a nebulizer or atomizer (which in this case is the spray nozzle) which converts the precursor solution to droplets. As these droplets touch the surface of the heated substrate, they undergo a pyrolytic decomposition, thus forming either a single crystalline or a cluster of crystalline films on the substrate surface. The reaction is carried out by subjecting the precursor solution to temperatures at which pyrolysis of the solute will occur (Kalyana *et al*., 2009).

The spray pyrolysis deposition technique is characterized by three major steps which are: atomizing the precursor solution into droplets, transportation of the droplets and finally the decomposition of the transported droplets via a spray nozzle on a heated substrate. In depositing a film using spray pyrolysis deposition technique, a number of factors have been identified as having a direct effect on the grown films. Some of these factors include

concentration of the precursor solution, distance of the spray nozzle from the substrate, temperature of the substrate, working air pressure, volume of the solution and the deposition time.

Spray pyrolysis is a physical method, which is relatively simple, reproducible, size controllable, low cost and continuous for synthesis of some nano metal oxides, mixed metal oxides and metals on metal oxides (Okuyama and Lenggoro, as cited in Ghaffarian *et al*., 2011).

2.7.2 Vacuum evaporation technique

Vacuum evaporation is a form of deposition technique designed for growing thin and nano films and this can be achieved by allowing the deposition process to take place inside a vacuum chamber. The vacuum chamber consists of a vapourization source and a substrate holder. Notable vapourization sources include highly resistive wires and boat or crucibles. Before deposition takes place, the vacuum chamber is sealed and connected to an external current source. In vacuum evaporation, the substrate is placed at some distance above the vapourization source (in this case, a boat). The material to be vapourized is normally crushed into a powder form and placed on the vapourization source. The vacuum chamber is then pumped to a pressure, say about 10^{-5} Torr or more. As the pressure of the vacuum chamber is raised, electric current from the external current source is applied and made to pass through the constructed boat. As this happens, the vapourization temperature is attained and molecules of the material to be deposited are evaporated from the surface of the vapourization source and travel in a straight path until they reach the surface of the substrate. Since the temperature of the substrate is lower than that of the vaporization temperature, the evaporated material on getting to the substrate, condense and adhere to the substrate thus forming the desired film.

Some of the materials will be lost by volatilization or expansion from the substrate surface during deposition; therefore approximately 20% in excess of material should be added to be sure that the wanted thickness will be achieved (Al-Mashhadany and Sadeq, 2007).

2.7.3 Chemical bath deposition technique

This technique is also known as solution growth technique. This deposition process is characterized by a very simple formulation, easy set up and requires low temperature for the entire process. This process can be conveniently carried out at room temperature. However, most films obtained by this process are generally amorphous. It is generally difficult to obtain crystalline films with this method at room temperature. However, if the temperature is raised above room temperature, say as high as 150 ^{o}C and above, crystalline films could be obtained. It is pertinent to state that this process can proceed through two main basic mechanisms. The two main basic mechanisms are what are commonly termed the cluster (or hydroxide, since it normally proceeds through a hydroxide cluster) mechanism and the ion-ion mechanism (Gorer *et al*., 1995), as illustrated in figure 2.5.

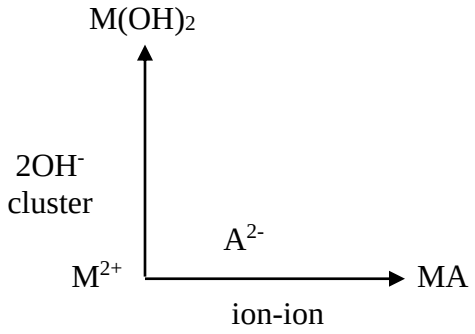

Figure 2.5: The two main basic mechanisms involved in a typical CBD process

In depositing a film using chemical bath deposition, several materials/equipments are required. Some of such materials/equipments include a set of beakers, chemicals, distilled water, thermometer, glass rod stirrer, microscopic glass slides (which serve as substrates), syringes, measuring cylinder, a weighing balance and a digital pH meter used for measuring the pH value of the mixture.

Figure 2.6 illustrates a simple setup of the chemical bath deposition technique.

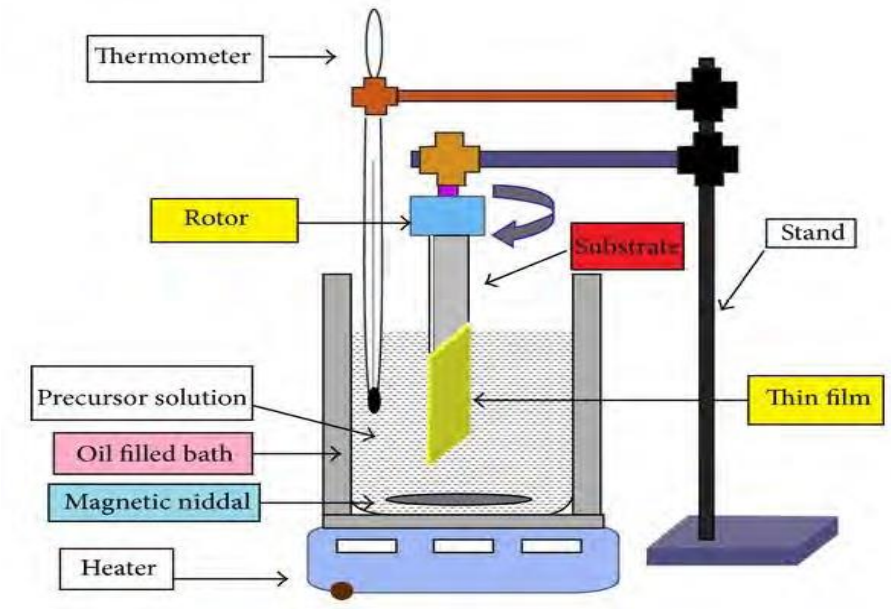

Figure 2.6: Chemical bath deposition technique (Tanvir, 2017)

2.7.4 Successive ionic layer adsorption and reaction technique

This process of film deposition is almost the same as chemical bath deposition with a slight difference. It can be performed using glass beakers of any size just as in chemical bath deposition technique. Hence scientists and researchers often refer to the SILAR technique as the modified version of chemical bath deposition technique. SILAR is a wet chemical route for the synthesis of thin films in which the basic building blocks are ions instead of atoms and

therefore the preparative parameters are easily controllable (Mitra and Mondal, 2013). The SILAR method is mainly based on the adsorption and reaction of the ions from the solution and rinsing between every immersion with de-ionized water to avoid homogeneous precipitation in the solution (Raidou *et al*., 2010). In this process, cationic and anionic precursors are prepared in separate beakers. The substrate is first immersed into a cationic solution for a while; thereafter it is removed and rinsed in de-ionized water. This same substrate is again immersed into the anionic solution for a while and then removed and also rinsed in de-ionized water. It is then kept in an air-tight box to prevent it from coming in contact with dirt and for further characterization. Raidou *et al*., (2010) reported that in general, the SILAR growth cycle contains four different steps: adsorption, rinsing, reaction and rinsing. Rinsing follows each reaction, which enables heterogeneous reaction between the solid phase and the solvated ions in the solution (Raidou *et al*., 2010).

Pathan and Lokhande, (2004) reports that in spite of its simplicity, SILAR has a number of advantages which include the following:

(a) it offers extremely easy way to dope film with virtually any element in any proportion by merely adding it in some form of the cationic solution.

(ii) unlike closed vapour deposition method, SILAR does not require high quality target and/or substrates nor does it require vacuum at any stage, which is a great advantage if the method will be used for industrial application.

(iii) the deposition rate and the thickness of the film can be easily controlled over a wide range by changing the deposition cycles.

(iv) operating at room temperature can produce films on less robust materials.

(v) unlike high power methods such as radio frequency magnetron sputtering (RFMS), it

does not cause local over heating that can be detrimental for materials to be deposited.

(vi) there are virtually no restrictions on substrate material, dimensions or its surface profile.

It is important to state that this process of film deposition is generally not expensive; it is simple and very convenient for the deposition of a film on a large surface.

2.7.5 Electrochemical deposition technique

Electrochemical deposition (ECD) is a term used for all types of electrochemical reactions leading to the deposition of a material (Tang, 2008). According to Mendelson (2010), the electrochemical deposition process is defined as the production of a coating on a surface from an aqueous solution composed of several substances. Electrochemical deposition process usually takes place inside an electrochemical cell. In this type of deposition technology, the film deposit can be formed on a substrate by allowing current to pass through an electrochemical cell with the aid of an external power source. Alternatively, it can be formed by making a complex solution where chemical reactions take place continuously without any power source due to the sufficiently high potential between the surface and a solution (Mendelson, 2010).

A typical electrochemical cell consists of a reaction vessel (a beaker in most cases) and maybe two or three electrodes. The two-electrode cell consists of a working electrode (substrate) and a counter electrode. The reactions can be controlled in the two-electrode cell by the application of current between the working electrode and the counter electrode. In the three-electrode cell, deposition of the required film on a substrate can be obtained either by controlling the potential or the current and the corresponding potential or current is measured.

In electrochemical deposition, when a potential different (PD) is applied across the system, a direct current (DC) source supplies current which flows in one direction through the external

circuit. Electrons are the main carriers of current in the external conductors. Electricity is transferred in the solution through electrically charged particles known as ions. When a potential difference is applied, the positive ions referred to as cations move towards the negative electrode while the negative ions known as anions move towards the positive electrode. As this mechanism takes place, deposition of films occur on the substrate from the aqueous solution. In an electrochemical cell the positive electrode is referred to as the anode while the negative electrode is called the cathode. Electrochemical deposition is an attractive method for preparation of thin films in commercial quantities because it uses relatively cheap equipment, enables the deposition in large area and easy control of growth parameters through applied potential, current, pH and temperature of the bath (Mammadov *et al*., 2012).

2.7.6 Chemical vapour deposition technique

Chemical vapor deposition (CVD) is a deposition process where chemical precursors are transported in the vapor phase to decompose on a heated substrate to form a film (Barron, 2009). The deposited films may either be amorphous, crystalline or polycrystalline depending on the deposition conditions such as deposition temperature, precursor materials, deposition substrates, substrate temperature, deposition pressure and so on. Carlsson and Martin, (2010) defined chemical vapor deposition (CVD) as a process whereby a solid material is deposited from a vapor by a chemical reaction occurring on or in the vicinity of a normally heated substrate surface. Chemical vapor deposition (CVD) is a widely used materials-processing technology which can be applied in solid thin-film coatings to surfaces, production of high-purity bulk materials and powders, as well as fabricating composite materials via infiltration techniques (Creighton and Ho, 2001).

In a typical CVD process, one or more gases are introduced into a reaction chamber, in most cases at low pressure. When this is done, the gases react on the surface of the substrate which leads to the desired film. After deposition occurs on the substrate surface, the gaseous by-products of the reactions are absorbed and ejected via an exhaust pipe from the reaction chamber. This completes the entire process of CVD. Thus, in a nutshell, we emphasize that a typical CVD process consists of the following four steps;

(a) reactant gases are introduced into the reaction chamber,

(b) the reactant gases move to the substrate and gets absorbed by the substrate,

(c) deposition takes place on the substrate,

(d) the gaseous by-products of the reactions are absorbed and ejected via an exhaust pipe from the reaction chamber.

2.8. Techniques for characterizing semiconductor films

Characterization of semiconductor films involves the use of several techniques which allows the deposited films to interact with electromagnetic radiation in a step by step procedure to obtain the optical properties, surface morphologies, film composition and other properties. Some of these techniques will be briefly explained in the subsections that follow.

2.8.1 Optical characterization

2.8.1.1 Ultra-violet/visible/near-infrared spectrophotometric measurement

The absorbance of semiconductor films can be measured by the use of spectrophotometers. The spectrophotometer consists of a number of high intensity lamps which provides radiation from the ultraviolet (UV) region to the near-infrared (NIR) region of the electromagnetic spectrum and a monochromator which is responsible for selecting the different wavelengths

striking the material. Depending on how the UV/VIS/NIR spectrophotometer is set to function, when a beam of electromagnetic radiation is incident on a material, part of the incident radiation, I_R, could be absorbed while the other part of it could either be reflected or transmitted (transmitted flux, I_x). The absorbed radiation at different wavelengths is detected by a photo detector and the results obtained are displayed on the screen of a computer monitor. In the case of UV/VIS region, the absorbance of the material can be read directly from the instrument while the transmittance can be calculated using equation 2.1 as shown below.

$$T = 10^{-A} \quad (2.1)$$

The reflectance values can be calculated using equation 2.2

$$R = [1 – (A + T)] \quad (2.2)$$

In the case of infrared region (IR), the transmittance values can be measured directly from the machine.

2.8.2 Surface characterization

2.8.2.1 Atomic force microscopy

The atomic force microscopy technique employs an atomic force microscope (AFM) to analyze and characterize samples. The atomic force microscope is an instrument which characterizes samples at the microscopic level.

The atomic force microscope consists of a flexible cantilever which is attached to a piezoelectric scanner. A sharp tip is mounted on the cantilever and the sample to be analyzed is made to come in contact with the sharp tip (contact mode) of the AFM. Once this is achieved, the sample undergoes a scanning process which is controlled by the piezoelectric scanner attached to the cantilever and moves the sample relative to the tip and vice versa.

Thereafter, the image of the sample at the microscopic scale is displayed on the screen of a computer attached to the AFM.

The major advantages of AFM are that it has a combination of high resolution in three dimensions, the sample does not have to be conductive and there is no requirement for operation within a vacuum (Natasha and Paul, as cited in Jeroh, 2012).

2.8.2.2 Transmission electron microscopy

This phenomenon involves the use of transmission electron microscope to analyze the microstructure of the sample under investigation. This is done by transmitting a high energy beam of electrons through the sample with atomic scale resolution. The transmission electron microscope consist of electromagnetic lenses which are used in focussing the electrons of the sample and then accelerated at several hundred kilovolts (kV) and thereafter the image is recorded on a fluorescent screen or a digital camera.

2.8.2.3 Scanning electron microscopy

Scanning electron microscopy is a technique used for analyzing the surface morphology of grown films. Scanning electron microscopy gives the surface micrographs of the deposited films and this is usually carried out using a scanning electron microscope (SEM). Just as the name suggests, the scanning electron microscope employs electrons for imaging of film samples.

The SEM consists of an electron column, a sample chamber and a thermal emission source. The sample to be analyzed is mounted on the sample chamber. A beam of incident electrons are then generated in the electron column which is located slightly above the sample chamber. The scanning electron microscope (SEM) uses a focused beam of high-energy electrons to

generate a variety of signals at the surface of solid specimens (Swapp, 2011). The signals that derive from electron-sample interactions reveal information about the sample including external morphology (texture), chemical composition, and crystalline structure and orientation of materials making up the sample (Swapp, 2011).

2.8.3 Elemental composition analysis

2.8.3.1 X-ray fluorescence spectroscopy

When a material is bombarded by high energy x-rays or gamma rays, the emission of fluorescent x-rays by the material is termed "x-ray fluorescence." The analysis of a sample using x-ray fluorescence (XRF) is known as x-ray fluorescence spectroscopy. This method of analysis is widely employed by various scientists and researchers in determining the elemental and chemical compositions of semiconductor thin and nanofilms respectively. The major advantage of this method is its non-destructive nature and also offers the advantage of being very fast in sample analysis.

2.8.3.2 Energy dispersive x-ray spectroscopy

Energy dispersive x-ray spectroscopy (EDX) is a chemical microanalysis method used for analyzing the elemental composition and chemical states of the film under study. It is used alongside with scanning electron microscopy. In the EDX analysis, a beam of electron is allowed to bombard the sample to be analyzed. When this happens, x-rays are emitted. These emitted x-rays are detected by the EDX machine and this helps to characterize the elemental composition of the sample under analysis.

The EDX spectrum obtained is displayed in a computer monitor attached to the EDX machine in digital form. The displayed spectrum comprises the x and y axes respectively. The x-axis represents the energy while the y-axis represents the number of counts per channel. The

resolution of the energy is defined as the full width of the peak at half maximum height (FWHM).

2.8.4 Structural characterization

2.8.4.1 X-ray diffraction analysis

The structural property of the grown film to be analyzed is determined by x-ray diffraction (XRD). This technique helps to determine the actual structure of the film under study. It is a non-destructive technique which reveals if the film under study is either amorphous, crystalline or polycrystalline as the case may be. XRD analysis is performed using an x-ray diffractometer. The x-ray diffractometer consists of a monochromatic source of x-rays, usually from a copper target or anode giving CuK_{α} ($\lambda = 0.154$ nm after passing through nickel filter), a sample holder and an x-ray detector (Sulabha, 2015). Both sample and the detector move around an axis passing through sample centre and normal plane of the paper (Sulabha, 2015).

The substrate containing the sample to be analyzed is placed in the sample stage compartment where incident x-rays from an x-ray tube are accelerated at a specified accelerating voltage and current and allowed to strike the substrate. As this happens, the films are separately scanned continuously between 0˚ and 80˚ or any chosen range of 2θ at a chosen step size and at a specified time per step. Typical diffraction patterns of the films are detected by the detector and are displayed on a computer monitor attached to the XRD equipment. The diffraction pattern is a plot of the intensity versus angle of diffraction (2θ) of the film under study. This technique plays a fundamental role in determining structural properties of films. These structural properties include grain size, lattice parameters, preferred orientation, strain and phase composition respectively.

2.9 Optical properties of semiconductor films

When semiconductor films interact with electromagnetic radiation, they exhibit certain properties which are referred to as optical properties. These optical properties when studied carefully help to reveal the industrial importance of semiconductor materials. Some of these optical properties include absorbance (A), transmittance (T), reflectance (R), absorption coefficient (α), refractive index (n), optical conductivity (σ), extinction coefficient (k), dielectric function (ε) and band gap energy (E_g).

2.9.1. Absorbance (A).

When a sample interacts with light, part of the incident light on the surface of the sample is absorbed. This process is known as absorption and the mathematical quantity of the light absorbed is termed "absorbance."

The absorbance of a sample can also be defined as the ratio of the absorbed beam of light to the incident beam of light. If the incident beam of the sample is I_o and the absorbed beam is I_A, then the absorbance of the sample is expressed by equation 2.3:

$$A = \frac{\text{Absorbed beam } (I_A)}{\text{Incident beam } (I_0)} \qquad (2.3)$$

Absorbance is measured in arbitrary unit (a.u).

2.9.2. Transmittance (T)

The transmittance of a sample is defined as the quantity of light at a particular wavelength which passes through the sample when light or electromagnetic radiation is incident on the sample. It can also be defined as the ratio of the transmitted light to the incident radiation. If

the transmitted light is designated by I_T and the incident radiation is given by I_o, then the transmittance can be expressed mathematically by the relation:

$$T_\lambda = \frac{I_T}{I_o} \qquad (2.4).$$

where T_λ = Transmittance of the sample at a particular wavelength,

I_T = Intensity of the transmitted light,

I_o = Intensity of the incident radiation.

However, it is pertinent to state that the term "transmission" is used to refer to the physical process of radiation which passes through a sample while "transmittance" refers to the mathematical quantity.

2.9.3. Reflectance (R)

When electromagnetic radiation strikes a sample at a particular wavelength, the portion of reflected light is called reflection and the quantity of the incident radiation at a given wavelength that is reflected back when it strikes a surface is referred to as the reflectance. Reflectance can also be defined as the ratio of the reflected light to the incident radiation. If the reflected light is designated by I_R and the incident radiation is given by I_o, then the reflectance can be expressed mathematically by the relation:

$$R = \frac{\text{Reflected Light } (I_R)}{\text{Incident Radiation } (I_0)} \qquad (2.5)$$

The spectral absorbance (A), transmittance (T) and reflectance (R) are related by a single equation as shown in equation 2.6.

$$A + T + R = 1 \qquad (2.6)$$

The value of reflectance (R) of a given sample can be calculated from equation 2.6 when the values of absorbance (A) and transmittance (T) are known.

2.9.4. Absorption coefficient (α)

The amount of light absorbed by a material is defined by its absorption coefficient. It can be seen as the decrease in the intensity of a beam of photons or particles when they pass through a particular sample or medium (Jeroh, 2012).

Consider an incident radiation I_o on a material having thickness t, then the transmitted intensity I_T can be expressed as:

$$I_T = I_o \exp(-\alpha t) \quad (2.7)$$

$$I_T / I_o = \exp(-\alpha t) \quad (2.8)$$

But, $T = I_T / I_o$

Therefore, $T = e^{-\alpha t}$ (2.9)

Where α = absorption coefficient.

Equation 2.9 can be re-written in the form:

$$\ln T = -\alpha t \quad (2.10)$$

$$\alpha = \frac{-[\ln T]}{t} \quad (2.11)$$

2.9.5 Refractive index

The refractive index of a material is defined as a measure of the speed of light in that material. It can be expressed as a ratio of the speed of light in vacuum relative to that in the considered medium. The refractive index of a material can be calculated as expressed in equation 2.12.

$$n = \frac{\text{Speed of light in vacuum}}{\text{Speed of light in medium}} \quad (2.12)$$

The refractive index can also be expressed as shown in equation 2.13.

$$n = \frac{1+ R^{1/2}}{1- R^{1/2}} \quad (2.13)$$

where R = reflectance of the film.

2.9.6. Optical conductivity

The frequency response of a material when it is irradiated by light is referred to as the optical conductivity of the material. The optical conductivity of a material directly depends on the absorption coefficient and is found to increase sharply for higher energy values due to large absorption coefficient for the values.

2.9.7 Extinction coefficient

The extinction coefficient of a sample is defined as a measure of the rate of diminution of transmitted light via scattering and absorption for the sample. The absorption and refraction of a medium can be described by a single quantity called the refractive index. This is usually given by the symbol; ñ and is defined through the equation:

$$\tilde{n} = n + ik. \tag{2.14}$$

The real part of ñ, namely n, is the normal refractive index while the imaginary part of ñ, namely k, is called the extinction coefficient.

2.9.8. Dielectric function

The dielectric function of a thin film is a complex quantity which consists of both the real and imaginary parts. It is a fundamental intrinsic property of a material. The real part indicates how the speed of light in the material can be slowed down while the imaginary part deals with the absorption of energy by a dielectric from electric field due to dipole motion.

2.9.9 Band gap energy

Band gap is defined as the distance between the upper valence band and the lower conduction band. The energy associated with band gap energy and transition type can be defined from

mathematical treatment of data obtained from optical absorbance versus wavelength with the following relationship for near edge absorption (Anuar *et al*., 2010).

The band gap energy of semiconductor thin/nanofilms can be calculated from the expression (Anuar *et al*., 2010):

$$\alpha = \frac{[k(h\nu - E_g)^{n/2}}{h\nu} \quad (2.15)$$

where α is absorption coefficient, υ is the frequency, h is Planck's constant, k is a constant and n= 1 or 4.

For a direct transition, n is equal to 1, while n is equal to 4 for an indirect transition.

Hence, the intercept of the plot of $(\alpha h\nu)^2$ versus the photon energy, hυ, gives the value of the band gap for a direct transition while the band gap energy for an indirect transition is obtained from the intercept of the plot of $(\alpha h\nu)^{1/2}$ versus the photon energy, hυ.

2.10 Methods of measuring the thickness of semiconductor films

Different techniques exist for measuring the thickness of semiconductor films. A brief appraisal of some of these techniques will be presented in the subsections that follow.

2.10.1 Gravimetric (microbalance) technique

For this method to be applied in calculating film thickness, the mass of the film, its area and density have to be known with great certainty. To get an approximate mass of the film, the microscopic glass slide serving as the substrate has to be weighed with a sensitive mass balance before and after the film has been deposited on it. The approximate mass of the film is then obtained by subtracting the mass before deposition from the mass after deposition.

Let M_1 be the mass of the substrate before deposition and M_2 the mass after the deposition. Then the thickness t can be calculated by the expression (Ompong, 2010):

$$t = (M_2 - M_1)/A\rho \quad (2.16)$$

where A = Lb is the area of the film surface, ρ is the density of the film.

This method has a number of challenges in measuring film thickness because film density is not known with certainty (Ompong, 2010).

2.10.2 Stylus (surface profile) technique

A profiler model can be used to determine the thickness of samples deposited on a substrate. The surface profiler consists of a marking tip used to scratch off a portion of the sample on the substrate. The sample whose thickness is to be determined is placed on a sample stage and the diamond tip stylus is then lowered onto the sample. The tip of the stylus makes a soft touch down on the sample and runs along the sample surface off the sample and down to the substrate. The drop off the sample surface onto the substrate helps to determine the thickness of the film grown/deposited on the substrate.

2.11 Empirical literature review

Over the years, several researches have been carried out by different research groups on pure II-VI semiconductors and II-VI semiconducting compounds doped with europium.

Deshpande *et al*., (2011) researched on nanoparticles of ZnSe prepared by chemical bath deposition. The water bath was maintained at a temperature of 343 K for about 3 to 4 hours before eventually allowed to cool to room temperature. Structural study conducted reveals the films are polycrystalline, characterized by a hexagonal phase system. The preferred orientation of the films was along the (102) lattice plane. Discrepancies arising between the particle sizes calculated from XRD analysis and those obtained from TEM measurements suggest the particle sizes are not uniformly distributed. SEM analysis confirmed the particles

are spherical. Photoluminescence (PL) spectra shows a red shift at 573 nm for ZnSe nanoparticles when compared to the bulk zinc selenide observed at 465 nm.

Bhuiyan *et al*., (2012) studied the effect of temperature on the structural and optical properties of zinc selenide thin films obtained by thermal vacuum evaporation technique. Different films were obtained by varying substrate temperature from room temperature to a maximum temperature of 200 ^{o}C. Optical analysis indicates the films deposited above room temperature had transmittance value above 80% at wavelengths longer than 550 nm. Less transmittance in the visible region was obtained for the films deposited at room temperature. Band gap energy obtained in this study varied between 2.799 eV to 2.803 eV for different substrate temperatures. X-ray diffraction studies reveal the polycrystalline nature of the films exhibiting the cubic phase crystal structure with preferred orientation along the (111) lattice plane.

Lohar *et al*., (2014) researched on the structural, optical, morphological, photoluminescence of ZnSe films deposited by pressurized spray pyrolysis with air as the carrier gas. In this experiment, substrate temperature was kept constant at 473 K. Further annealing of the deposited films was performed at 573 K for 60 mins. Optical analysis was studied in the wavelength range of 350 nm to 1100 nm. Maximum transmittance of 50% and reflectance of 40 % were obtained for the deposited films. XRD study reveals polycrystalline nature with a hexagonal structure for the deposited films. SEM images reveal a cotton-like morphology which was attributed to high deposition and annealing temperature which was responsible for the water content evaporation. Photoluminescence (PL) study showed strong emission for the film at 497 nm which implies that ZnSe is a good material for blue light emission.

Khairnar *et al*., (2012) studied the optical properties of polycrystalline zinc selenide thin films. The films were obtained by thermal evaporation technique. In this research, substrate

temperature was maintained at 373 K. The films obtained have thicknesses of 50 nm, 100 nm, 200 nm, 300 nm, 400 nm and 500 nm respectively. Optical studies reveal increase in band gap energy as film thickness increases. XRD analysis indicates the films are polycrystalline, possessing the cubic crystal structure with preferred growth orientation along the (111) plane.

Igwebuike and Okoli (2017) studied the optical, electrical and structural properties of zinc selenide films grown by electrodeposition technique. The deposition was carried out at room temperature at different time intervals ranging from 1 min to 5 mins at one step interval. Optical measurements reveal a low absorbance and reflectance values for the films in the visible region. However, the films were reported to be highly transparent in the visible region with maximum transparency of about 90%. Electrical studies show the films have high sheet resistivity with a corresponding low electrical conductivity.

Park *et al*., (2005) reported the effect of photoluminescence intensity of Eu-doped Y_2O_3 nanocrystals. Nanoparticles which comprises Y_2O_3: Eu (at 15, 20, 25 wt.%) were synthesized by the liquid-phase reaction technique and the luminescence characteristics of the nanocrystals were studied according to the amount of doped europium. Some of the synthesized nanocrystals (15, 25 at wt.%) were annealed in air at 500 ^oC while the remaining (20 at wt%) were annealed in oxygen also at 500 ^oC. Results indicated that the particle size and luminescence intensity of the synthesized nanocrystals annealed at 500 ^oC in air depended on the concentration of europium. These nanocrystals were compared with Y_2O_3:Eu (20 wt.%) annealed in oxygen at 500 ^oC. Analysis showed that the nanocrystal annealed in oxygen showed a better luminescence characteristic and crystalline orientation. Hence, it was concluded that with these annealing conditions, the crystallinity and luminescence characteristic of the Y_2O_3:Eu nanocrystals were improved.

Paritosh *et al*., (2007) studied the synthesis of single crystalline europium-doped zinc oxide (ZnO) nanowires using vapour deposition method under a controlled oxidative atmosphere. It was observed that when compared with the un-doped counterpart, the lattice parameters were increased by europium doping because of the bigger size of Eu^{3+} cations. XRD studies reveals that the nanowires are single crystalline with ± (0001) growth direction. The concentration of Eu^{3+} in the nanowires was below 1 atomic %, and such a small amount of the dopant (Eu^{3+}) concentration is useful for studying their optical absorption and emission properties.

Atsuya *et al*., (2008) reported the synthesis of europium-doped yttrium hydroxide ($Y(OH)_3$:Eu) and yttrium oxide (Y_2O_3:Eu) nanosheets using the sol-gel technique and hydrothermal reactions. XRD patterns indicated that the product was purely hexagonal phase $Y(OH)_3$. Transmission electron microscopy (TEM) images revealed that the nanosheets are square shaped (1 x 1 μm^2) having thickness of several tens of nanometers. In conclusion, the prepared $Y(OH)_3$:Eu and Y_2O_3:Eu nanosheet phosphors were found to exhibit a relatively high photoluminescence (PL) intensity.

Yadev *et al*., (2009) reported the optical properties of Europium-doped bunches of ZnO nanowires synthesized by co-precipitation method. The synthesized nanowires have diameter between 60 nm and 100 nm and length up to several microns. Photoluminescence study revealed a wide band emission from europium doped bunches of ZnO nanowires. The wide band is as result of the presence of emission peaks at 520 nm, 550 nm, 580 nm, 620 nm and 650 nm. The photoluminescence intensity decreases with increasing annealing temperature. The generation of green emission is associated with recombination of delocalized electrons at singly occupied oxygen vacancies with deep trapped holes in ZnO and red emission is due to

europium ion transitions by single wavelength light excitation at 325 nm in europium doped bunches of ZnO nanowires.

Dongsheng *et al*., (2010) reported the structure and luminescence evolution of annealed europium-doped silicon oxides films. The concentration of europium (Eu) was varied from 2.1% to 4.7%. The doped films were deposited on P-type (100) silicon substrates at 300 ^{o}C by electron beam evaporation (EBE). In this study, the photoluminescence (PL) intensity of the samples decreases with annealing temperatures from 400 °C to 800 °C, and then increases greatly at higher temperatures. It was suggested further that the photoluminescence (PL) intensity of the samples annealed at temperatures higher than 800 °C can be further enhanced by increasing the annealing duration. Transmission electron microscopy (TEM) images indicated that nano-size clusters were formed when the samples were annealed above 800 °C.

Luo *et al*., (2010) focused on enhanced ultraviolet lasing from europium-doped zinc oxide nanocrystals. Zinc oxide (ZnO) and europium-doped zinc oxide (ZnO:Eu) nanocrystals were prepared using the sol–gel technique. The effects of europium (Eu) as doping element on the morphology, crystal structure, surface chemical composition, and optical properties were investigated by scanning electron microscopy (SEM), X-ray diffraction (XRD), X-ray photoelectron spectra (XPS) and photoluminescence (PL) spectra, respectively. The effect of Eu doping on the optical properties of ZnO nanoparticles was also investigated by measuring the photoluminescence (PL) spectra under different excitation power. Scanning electron microscopy (SEM) analysis indicated that all the samples are polycrystalline, and the nanoparticles of the Eu-doped ZnO are smaller than that of the un-doped ZnO. X-ray diffraction (XRD) showed that the grown nanocrystals all had a hexagonal wurtzite structure. The results suggest that Eu-doped ZnO nanocrystals are very promising UV lasing materials.

Putut *et al*., (2012) prepared europium-doped gallium oxide thin films (Ga_2O_3:Eu) by homemade direct current (DC) magnetron sputtering with varying concentrations of Europium (2% and 5%) respectively. The films were grown on Si (100) substrates. The deposition temperature, plasma power, argon pressure, oxygen pressure, and deposition time were set at 600 °C, 40 W, 600 mTorr, 100 mTorr, and 3 hr, respectively. Scanning electron microscopy (SEM) images reveals that the morphology of Ga_2O_3:Eu thin film indicates a granulated nano-size configuration. UV-visible spectrophotometer results indicated that the variation of Eu doping concentration had no significant change on the optical band gap of the grown films. Photoluminescence emissions of all samples were observed in the red area with the emission peak between 593 nm and 602 nm. The grown Ga_2O_3:Eu thin film was noted to have a granulated configuration with a single orientation. Therefore, Ga_2O_3:Eu thin film has a low degree of magnetic anisotropy but a high magnetic permeability degree. Based on this characteristics, Ga_2O_3:Eu film can be viewed to be suitable for thin-film electroluminescence (TFEL) device application.

Lupan *et al*., (2013) studied Eu-doped ZnO nanowire arrays grown by electrodeposition under low temperature and at atmospheric pressure. XRD measurement indicated that Zn was substituted by Eu in the crystal lattice. Eu doping was quite uniform along the nanowires. High-resolution transmission electron microscopy (TEM) studies indicated a (0 0 0 1) growth direction along the c-axis of the hexagonal ZnO and the associated selected electron diffraction showed the single crystal structure without noticeable defects in the ZnO:Eu nanowires. SIMS and XPS studies indicated that only cationic Eu species were detected suggesting the incorporation of Eu into the ZnO lattice. Direct resonant excitation of Eu in the material led to the sharp red emission at around 612 nm due to $^5D_0$–$^7F_2$ transition of the Eu^{3+}

ion, hence, Eu-doped ZnO nanowires could pave the way for efficient, multispectral LEDs and optical devices.

Ivashchenko *et al*., (2017) deposited pure and Eu-doped zinc selenide films by the close-spaced vacuum sublimation (CSVS) method at substrate temperatures of 100 ^{o}C (373 K), 200 ^{o}C (473 K) and 300 ^{o}C (573 K) respectively. The optical properties of the pure and doped films were studied and their analysis revealed that the doped films show high transmittance values (80% - 90%) than the pure films (55 % - 65 %). It was established that the band gap energy increases with temperature. A band gap energy in the range of 2.63 eV - 2.69 eV for the pure ZnSe films while that of the Eu-doped ZnSe is within the range of 2.77 eV - 2.81 eV was reported. Fourier-transformed infra-red (FTIR) analysis conducted on the films indicated that the films grown are all crystalline.

Kumar *et al*., (2018) reports the optical, electrical and structural properties of ZnSe films doped with Europium grown electrochemically. Optical studies indicated that the doped films possess higher band gap energy than the un-doped films. Structural study from XRD analysis revealed the films were polycrystalline and possess the hexagonal structure with preferential orientation along the (101) plane. The formation of different phases of the films attributed to the growth conditions such as the pH of the growth solution and the complexing agent was reported.

2.12 Gap in literature

This research focused on the deposition of zinc selenide (ZnSe), europium-doped zinc selenide (ZnSe:Eu), europium-doped cadmium selenide (CdSe:Eu) and europium-doped magnesium selenide (MgSe:Eu) using electrostatic spray pyrolysis technique. In available literatures, a number of researches on the growth of ZnSe films with different deposition

technologies exist. Very few reports on ZnSe:Eu and CdSe:Eu exist in previous literatures. In the case of MgSe:Eu films, to the best of my knowledge, I have not come across any research either in electronic or in print on the deposition of MgSe:Eu films.

In this research, ZnSe, ZnSe:Eu, CdSe:Eu and MgSe:Eu films were deposited for the first time using electrostatic spray pyrolysis. The temperature range considered for growing all the films using electrostatic spray pyrolysis is novel.

In the case of ZnSe, the variation in the volume of precursor solution has not been previously reported. Also, the optical properties based on variation of flow-rate of precursor solution are missing in previous literatures.

As regards ZnSe:Eu, the deposition technique used for growing the films is novel. The temperature range, variation in flow-rate of precursor solution and dopant concentrations considered to explain the optical, structural and morphological properties are novel.

For CdSe:Eu films, the deposition technique, the temperature range and other variations considered are all novel. No previous literature has reported a detailed analysis of the optical and structural properties of CdSe:Eu films.

In the case of MgSe:Eu films, few literatures on pure MgSe films can be found in the literature. However, the study of the optical, structural and morphological properties of MgSe:Eu films reported in this research is novel.

CHAPTER THREE

MATERIALS AND METHODS

3.1 Materials

The materials for the deposition process of all the doped and un-doped semiconductor films include a number of 50 ml and 100 ml beakers, syringes, a measuring cylinder, microscopic glass slides, an electronic compact digital weighing balance and a magnetic stirrer hot plate. Others include spray pyrolysis deposition chamber, distilled water and a number of chemicals. All the proposed chemicals used for the deposition process are analytical grade (AR), 99.9% purity. Europium trioxide (Eu_2O_3) was obtained from Sigma Aldrich Company, Germany through Bristol Scientific Company Limited, Lagos-Nigeria. Zinc acetate dehydrate {$Zn(CH_3COO)_2.2H_2O$}, magnesium acetate tetrahydrate {$Mg(CH_3COO)_2.4H_2O$}, nitric acid (HNO_3) and ethanol (C_2H_5OH) were obtained from JHD chemicals, China. Selenium dioxide (SeO_2) and cadmium acetate dehydrate {$Cd(CH_3COO)_2.2H_2O$} were obtained from Loba Chemie chemicals in China and India respectively.

During the deposition process, Eu_2O_3 and SeO_2 served as the sources of europium ion (Eu^{3+}) and selenium ion (Se^{2-}) respectively. {$Zn(CH_3COO)_2.2H_2O$} served as the source of zinc ion while {$Mg(CH_3COO)_2.4H_2O$} and {$Cd(CH_3COO)_2.2H_2O$} served as the sources of magnesium ion and cadmium ion respectively. Hydrochloric acid (HCl) was added as a complexing agent, nitric acid was used to dissolve the europium trioxide salt while absolute ethanol served as the solvent for the other salts.

3.2 Instrumentation

The equipment used for the deposition of films in this research is based on electrostatic spray deposition technique. It comprises an enclosed chamber where the actual deposition takes

place. The enclosed chamber has a hot plate embedded in it where the substrate is placed. The syringe needle which served as the nozzle was connected to a syringe pump outside the deposition chamber. The hot plate was connected to an external digital heater which was used to vary the temperature of the substrate. The heater is capable of measuring temperature up to 480 ^{o}C. A chromel-nickel thermocouple was connected to the hot plate; which helps to give the actual temperature reading of the substrate. The entire deposition unit is connected to an exhaust pipe which releases the toxic gases into the atmosphere. The mechanism involved in this process is that a wire is connected to the tip of the needle (nozzle), the voltage switch is turned on and the films are deposited on the substrate with the aid of the voltage source. Depositing films through this method is very effective as small and fine droplets of film can be deposited without much stress. The spray pyrolysis unit used for the deposition process in this research is shown in figure 3.1.

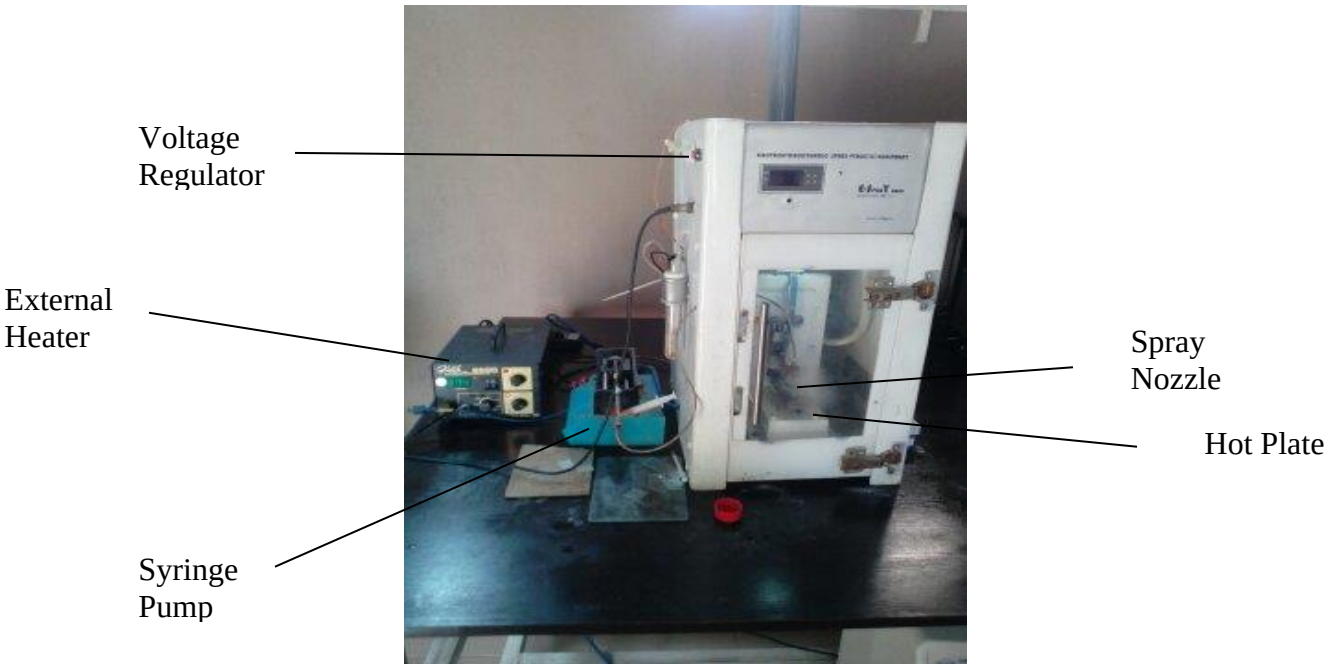

Figure 3.1: Electrostatic spray pyrolysis deposition unit

3.3 Preparation of bulk/stock solutions

The required solutions were prepared using the required solvents. All the preparations were carried out at room temperature.

Prior to the preparation, the salts were weighed using an electronic compact digital weighing balance. This is necessary in order to ascertain their respective masses in grams needed to form the respective solutions. The preparation and required masses of europium trioxide, zinc acetate dehydrate, cadmium acetate dehydrate, magnesium acetate dehydrate and selenium dioxide are found in appendixes E1 to E5 respectively.

3.4 Surface preparation of glass slides/substrates

A clean surface that contains no dirt or unwanted particles is particularly required for the deposition process of any semiconducting film. This has become a necessary step to take due to the fact that the nature and surface of the substrate tend to have adverse effect on the properties of the deposited films. It is therefore of great importance that prior to the deposition of any semiconducting thin film on a substrate, the substrate should be washed thoroughly to remove any unwanted substance from it (Jeroh, 2012).

All the glass substrates used in this research were ultrasonically cleaned with the aid of a sonicator containing an ultrasonic bath. The model number of the sonicator is KOOCU-388. To form the ultrasonic bath, 2.88 g of sodium lauryl sulphate was dissolved in 200 ml of pure laboratory distilled water forming a 0.05 M solution. The salt (sodium lauryl) dissolved completely. The glass slides which served as substrate for this research were agitated in the ultrasonic bath for approximately six (6) minutes (a complete cycle) after which they were removed and kept for two hours in a clean glass jar containing pure laboratory distilled water. The glass substrates were later removed from the distilled water and placed in a soxhlet

apparatus containing methanol which was employed for refluxing the cleaned substrate. The apparatus was filled with methanol and heated to its boiling point. The glass slides rinsed in distilled water were carefully placed inside the apparatus and refluxing was performed through five cycles. Each cycle of refluxing lasted for about seven minutes. After the process of refluxing, the glass substrates were removed from the soxhlet apparatus and dried with an air blower at room temperature. After drying, they were placed in an air-tight clean glass jar to avoid contamination. The reason for refluxing was to ensure that the glass substrates were properly cleaned and devoid of dirt prior to deposition. The dimension of the microscopic glass slides which served as the substrate in this work is 76 mm x 26 mm x 1 mm.

3.5 Choice of stabilizing agent

A stabilizing agent is used to stabilize the rate of reaction between different chemical compounds. Normally in spray pyrolysis deposition technique, the reaction is expected to occur on the surface of the hot glass substrate. Here, the reacting compounds undergo a pyrolytic decomposition on the substrate surface.

However, in the course of this research, it was observed that a mixture of zinc acetate and selenium dioxide reacted immediately they were mixed together in a beaker. The same effect was observed when magnesium acetate and cadmium acetate were mixed separately with selenium dioxide. It was therefore necessary to stabilize the reaction using a stabilizing agent. Different stabilizing agents such as citric acid, acetic acid and triethanolamine (TEA) were used but did not result in the formation of good films. Finally, concentrated hydrochloric acid (HCl) was used because it is volatile at the decomposition temperature and produced good and adherent films.

3.6 Experimental procedure

Experimental procedure entails the description of the method employed in the deposition process. The experimental procedure for each of the compounds will be explained in the subsections that follow.

3.6.1 Experimental procedure of ZnSe films (0% doping)

A mixture of 3 ml of 0.4 M solution of zinc acetate, 0.6 ml of concentrated hydrochloric acid (HCl) and 3 ml of 0.4 M of selenium dioxide were measured into the solution chamber of the expermimental setup and stirred for about 30 seconds. The solution chamber of the spray pyrolysis setup was connected to the spray nozzle. The precursor solution was sprayed onto the heated glass substrates via a syringe pump at a steady flow rate of 400 μL/spray. The nozzle to substrate distance was optimized at 5.67 mm, applied voltage was optimized at 3.5 kV, while temperature was varied between 300 ^{o}C and 400 ^{o}C at intervals of 25 ^{o}C . This range of temperature was preferred because after series of trials, it was observed that good films were obtainable as from 300 ^{o}C. Before each spray, the tube carrying the spray solution to the nozzle is flushed with fresh ethanol to avoid contamination of the solution. After variation of temperature, volume of spray solution was varied at 400 μL/spray, 480 μL/spray, 560 μL/spray, 640 μL/spray and 720 μL/spray respectively while the temperature of the substrate was kept constant at 350 ^{o}C.

3.6.2 Experimental procedure for ZnSe:Eu films

2.7 ml of 0.4 M of zinc acetate was measured into a beaker while 0.5 ml of HCl was measured and added. 3 ml of selenium dioxide was also added to the solution. The overall mixture was stirred to allow for homogeneity of the solution. Next, 0.3 ml of Eu_2O_3 (representing 10%

volume doping concentration due to the fact that the overall volume of the source of zinc ion is 3 ml) was added to the mixture and stirred continuously for 2 mins. Thereafter, the solution was fed into the solution chamber and eventually sprayed on the hot glass substrate by electrostatic spray pyrolysis deposition technique at a deposition temperature of 375 ^{o}C and constant flow rate of 400 μL/spray. This process was repeated for doping concentrations of 15%, 20%, 25% and 30% respectively. Applying similar experimental technique, volume of spray solution was varied at 400 μL/spray, 480 μL/spray, 560 μL/spray, 640 μL/spray and 720 μL/spray while keeping temperature and dopant concentration constant at 375 ^{o}C and 20% respectively. Also while keeping volume of spray solution and doping concentration constant at 400 μL/spray and 10% respectively, temperature was varied between 300 ^{o}C and 400 ^{o}C at 25 ^{o}C intervals. Throughout the entire experimental procedure, applied voltage and nozzle-substrate distance were optimized at 3.5 kV and 5.67 mm respectively.

3.6.3 Experimental procedure for CdSe:Eu films

The initial spray solution of CdSe:Eu comprises 2.55 ml of cadmium acetate dehydrate, 0.4 ml of HCl (for stabilizing the solution) and 3 ml of selenium dioxide. Europium trioxide (15% volume concentration due to the fact that the overall volume of the source of cadmium ion is 3 ml) which served as the dopant was added to the spray solution. The resulting solution was sprayed onto a hot glass substrate using electrostatic assisted aerosol deposition technique. The flow rate was kept constant at 400 μL/spray. The CdSe:Eu films were sprayed for 10 mins at a deposition temperature of 300 ^{o}C with an applied voltage of 7 kV. The nozzle-substrate distance was optimized at 7.98 mm. Different parameters were varied throughout the entire experimental process. At a constant flow rate of 2400 μL/hr, volume of spray solution at 400 μL/spray, doping percentage of 15% and optimized nozzle-substrate distance of 7.98

mm, temperature was varied between 300 ^{o}C and 380 ^{o}C at intervals of 20 ^{o}C respectively. In likewise manner, volume of spray solution was varied at 400 μL/spray, 480 μL/spray, 560 μL/spray, 640 μL/spray and 720 μL/spray while other parameters were kept constant. Also keeping other parameters constant, doping concentration was varied between 10% and 30% at intervals of 5%.

3.6.4. Experimental procedure for MgSe:Eu films

1.8 ml of magnesium acetate was measured and put into the precursor solution chamber. 6 ml of selenium dioxide was added to the spray solution and mixed continuously with the aid of a magnetic stirrer hot plate. Thereafter, 0.2 ml of europium trioxide (dopant) representing 10% volume concentration of dopant (the overall volume of the source of magnesium ion is 2 ml) was added to the spray solution and agitated for ten minutes before being sprayed onto the hot glass substrate at substrate temperature of 350 ^{o}C, while the volume of spray solution was maintained at 400 μL/spray. This process was repeated at different substrate temperatures of 300 ^{o}C, 325 ^{o}C, 375 ^{o}C and 400 ^{o}C, while the volume of spray solution and dopant concentration were kept constant at 400 μL/spray and 10% respectively.

The process described in the above paragraph was also used in varying the volume of spray solution of the films. Volume of spray solution was varied between 400 μL/spray and 720 μL/spray while keeping temperature and dopant concentration constant at 350 ^{o}C and 20% respectively.

For the variation of dopant concentration, substrate temperature and volume of spray solution were kept constant at 350 ^{o}C and 400 μL/spray respectively while dopant concentration was varied between 10% and 50% at a step of 10% apart. The voltage and nozzle-substrate

distance throughout the entire deposition process were optimized at 5.5 kV and 5.82 mm respectively.

3.7. Preserving the substrate containing the deposited films

After successfully depositing the required films on the glass substrates, they were allowed to cool before they were removed from the surface of the hot plate. This was done so as to avoid cracking of the hot substrates. After removing the substrates from the top of the hot plate, they were allowed to cool down to room temperature and further placed in petri dishes and slide box to avoid the slides from coming in contact with dirt and unwanted materials.

3.8 Characterization techniques for all deposited films

In this research, different techniques were employed to obtain the thickness, optical properties, surface morphologies, structural properties and elemental compositions of all the films under study. After characterization of the respective films, they were then analysed and studied for their respective applications.

3.8.1 Surface profile analysis

The thickness of all the films under study was obtained by surface profile analysis with the aid of a surface profiler (Model: Veeco Dektak 150) located at Sheda Science and Technology Complex (SHESTCO), Abuja. The sample was placed on a sample stage and a diamond tip stylus was lowered on to the sample. The marking tip was used to scratch off a portion of the sample on the substrate. The tip of the stylus makes a soft touch down on the sample and runs along the sample surface and down to the substrate. The drop off the sample surface on to the substrate helps to determine the thickness of the film grown on the substrate which is displayed on a computer monitor attached to the surface profiler.

3.8.2 Optical studies

The absorption measurement of all the deposited films were obtained in the electromagnetic spectrum between 200 nm and 800 nm with the aid of a Cary ultraviolet visible (UV-VIS) spectrophotometer located at the Department of Chemical Engineering, Ahmadu Bello University (ABU), Zaria. In each case, to obtain the absorbance of the films, the glass substrate containing the respective films was mounted on a sample stage of the UV-VIS spectrophotometer. Light from a source was passed through the sample. The UV-VIS spectrophotometer was connected to a computer monitor. As the sample interacts with light, the portion of absorbed radiation was displayed on the computer monitor, thus revealing the absorbance values of the film. The transmission values of all the deposited films were calculated from absorption values using equation 2.1.

The reflectance values for all the deposited films were calculated from equation 2.7.

The absorption coefficient of all the deposited films at different substrate temperatures was calculated using equation 2.12.

In this research, the refractive index of all the films was calculated from equation 2.13.

The optical conductivity of all the films was calculated using equation 3.1.

$$\sigma = \frac{\alpha n c}{4\pi} \tag{3.1}$$

where, α is absorption coefficient of the material, n is the refractive index of the material, c is speed of light while π is a constant.

The extinction coefficient of all the deposited films was calculated using the expression:

$$k = \alpha \lambda / 4\pi \tag{3.2}$$

where α is the absorption coefficient of the material, λ is the wavelength and π is a constant.

The dielectric function of all the films under study was calculated from the expression:

$$\varepsilon_T = \varepsilon_1 + \varepsilon_2 \quad (3.3)$$

where ε_1 is used to represent the real part while ε_2 represents the imaginary part respectively and they are given by the relation:

$$\varepsilon_1 = n^2 - k^2 \quad (3.4a)$$

$$\varepsilon_2 = 2nk \quad (3.4b)$$

where n is refractive index and k is extinction coefficients of the films.

The direct band gap of all the films at different substrate temperatures was calculated from equation 2.15.

3.8.3 Surface morphology and elemental composition

The surface morphology of all the films under study was obtained using a Leo-Zeiss scanning electron microscope while the elemental (chemical) composition of the films was determined by energy dispersive x-ray spectroscope attached to the scanning electron microscope. The scanning electron microscope (SEM) which was used for imaging the films under study consists of an electron column, a sample chamber and a thermal emission source. The overall SEM equipment is connected to a computer monitor. In each case of characterization, the sample was mounted on the sample chamber. High-energy incident electrons were generated in the electron column and are made to interact with the sample under study. As the incident electrons strike the sample, the samples undergo scanning by the electron microscope wherein surface imaging of the film and the chemical composition of the film were generated and displayed on a computer monitor. This information was further used for the analysis of the films under study in this research.

3.8.4 Structural studies

The XRD patterns of all the films in this research were recorded using a SmartLab X-ray diffractometer. The glass substrate containing the sample was mounted on a sample stage in the x-ray diffractometer and scanned between 0^o and 80^o with operating voltage and current of 45 kV and 200 mA respectively with Cu-kα1 radiation and wavelength, λ set at 1.540593Å. The x-ray diffractometer was connected to a computer monitor. As the films were being scanned, the diffraction patterns were recorded and displayed on the computer monitor.

For an effective understanding of the diffractogram, structural parameters such as the grain size, inter-planar distance, strain, lattice constant, dislocation density and number of crystallites per unit area have been calculated and presented in appendixes A15 and A16.

The grain size, D, was calculated from the Debye-Scherer expression (Gnanamuthu *et al*., 2015):

$$D = \frac{0.94\lambda}{\beta\cos\theta} \tag{3.5}$$

where λ is the diffraction wavelength given by 1.540593Å, β is the Full Width at Half Maximum (FWHM) while θ is the Bragg's diffraction angle.

The inter-planar distance, d, was calculated from the expression (Kissinger, 2007):

$$d = \frac{\lambda}{2\sin\theta} \tag{3.6}$$

The strain, ε, was calculated from the expression (Muthumari *et al*., 2012):

$$\varepsilon = \frac{\beta\mathrm{Cos}\theta}{4} \tag{3.7}$$

The dislocation density, δ, was calculated from the mathematical expression (Dawood *et al*., 2014):

$$\delta = \frac{1}{D^2} \tag{3.8}$$

where D is the grain size.

The lattice constant for the hexagonal phase of ZnSe was calculated from the relation (Mote *et al*., 2013):

$$\frac{1}{d^2} = \frac{4}{3a^2}\ (h^2 + hk + k^2) + \frac{l^2}{c^2} \tag{3.9}$$

where a is lattice constant, d is the inter-planar spacing and hkl represents the miller indices.

The number of crystallites per unit area was calculated using the relation (Aly *et al*., 2015):

$$N = \frac{t}{D^3} \tag{3.10}$$

Where t, is the thickness of the ZnSe film and D is the crystallite size corresponding to each plane.

CHAPTER FOUR

RESULTS AND DISCUSSIONS

4.1 Thickness variation of pure ZnSe

The varying thickness obtained for the ZnSe films at different substrate temperature and different flow rate are shown in tables 4.1a and 4.1b respectively.

Table 4.1a: Thickness variation of pure ZnSe films with temperature

Temperature (ºC)	Thickness (nm)
300	100
325	105
350	138
375	200
400	150

Table 4.1b: Thickness variation of pure ZnSe films with flow rate

Flow Rate (µL/spray)	Thickness (nm)
400	138
480	183
560	210
640	150
720	110

From table 4.1a, the thickness of the ZnSe films increases with increase in substrate temperature up to 375 ^{o}C and thereafter decreased at 400 ^{o}C. This sudden decrease of film thickness at higher substrate temperature may be as a result of reduced transfer of precursor to the substrate. This can be attributed to gas convection emanating from the chamber, hence pushing the droplets away from the substrate leading to the development of crystallites within the vapour (Gnanamuthu *et al*., 2015).

From table 4.1b, the thickness of the film increases with flow rate up to 560 μL/spray and thereafter decreases.

4.2 Optical studies of the ZnSe films

4.2.1 Spectra absorption of ZnSe films

The spectra absorption curves of ZnSe films deposited at different substrate temperatures and flow rate at 0% doping are presented in figures 4.1a and 4.1b respectively.

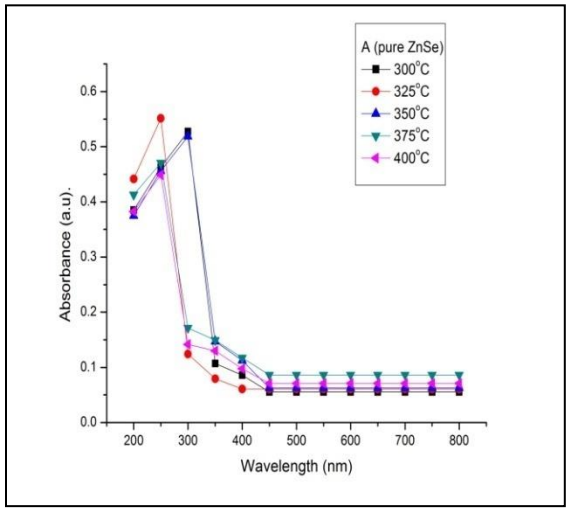

Figure 4.1a: Plot of absorption versus wavelength for ZnSe films deposited at different substrate temperatures

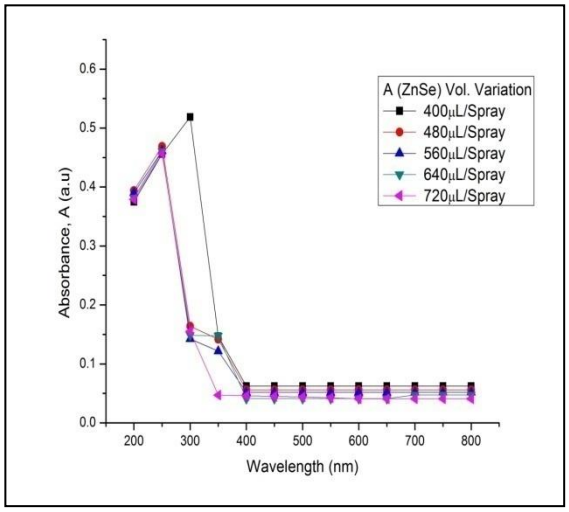

Figure 4.1b: Absorption curves of ZnSe films deposited at different flow rates

From figure 4.1a, all the ZnSe films show very poor absorption of light in the visible region of the electromagnetic spectrum and moderate absorption in the ultraviolet region with the highest absorption of about 55.17% observed for the film deposited at 325 ^{o}C. (Any number can be expressed as a percentage by multiplying that number by 100. Hence, 0.5517 can be expressed as 55.17%).

Figure 4.1b indicates that the ZnSe films deposited at different flow rates exhibited very poor absorption of radiation in the visible region. In the UV region, an absorbance value of about 51.88 % was observed for the film deposited at a flow rate of 400 μL/spray. However, the films deposited at 480 μL/spray, 560 μL/spray, 640 μL/spray and 720 μL/spray exhibited poor absorption within the range of 12.17% to 46.87% in the UV region. The poor absorption exhibited by ZnSe material in the visible region indicates a high transmission in this region. The result agrees with previous report of Okereke and Ekpunobi (2011) for chemical bath deposited ZnSe Films for buffer layers.

Figures 4.1a and 4.1b reveal a sharp decrease in the absorption spectra for all the films below 400 nm which can be attributed to the onset of electronic transitions between the valence and conduction bands occurring at the band edge. This observation is referred to as fundamental absorption. This result follows the same trend as the report of Ozutok *et al*., (2012) for Mn-doped ZnS films and Okereke and Ekpunobi (2011) for chemical bath deposited ZnSe films.

The absorption values (appendixes A1 and A2) for zinc selenide films deposited at different substrate temperatures and flow rates are presented.

4.2.2 Optical transmission spectra of the pure ZnSe films

The optical transmission spectra of the pure zinc selenide films deposited at different substrate temperatures and different flow rates are presented in figures 4.2a and 4.2b respectively.

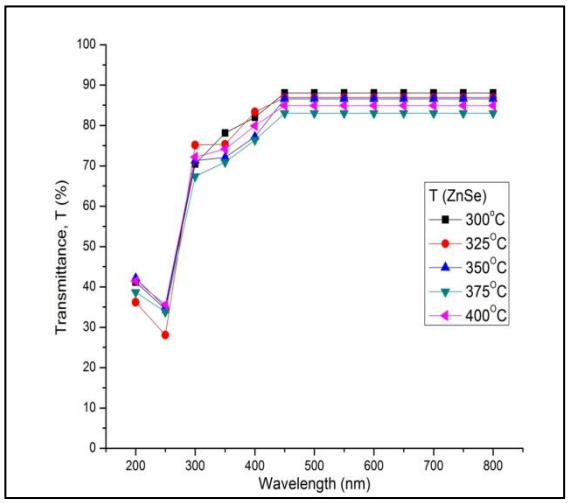

Figure 4.2a: Transmission spectra of ZnSe films deposited at different substrate temperatures

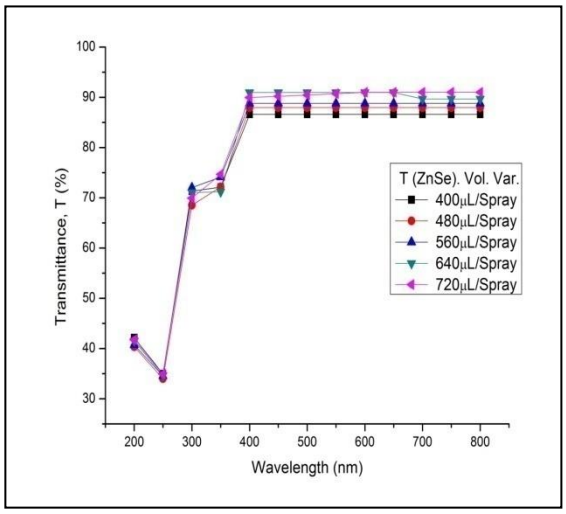

Figure 4.2b: Optical transmission spectra for spray deposited ZnSe films at different flow rates

The transmission of the spray deposited ZnSe films decreases in the visible region as temperature increases from 300 ^{o}C to 375 ^{o}C. Thereafter, the transmission slightly increased in the visible spectrum at 400 ^{o}C. This behaviour may be attributed to the presence of some structural or phase defects in the crystal structure of the films. From figure 4.2a, it is observed that the deposited films exhibited low transmission in the wavelength region of 200 nm to 300 nm. However, in the region of 450 nm to 800 nm, the films show high transmission in the range of 83.04% to 88.06%. Figure 4.2b displays the plot of transmission of pure ZnSe films against wavelength at different flow rates.

A clear observation of figure 4.2b reveals that all the deposited films exhibited high transmission (86.60% to 91.01%) in the visible region with very minimal transmission in the ultraviolet region. The deposited films show some interference pattern around 350 nm and 400 nm. The interference pattern exhibited by the films suggests that the films are specular (smooth) to some extent (Lohar *et al*., 2014) and confirm the films homogeneity (uniformity) (Ivashchenko *et al*., 2017).

In both figures 4.2a and 4.2b, all the deposited ZnSe films show high transmission in the visible region. The high transmission exhibited by the ZnSe films in the entire visible region makes the material very useful in fabricating optoelectronic devices. The results presented in this research are in agreement with the works reported by Kathalingam *et al*., (2007), Murali *et al*., (2008), Meshram and Thombre (2016).

The transmission values at different deposition conditions for un-doped ZnSe films are presented in appendixes A3 and A4 respectively.

4.2.3 Reflection spectra of pure ZnSe films

The reflection spectra for ZnSe deposited at different substrate temperatures and flow rates are presented in figure 4.3a and 4.3b.

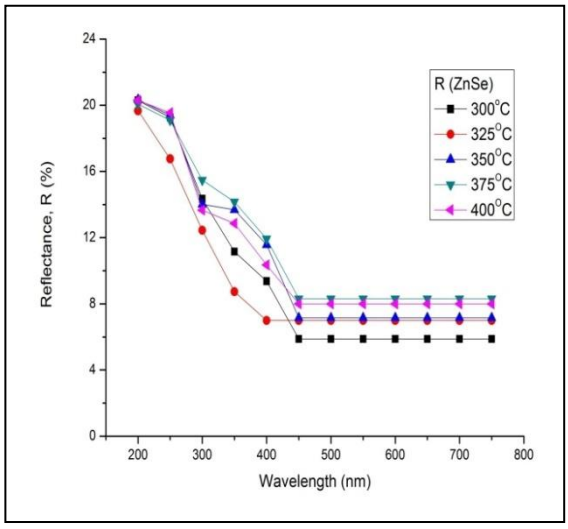

Figure 4.3a: Reflection spectra of ZnSe films deposited at different substrate temperatures

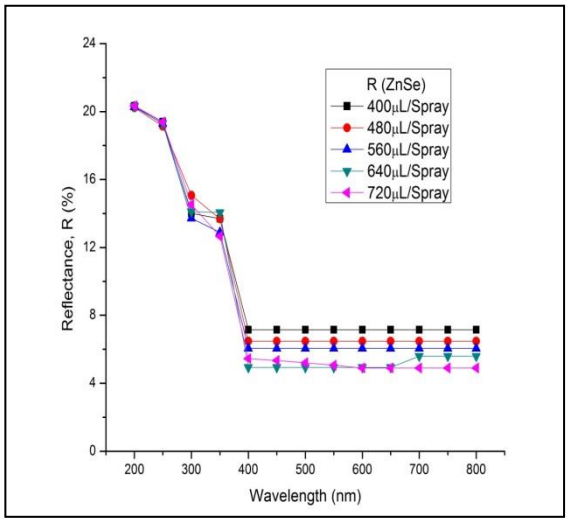

Figure 4.3b: Reflection spectra of ZnSe films deposited at different flow rates

All the ZnSe films prepared at different substrate temperature exhibited poor reflection of light in the UV-VIS region of the electromagnetic spectrum. The reflection of the ZnSe films

has values within the range of 5.88% to 20.33% with the film deposited at 350 ^{o}C recording the highest reflection (20.33%).

The film deposited at a flow rate of 400 μL/spray recorded reflection values in the range of 7.15% to 20.33% while the film deposited at a flow rate of 480 μL/spray show reflection within the range of 6.48% to 20.23%. The films deposited at flow rates of 560 μL/spray, 640 μL/spray and 720 μL/spray had reflection values within the range of 6.05% to 20.26%, 5.59% to 20.30% and 4.9% to 20.32% respectively. A clear observation of figure 4.3b indicates that all the deposited films exhibited poor reflection of light throughout the ultraviolet and visible regions of the electromagnetic spectrum. Lohar *et al*., (2014), Okereke and Ekpunobi (2011), Desai *et al*., (2015) and Islam *et al*., (2014) have also previously reported low reflection values for ZnSe films. The low values of reflection obtained in all cases of deposition at overall spectral ranges indicates their probability of being used as an anti-reflective coating material deployed in high efficiency solar cells (Ivashchenko *et al*., 2017).

The reflection values obtained at different spray conditions are presented (Appendixes A5 and A6).

4.2.4 Refractive index of pure ZnSe films

The refractive index of the pure ZnSe films for different deposition temperatures was plotted against photon energy as shown in figure 4.4.

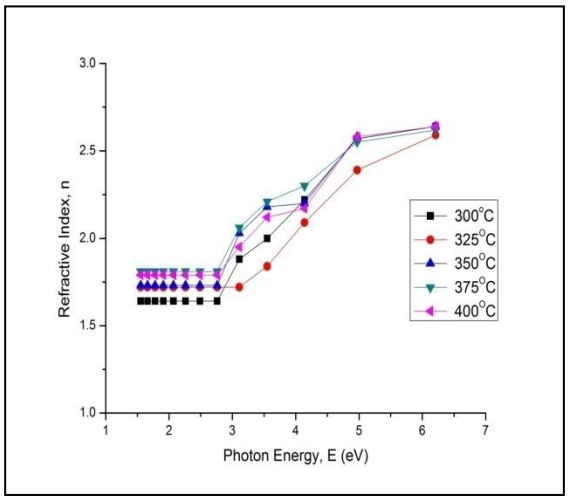

Figure 4.4: Refractive index of ZnSe films obtained at different temperatures

The films deposited at 300 ^{o}C recorded refractive index within the range of 1.64 to 2.64 while the films obtained at 325 ^{o}C have refractive index values between 1.72 and 2.59 respectively. For the films deposited at substrate temperatures of 350 ^{o}C, 375 ^{o}C and 400 ^{o}C, refractive index values are between 1.73 and 2.64, 1.81 and 2.62, 1.79 and 2.64. All the films were however observed to possess high refractive index values. The high refractive index exhibited by ZnSe films suggests that ZnSe films could prove very useful in fabricating optoelectronic devices. The values of the refractive index of ZnSe films obtained at different substrate temperatures are given in appendix A7.

4.2.5 Absorption coefficient of pure ZnSe films

Figure 4.5 is a plot of the absorption coefficient of ZnSe films obtained at different substrate temperatures against photon energy.

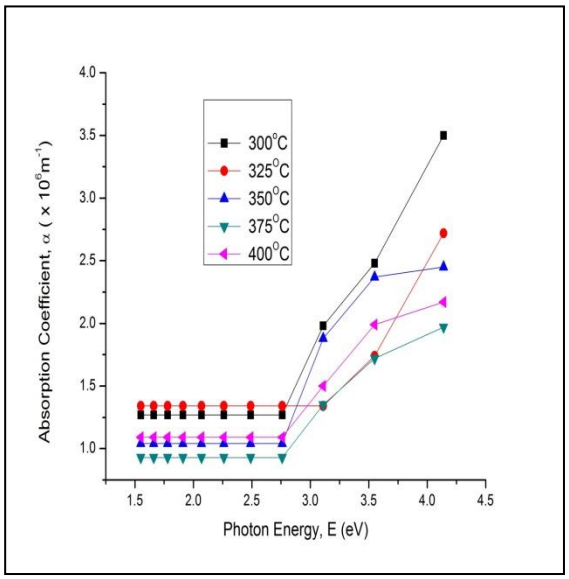

Figure 4.5: Plot of absorption coefficient of ZnSe films versus photon energy at different substrate temperatures

From figure 4.5, a similar trend is observed for all the ZnSe films. An almost constant value is observed at photon energies up to about 2.75 eV and thereafter increases. This behaviour is an indication that the material possesses high absorbance at short wavelengths and low absorbance values at longer wavelengths. The values of absorption coefficient are very large, which is a consequence of the very large density of states in the solid phase (Fox, 2001).

The values of absorption coefficient for ZnSe films at different deposition temperatures are presented in appendix A8.

4.2.6 Optical conductivity of pure ZnSe films

The optical conductivity values for the ZnSe films are plotted against photon energy as depicted in figure 4.6.

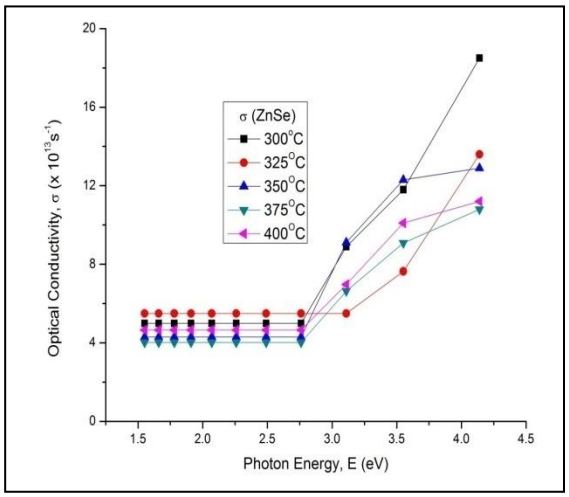

Figure 4.6: Plot of optical conductivity of ZnSe films versus photon energy at different substrate temperatures

From figure 4.6, it is observed that at different substrate temperatures, the optical conductivity for ZnSe films is high and increases sharply at high energies for all the films. Optical conductivity values for ZnSe are presented (appendix A9).

4.2.7 Extinction coefficient of pure ZnSe films

The values of extinction coefficient of the ZnSe films prepared at different substrate temperatures are plotted against photon energy and displayed in figure 4.7.

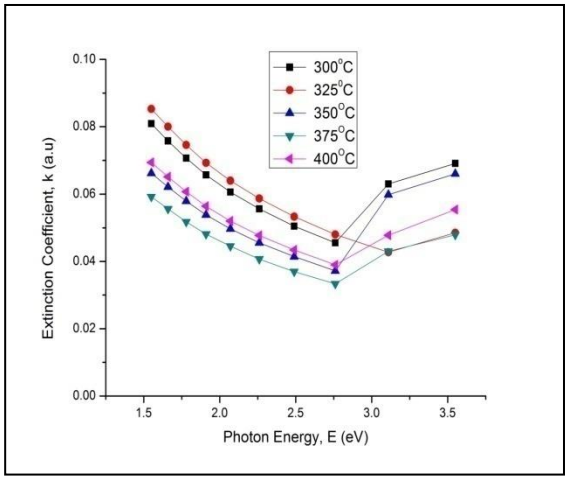

Figure 4.7: Extinction coefficient of ZnSe films at different substrate temperatures plotted against photon energy

In all cases of temperature variations, the extinction coefficient of the ZnSe films are observed to decrease as photon energy increases and slightly increased at energies above 2.5 eV. Such steady increase of extinction coefficient above 2.5 eV has also been previously reported by Howari (2012) and Khairnar *et al*., (2012) for ZnSe films. Appendix A10 contains the extinction coefficient values of ZnSe at different deposition temperatures.

4.2.8 Dielectric constant studies of ZnSe films

The dielectric constant is composed of two parts; the real and imaginary parts respectively. Both parts were calculated and plotted against photon energy for different substrate temperatures as shown in figures 4.8 (a-b).

4.2.8.1 Real part of dielectric constant

Figure 4.8a is a plot of the real dielectric constant against photon energy.

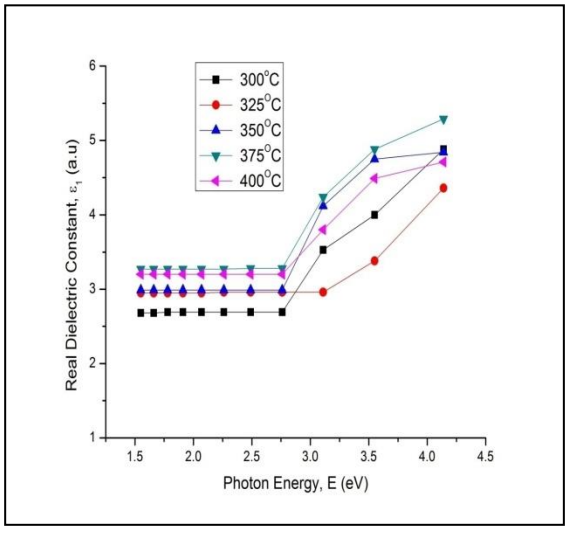

Figure 4.8a: Real dielectric constant plotted against photon energy for ZnSe films at different substrate temperatures

It is observed from figure 4.8a that the real dielectric constant has high values at high photon energies for different substrate temperatures. See appendix A11 for values of real part of dielectric constant of ZnSe films.

4.2.8.2 Imaginary part of dielectric constant of ZnSe films

Figure 4.8b displays the values of imaginary dielectric constant of pure ZnSe films at different substrate temperatures plotted against photon energy.

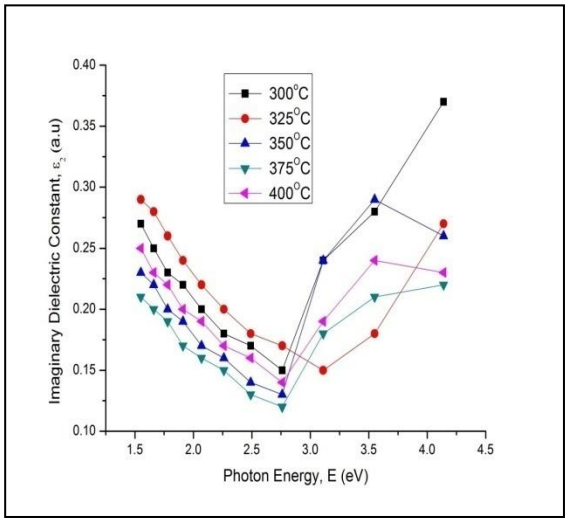

Figure 4.8b: Imaginary dielectric constant plotted against photon energy for ZnSe films at different substrate temperatures

The imaginary dielectric constant decreases steadily with increasing photon energy and thereafter exhibited increment at high photon energies for all the films. Appendix A12 contains the values of imaginary dielectric constant of ZnSe films.

4.2.9 Band gap energy of ZnSe films

Figure 4.9 reveals the plot of $(\alpha h\nu)^2$ versus photon energy for the ZnSe films for different deposition temperatures while the values are presented in appendix A13.

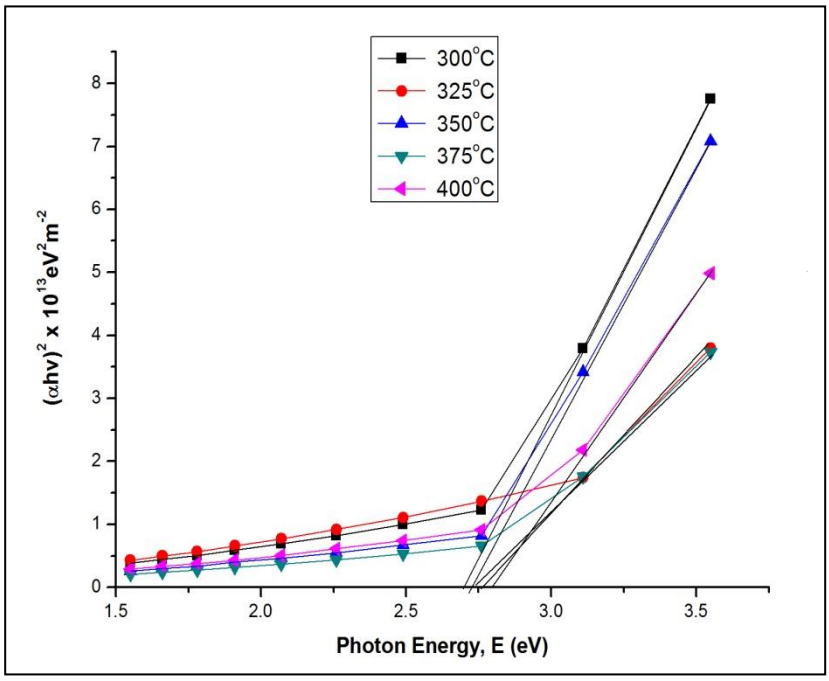

Figure 4.9: Band gap energy of ZnSe films at different substrate temperatures

The direct band gap of the ZnSe films at different temperature were obtained from the plot of $(\alpha h\nu)^2$ versus photon energy and the band gap obtained by extrapolating the linear portion of the curve to the point where $(\alpha h\nu)^2$ equals zero. The band gap was found to vary between 2.65 eV and 2.71 eV for substrate temperature between 300 ^oC and 400 ^oC.

4.3 Structural characteriation of ZnSe

4.3.1 X-ray diffraction (XRD) patterns

The x-ray diffraction pattern for the ZnSe films obtained at 300 ^oC is displayed in figure 4.10a while the diffractogram of ZnSe films at deposition temperature of 350 ^oC is displayed in figure 4.10b.

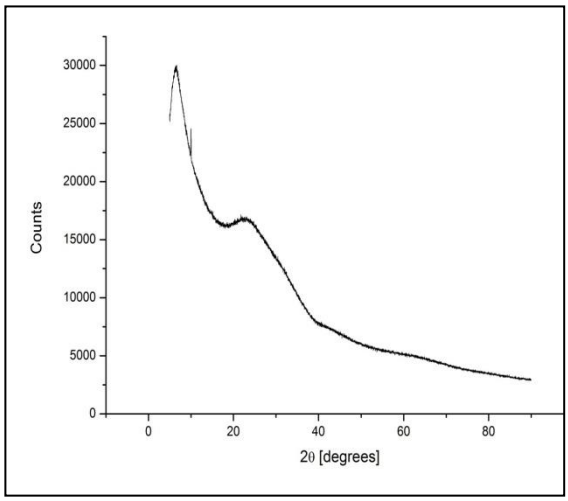

Figure 4.10a: X-ray diffractogram of ZnSe films obtained at 300 ºC

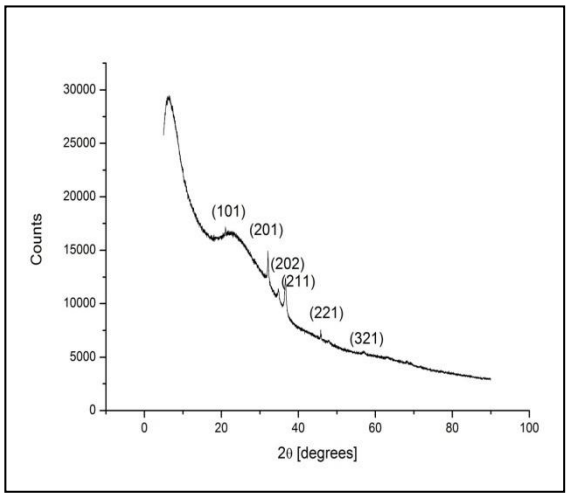

Figure 4.10b: X-ray diffraction pattern for nanocrystalline ZnSe films obtained at 350 ºC

From figure 4.10a, there are no displayed sharp peaks corresponding to reflections from ZnSe crystals. However, broad peaks are obvious in the observed pattern indicating the amorphous nature of the films which can be attributed to the low deposition temperature. At low deposition temperature for ZnSe films, the resulting films were amorphous in nature.

Reflection peaks slightly visible around 2θ values of 21.04º, 45.78º and 57.05º corresponding to diffraction planes of (101), (221) and (321) while slightly sharp reflection peaks with the values of 2θ obtained at 32.06º, 34.77º and 36.50º corresponds to diffraction planes of (201), (202), (211) were observed (figure 4.10b) which are all consistent with the hexagonal phase structure.

The lattice constant for the (201) plane (preferred growth plane) of ZnSe in this research was calculated to be 5.953 Å, which is close to the reported standard value of a = 5.667 Å (JCPDS 5-552).

4.4 Surface morphology of ZnSe film

The surface morphology of the deposited ZnSe film was determined for deposition temperature maintained at 350 ^{o}C, 10 mins and 12 mins deposition time respectively. The surface morphology of the films were obtained by scanning electron microscopy (SEM) technique at different resolutions and are presented in figures 4.11 (a-c).

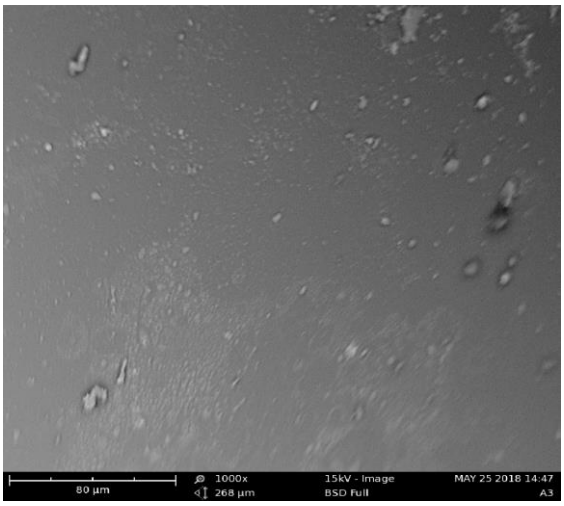

Figure 4.11a: SEM image of ZnSe at 350 ^{o}C (10 mins) at a resolution of 1000x

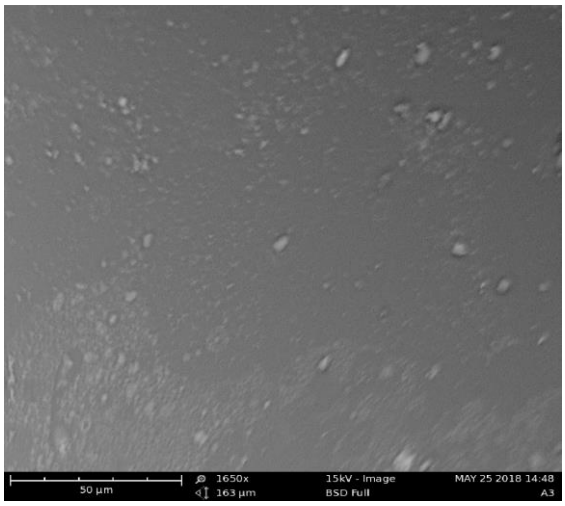

Figure 4.11b: SEM image of ZnSe at 350 ^{o}C (10 mins) at a resolution of 1650x

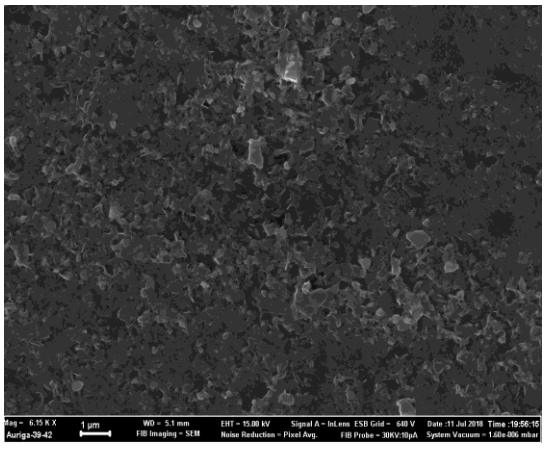

Figure 4.11c: SEM image of ZnSe film at 350 ^{o}C (12 mins) at a resolution of 2150x

In figures 4.11a & b, the SEM images indicate that the films are smooth with some small spots observed on the surface which may be a collection of some smaller grains. Similar observation has been reported by Khan and Bibi (2012), Venkatachalam *et al*., (2007) for ZnSe films. Figure 4.11c indicates the agglomeration of particles which may have resulted from the formation of smaller grains due to increased deposition time.

4.5 Thickness variation of Eu-doped ZnSe

The varying thickness obtained for the ZnSe:Eu films at different substrate temperatures and a constant dopant concentration of 10% is shown in table 4.2a while the thickness obtained at a constant temperature of 350 ^{o}C and varying dopant concentrations are shown in table 4.2b respectively.

Table 4.2a: Thickness variation of Eu-doped ZnSe films with temperature

Temperature (^{o}C)	Thickness (nm)
300	50
325	80
350	100
375	183
400	120

Table 4.2b: Thickness variation of Eu-doped ZnSe films with dopant concentrations

Dopant Concentration (%)	Thickness (nm)
10	183
15	150
20	200
25	220
30	225

From table 4.2a, ZnSe:Eu film thickness increases with temperature and further decreased at 400^{o}C.

From table 4.2b, film thickness decreased as dopant concentration increased from 10% to 15%. However, the thickness of the film increases as dopant concentration increases from 15% to 30%.

4.6 Optical studies of ZnSe:Eu films

4.6.1 Absorption spectra of ZnSe:Eu films

The absorption spectra of the Eu-doped zinc selenide films obtained at different deposition temperatures, flow rates and dopant concentrations are presented in figures 4.12a, 4.12b and 4.12c respectively.

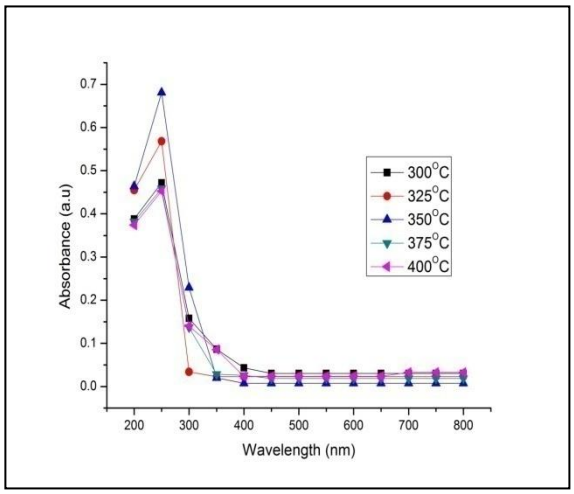

Figure 4.12a: Absorption spectra of Eu-doped ZnSe films at different substrate temperatures

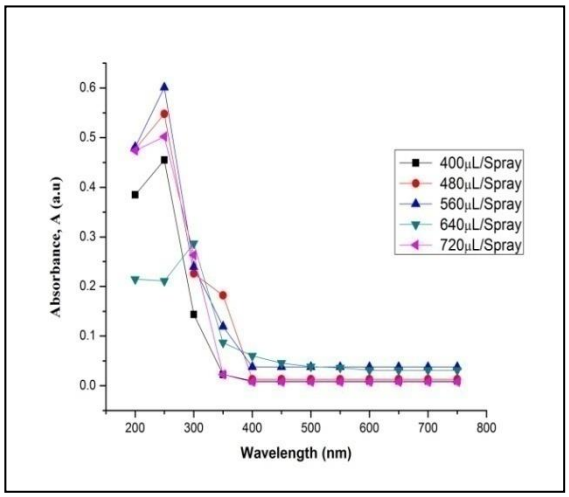

Figure 4.12b: Absorption spectra of Eu-doped ZnSe films at different flow rates

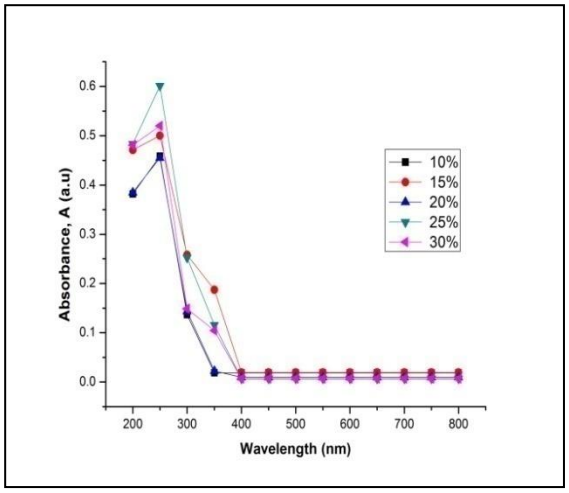

Figure 4.12c: Absorption spectra of Eu-doped ZnSe films at different europium concentrations

From figure 4.12a, the ZnSe:Eu films deposited by varying substrate temperatures exhibited very poor absorption of radiation in the entire visible region of the electromagnetic spectrum. All the absorption curves slightly increases and further decreases sharply at wavelengths below 400 nm. The films are seen to have high absorbance up to 68.12% at 250 nm for film deposited at 350 ^{o}C. The deposited films exhibited peaks at 250 nm. The peaks observed may

be due to the absorption of SeO_2 since selenium is unstable in air and therefore reacts with oxygen in air (Shinde *et al*., 2010; Lohar *et al*., 2014).

From figure 4.12b, the films deposited at different flow rates of 400 μL, 480 μL, 560 μL and 720 μL recorded highest absorbance of 45.5%, 54.8%, 60.1%, and 50.2% in the UV region respectively while the highest absorbance value for the film deposited at a flow rate of 640 μL was about 28.7% in the ultraviolet region. However, all the Eu-doped zinc selenide films deposited with different flow rates exhibited very poor absorption of radiation in the entire visible region of the electromagnetic spectrum.

From figure 4.12c, highest absorbance value of 60.1% was observed for the film deposited at 25% dopant concentration. However, just like the other films deposited by varying temperature and flow rate, the ZnSe:Eu films deposited by varying the dopant concentration also exhibited very poor absorption in the entire visible region of the electromagnetic spectrum.

Appendixes B1, B2 and B3 displays the absorbance values for Eu-doped zinc selenide films for different deposition conditions.

4.6.2 Optical transmission spectra of ZnSe:Eu films

The optical transmission spectra of the Eu-doped zinc selenide films deposited at different substrate temperatures, flow rates and dopant concentrations are presented in figures 4.13a, 4.13b and 4.13c respectively.

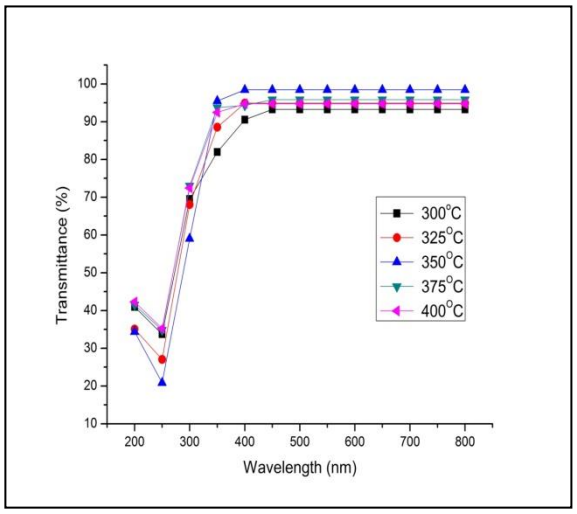

Figure 4.13a: Optical transmission spectra of ZnSe:Eu films at different substrate temperatures

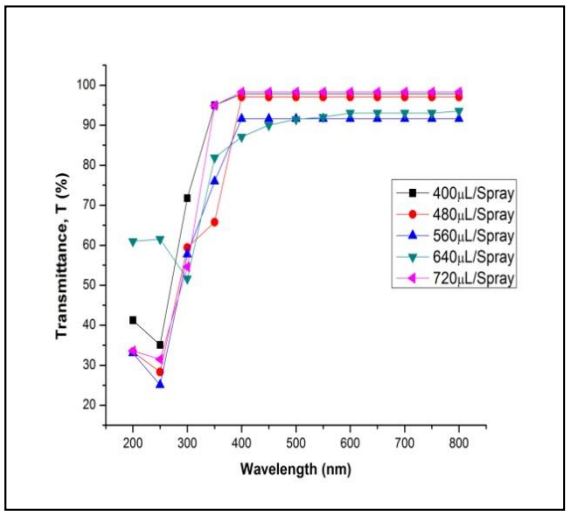

Figure 4.13b: Optical transmission spectra of Eu-doped ZnSe films at different flow rates

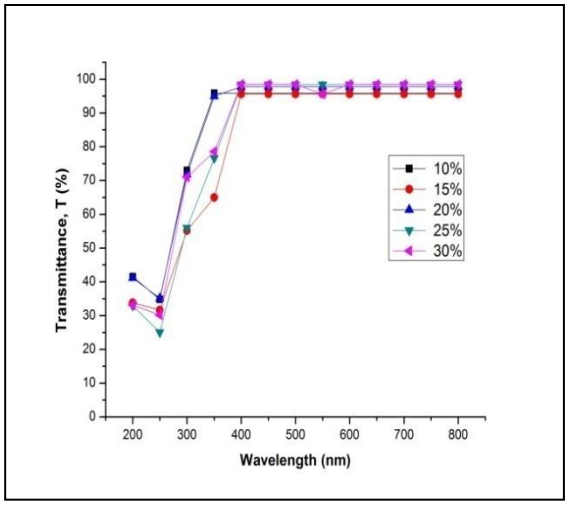

Figure 4.13c: Optical transmission spectra of Eu-doped ZnSe films at different concentrations of dopant

From figure 4.13a, transmission spectra reveal that the transmission of the films was within the range of 59% to 72% in the UV region while the films recorded very high transmission between 91% and 98% in the visible region. The transmission values obtained in this research at different deposition temperatures appear to be slightly higher than the values (80% to 90%)

reported by Ivashchenko *et al*., (2017) for Eu-doped ZnSe films fabricated by close-spaced vacuum sublimation (CSVS) technique. This difference could be due to the different deposition process and growth conditions. However, both results are similar to some extent since by comparison, both results show very high transmittance behaviour for the films in the visible region.

Figure 4.13b reveals that the optical transmission of the ZnSe:Eu films obtained at different flow rates exhibit very high transmission in the visible region. The transmittance is within the range of 87.06% to 98.29% in the wavelength range of 400 nm to 800 nm, with the highest transmittance (98.4%) observed for the film deposited when the flow rate was 720 μL/spray.

From figure 4.13c, the transmission spectra of the films deposited at different dopant concentrations show that ZnSe:Eu films also exhibited very high transmittance within the range of 95.63% to 98.52% in the visible region.

The very high transmission exhibited by all the ZnSe:Eu films at different deposition conditions in the visible region of the electromagnetic spectrum implies that Eu-doped zinc selenide films will be very useful for the fabrication of optical materials for use in lasers, optoelectronic devices, optical lenses, glasses, etc.

The optical transmission values obtained at different deposition conditions for the Eu-doped ZnSe films are presented in appendixes B4, B5 and B6 respectively.

4.6.3 Reflectance spectra of ZnSe:Eu films

The reflection spectra of the Eu-doped zinc selenide films deposited at different substrate temperatures, flow rates and dopant concentrations are presented in figures 4.14 (a-c).

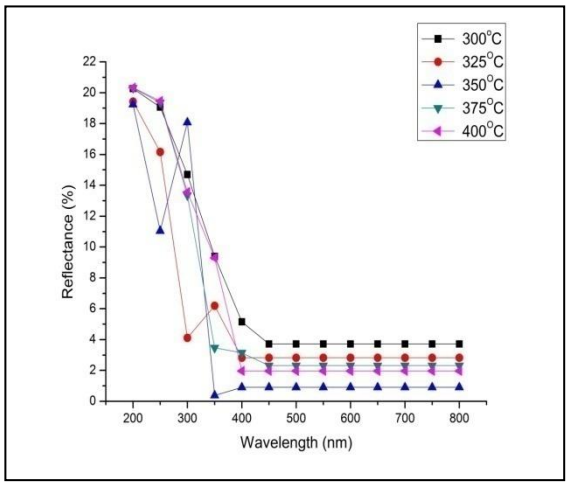

Figure 4.14a: Reflection spectra of spray deposited ZnSe:Eu films at different substrate temperatures

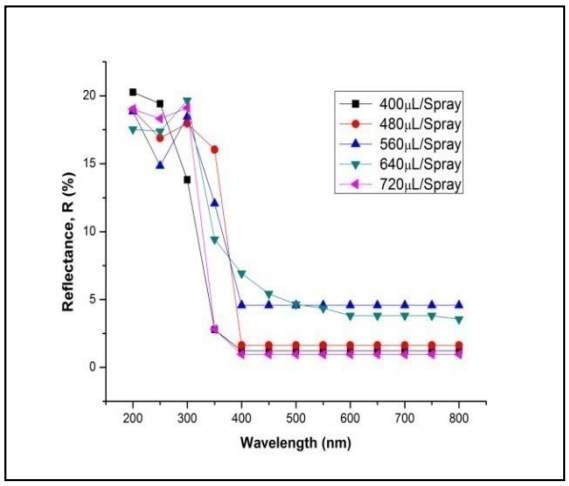

Figure 4.14b: Reflection spectra of spray deposited ZnSe:Eu films at different flow rates

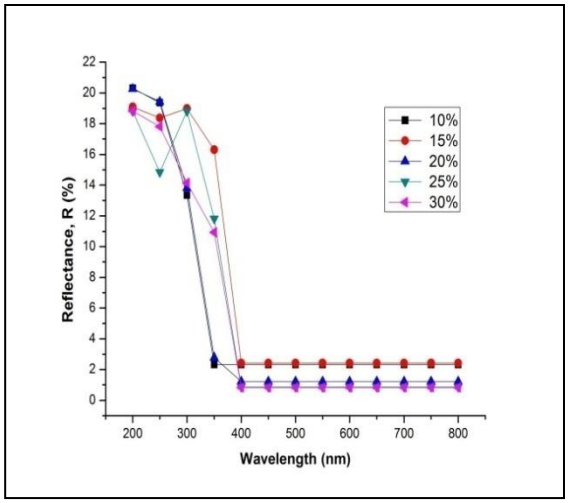

Figure 4.14c: Reflection spectra of spray deposited ZnSe:Eu films at different dopant concentrations

From figure 4.14a, the ZnSe:Eu films deposited at different substrate temperatures exhibited very poor reflection of radiation in both the UV and visible region respectively. Reflection values of the ZnSe:Eu films obtained for the different substrate temperatures are within the range of 0.9% to 20.33%. The film deposited at 300 ^{o}C show reflection in the range of 3.71%

to 20.27% while the film deposited at 325 ^{o}C show reflection within the range of 2.82% to 19.42%. The reflection range of 0.9% to 19.24% was recorded for the film deposited at 350 ^{o}C. The films deposited at 375 ^{o}C and 400 ^{o}C exhibited poor reflectance values within the range of 2.32% to 20.3% and 1.97% to 20.33% respectively. The information provided above can be observed in figure 4.15a.

From figure 4.14b, all the ZnSe:Eu films deposited at different flow rates show very poor reflectance (0.96% to 20.26%) of light throughout the ultraviolet and visible regions. The ultraviolet region recorded reflectance values of 2.78% to 20.26% while the visible region had reflectance values within the range of 0.96% to 6.92% for all the deposited films as indicated in figure 4.14b.

From figure 4.14c, the ZnSe:Eu films deposited at different dopant concentrations also reveal very poor reflectance values within the range of 2.32% to 20.30% in the UV region and 0.83% to 2.43% in the visible region for all the films within the same spectra range.

In all cases of investigation, the ZnSe:Eu films exhibited poor reflectance in the UV and visible region respectively and as such can be exploited as an anti-reflective coating to be used in solar cell fabrication. The results presented in this research agree with previous report of Ivashchenko *et al*., (2017). The values of reflectance of the ZnSe:Eu films for different deposition conditions are given in appendixes B7, B8 and B9 respectively.

4.6.4 Refractive index of ZnSe:Eu films

The refractive index of the Eu-doped ZnSe films was calculated at different temperatures and plotted against photon energy, E as indicated in figure 4.15.

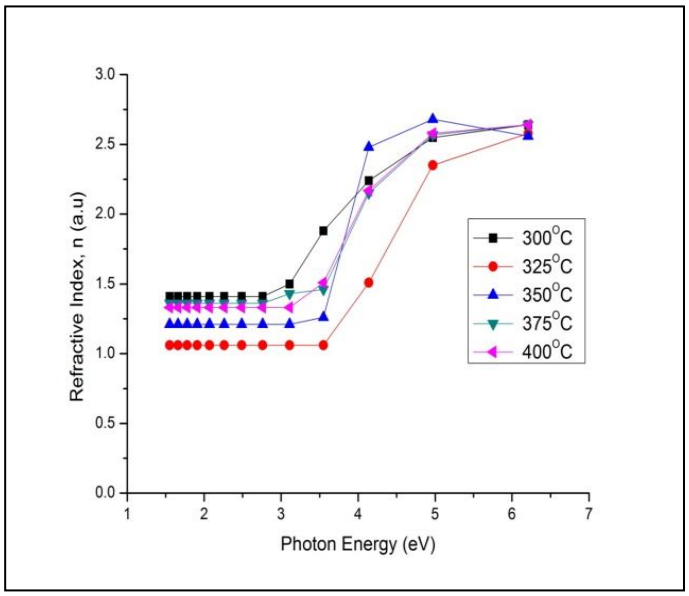

Figure 4.15: Refractive index of ZnSe:Eu films at different substrate temperatures

From figure 4.15, the refractive index of ZnSe:Eu films obtained at different substrate temperatures of investigation reveal an almost constant value within the range of 1.06 to 1.41 at photon energies below 3.11 eV. Constant refractive index value for the visible region of the electromagnetic spectrum is observed. At increased wavelength (lower photon energy), a constant value of refractive index of the ZnSe:Eu films is observed for all temperature variations. This may be due to the fact that at lower photon energy, there is no sufficient energy for the ZnSe:Eu material to release a photoelectron. As a result, maximum number of photons are transmitted through the band gap and a fewer number of photons interacts with the molecule (Tanvir, 2017).

However, at higher photon energies, the films recorded high refractive index between 2.24 to 2.64 for the range of temperature (300 ^{o}C to 400 ^{o}C) under study. This property of high refractive index exhibited by the films at high photon energies suggests that they can be useful in the manufacture of optoelectronic devices.

The values used in plotting the refractive index of ZnSe:Eu films against photon energy, E at different substrate temperatures are presented in appendix B10.

4.6.5 Absorption coefficient of ZnSe:Eu films

The absorption coefficient of the ZnSe:Eu films at different substrate temperatures were calculated from transmittance and thickness values and plotted against photon energy. This is shown in figure 4.16.

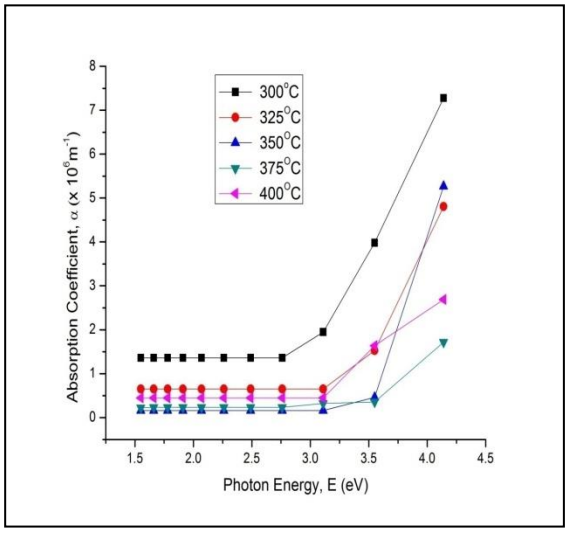

Figure 4.16: Absorption coefficient of ZnSe:Eu films at different substrate temperatures

All the ZnSe:Eu films are observed to show similar behaviour. An almost constant value is observed at photon energies below 3 eV and thereafter increases. This behaviour implies that the material has high absorbance at short wavelengths and low absorption coefficient at longer wavelengths. The absorption coefficient values of ZnSe:Eu films obtained at different substrate temperatures are presented in appendix B11

4.6.6 Optical conductivity study of ZnSe:Eu films

The optical conductivity of the ZnSe:Eu films under study was calculated for different substrate temperature and are plotted against photon energy as revealed in figure 4.17.

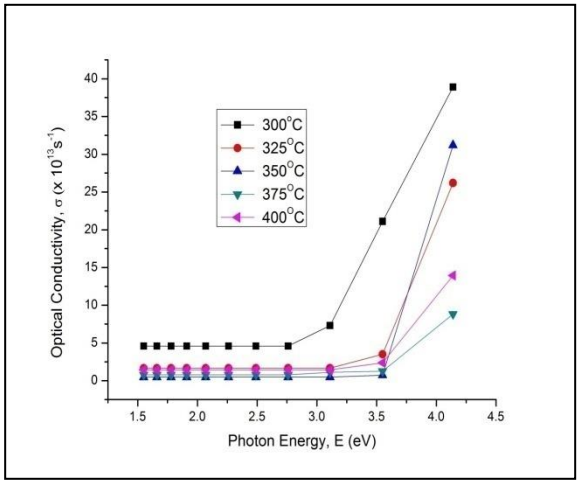

Figure 4.17: Plot of optical conductivity versus photon energy for ZnSe:Eu films at different substrate temperatures

Low optical conductivity was recorded for the ZnSe:Eu films at low photon energy and thereafter, the films exhibited some form of sharp increment at photon energy above 3 eV (about 3.5 eV), except for the film deposited at substrate temperature of 300 ^{o}C which increased at a photon energy of about 3.11 eV. For semiconductors, the optical conductivity increases sharply for higher photon energy which is in good agreements with the results reported in this research. The values of the optical conductivity of ZnSe:Eu films at different temperatures and photon energies are displayed in appendix B12.

4.6.7 Extinction coefficient of ZnSe:Eu films

The extinction coefficient of the ZnSe:Eu films at different substrate temperatures plotted against photon energy is shown in figure 4.18.

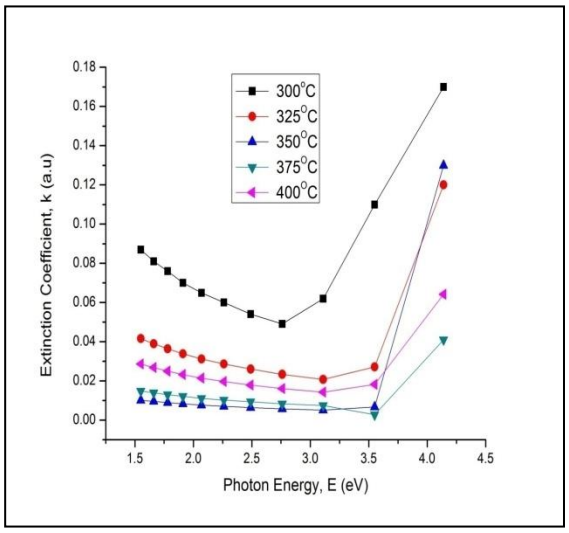

Figure 4.18: Plot of extinction coefficient versus photon energy for ZnSe:Eu films at different substrate temperatures

From figure 4.18, it is observed that the extinction coefficient of all the ZnSe:Eu films decreased as photon energy increased and thereafter increases sharply. This behaviour may be due to the absorption of light at the grain boundaries (Tanvir, 2017). The sharp increase of extinction coefficient with photon energy indicates the probability of raising the electron transfer across the mobility gap with photon energy and greater attenuation of light (Howari, 2012).

4.6.8 Real part of dielectric constant of ZnSe:Eu films

The real part of the dielectric constant of ZnSe:Eu films was calculated for different substrate temperatures. Figure 4.19 shows a plot of the real part of dielectric constant versus photon energy for ZnSe:Eu films for different substrate temperatures.

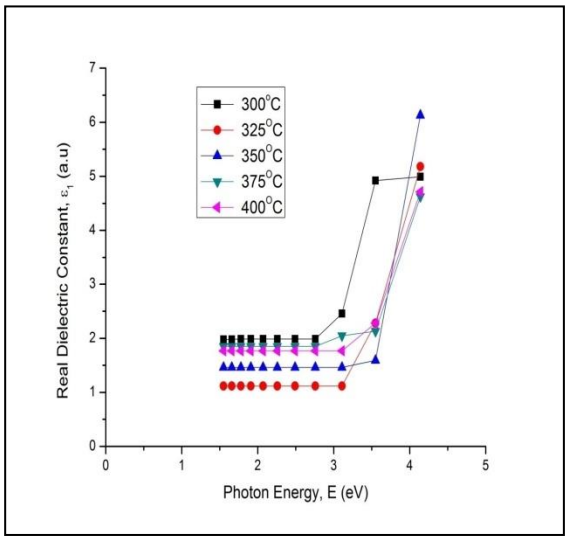

Figure 4.19: Plot of real dielectric constant versus photon energy for ZnSe:Eu films at different substrate temperatures

For all the deposited ZnSe:Eu films, the real dielectric constant assumes a constant value at low photon energy (visible region) and increases spontaneously above 2.5 eV near the UV region as observed in figure 4.19.

The values of extinction coefficient for ZnSe:Eu films are shown in appendix B14.

4.6.9 Imaginary part of dielectric constant of ZnSe:Eu films

The imaginary dielectric constant was calculated for different substrate temperatures. It was plotted against photon energy as depicted in figure 4.20.

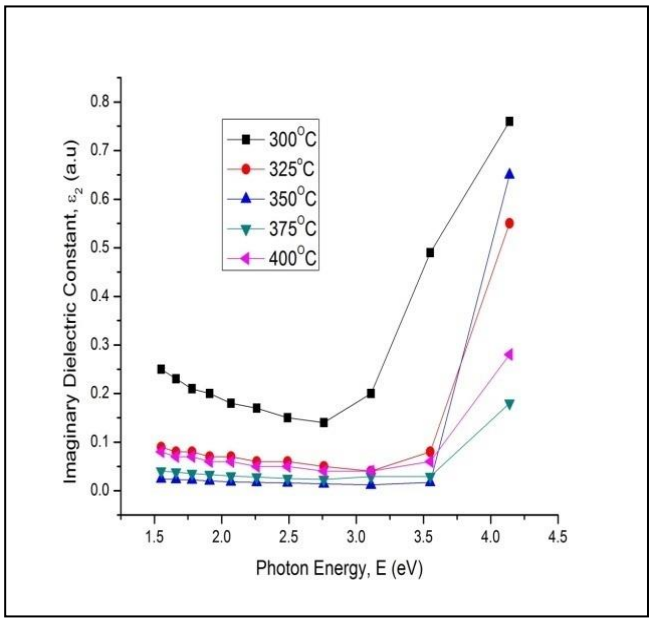

Figure 4.20: Plot of imaginary dielectric constant versus photon energy for ZnSe:Eu films at different substrate temperatures

The imaginary dielectric constant values of the ZnSe:Eu films assumes a steady decline as the photon energy approaches higher values (UV region). Nevertheless, the films exhibited steep increase around 2.8 eV (for the film at 300 ^{o}C) and about 3.4 eV (for films at 325 ^{o}C to 400 ^{o}C).

The values of imaginary dielectric constant used for plotting figure 4.20 are presented in appendix B15.

4.6.10 Band gap energy of ZnSe:Eu films

Figures 4.21 (a-e) shows the plot of $(\alpha h\nu)^2$ versus photon energy for the ZnSe:Eu films for different substrate temperatures while the values of $(\alpha h\nu)^2$ are presented in appendix B16.

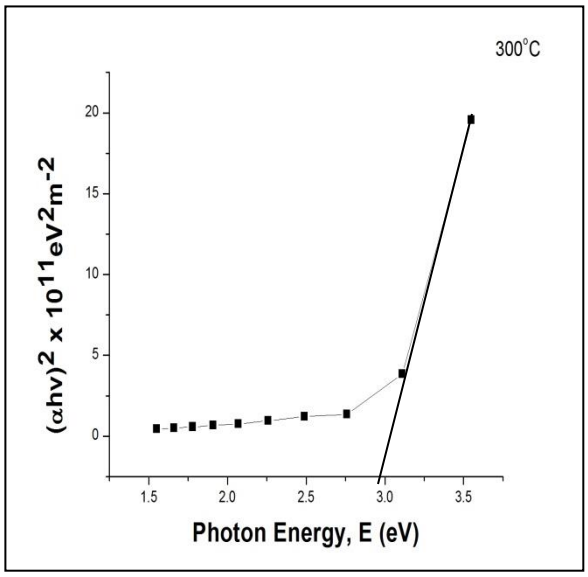

Figure 4.21a: Plot of $(\alpha hv)^2$ versus photon energy for ZnSe:Eu films at substrate temperature of 300 °C

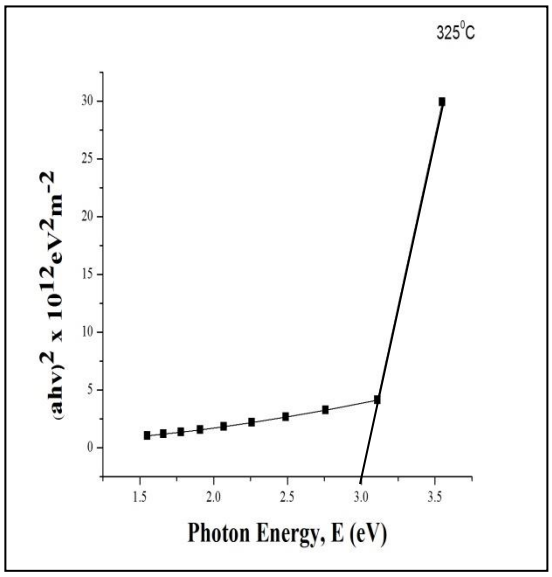

Figure 4.21b: Plot of $(\alpha hv)^2$ versus photon energy for ZnSe:Eu films at substrate temperature of 325 °C

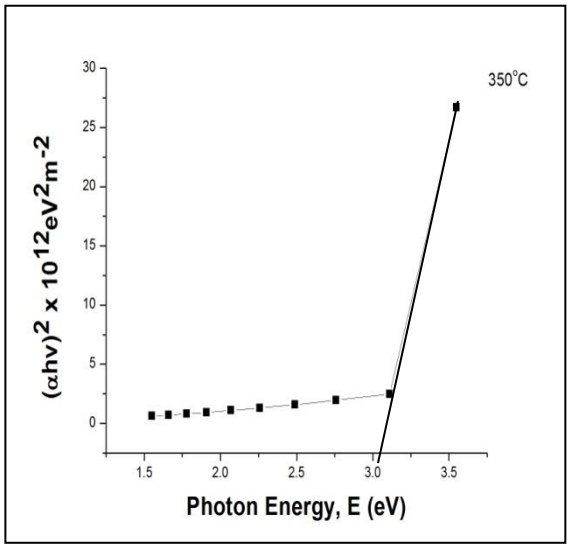

Figure 4.21c: Plot of $(\alpha hv)^2$ versus photon energy for ZnSe:Eu films at substrate temperature of 350 °C

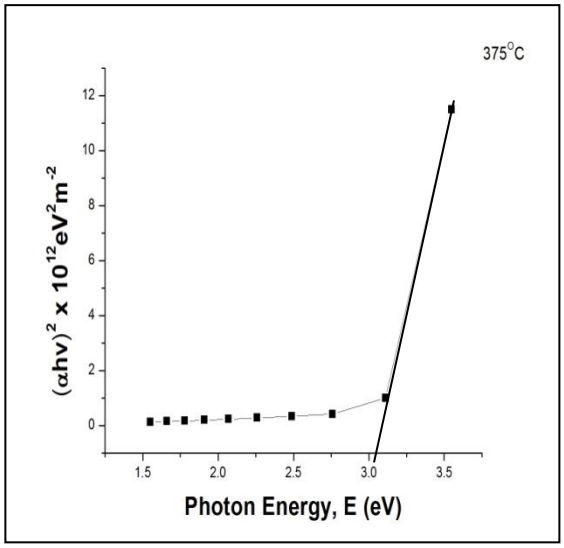

Figure 4.21d: Plot of $(\alpha hv)^2$ versus photon energy for ZnSe:Eu films at substrate temperature of 375 °C

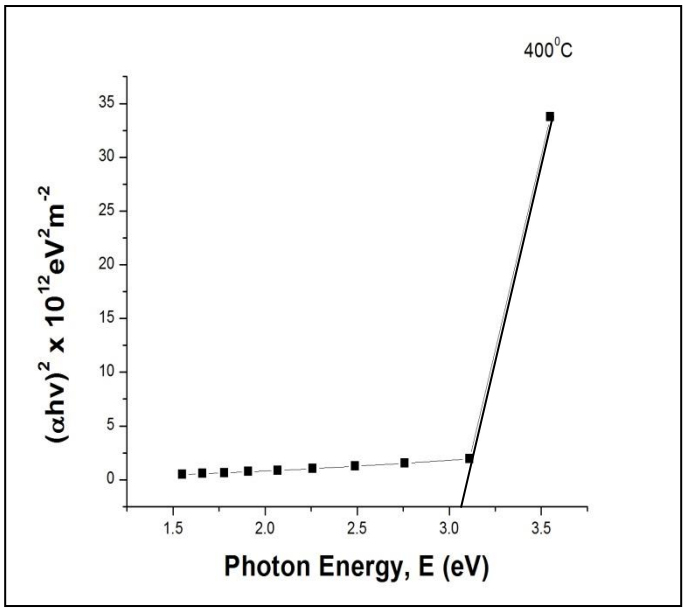

Figure 4.21e: Plot of $(\alpha h\nu)^2$ versus photon energy for ZnSe:Eu films at substrate temperature of 400 ºC

As observed in figures 4.21 (a-e) above, the calculated direct band gap at different substrate temperature of ZnSe:Eu are all blue-shifted with respect to the bulk value (2.72 eV) of ZnSe. This could be attributed to the incorporation of Eu^{3+} ions into the pure ZnSe films and also indicates enhancement of the films. The band gap values obtained in this research are within the range of 2.99 eV to 3.12 eV for substrate temperature between 300 ºC and 400 ºC respectively. The results also indicate that the band gap increases as substrate temperature increases. The values of band gap for ZnSe:Eu obtained in this research are well within the range reported by previous research by Muthumari *et al;* (2012), Buba (2016), Kumar (2015), Amatalo (2014), Fakhrurrazi, *et al;* (2016) and Kumar, *et al;* (2012) for ZnSe films.

4.7 Structural characterization of ZnSe:Eu nanofilms

4.7.1 X-ray diffraction (XRD) analysis

The XRD pattern of the ZnSe:Eu films obtained at 350 ^{o}C and 10% dopant concentration is presented in figure 4.22, while the XRD pattern of the ZnSe:Eu films obtained at 350 ^{o}C and 20% doping concentration is displayed in figure 4.23.

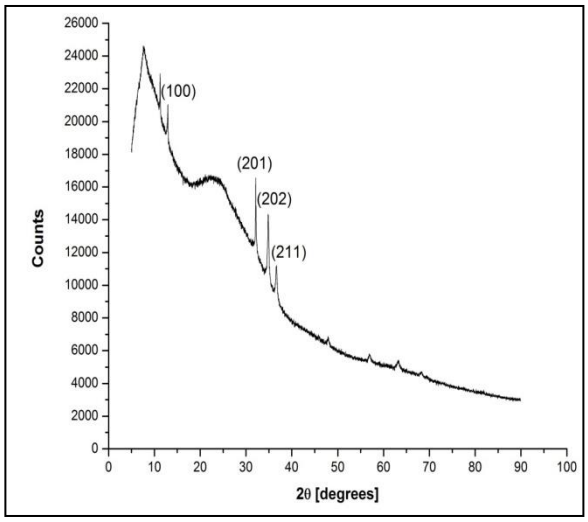

Figure 4.22: X-ray diffractogram for ZnSe:Eu films obtained at 350 ^{o}C and 10% dopant concentration

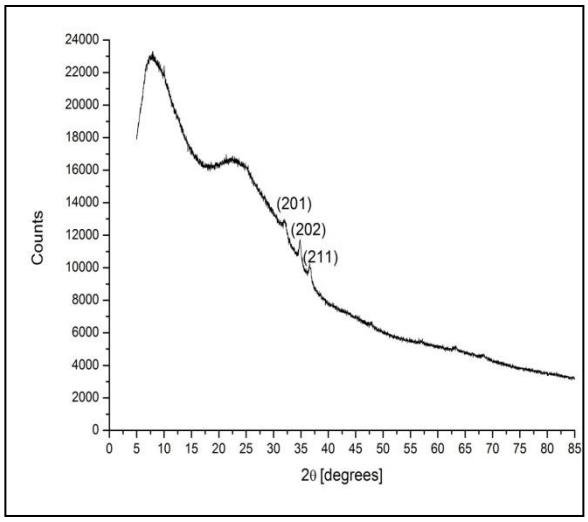

Figure 4.23: X-ray diffractogram for ZnSe:Eu films obtained at 350 ^{o}C and 20% dopant concentration

The x-ray pattern displayed in figure 4.22 suggests the films are polycrystalline with indexed lattice planes at (100), (201), (202) and (211) at Bragg's diffraction angles of 12.99^{o}, 32.12^{o}, 34.82^{o} and 36.63^{o}. The indexed planes reveal the films possess the wurtzite (hexagonal) structure of zinc selenide. Due to the highest intensity observed at 2θ equals 32.12^{o} indexed to the reflection plane of (201), this angle was chosen as the preferred growth plane of the film. The lattice constant calculated for the (201) plane is 5.946 Å which is a bit higher than the value (5.667 Å) for bulk zinc selenide.

The crystallite size, the lattice spacing and other lattice parameters have been calculated from the relevant equations and presented in appendixes B17 and B18 respectively.

In figure 4.23, less sharp peaks are observed. Increasing the volume of dopant concentration from 10% to 20% resulted in a reduction of the number of peaks observed for the ZnSe:Eu films. As observed in figure 4.23, the intensities of the peaks were greatly reduced as a result of the increased dopant concentration. This behaviour is an indication of a loss in crystallinity due to distortion in the crystal lattice (Pal *et al*., 2012). The resulting reflection peaks were indexed to the (201), (202) and (211) planes with corresponding Bragg's angle (2θ) of 31.99^{o}, 34.75^{o} and 36.55^{o} respectively. The observed planes are consistent with the wurtzite (hexagonal) structure of ZnSe. The (202) plane has the highest intensity, hence is seen as the desired growth plane. The particle size for this plane was calculated to be about 31.05 nm. Other lattice parameters corresponding to the desired growth plane and the other reflection planes were estimated and presented in appendixes B19 and B20.

4.8 Surface morphology of ZnSe:Eu film

4.8.1 Scanning electron microscopy (SEM) study

The SEM micrograph of the ZnSe:Eu film grown at 350 ^{o}C, 10% dopant concentration and flow-rate of 400 μL/spray is displayed in figure 4.24 (a-b) for different resolutions. Figure 4.24c displays the SEM image of ZnSe:Eu film obtained at 375 ^{o}C at 10% dopant concentration while figure 4.24d is the SEM image obtained at 375 ^{o}C at 20% dopant concentration.

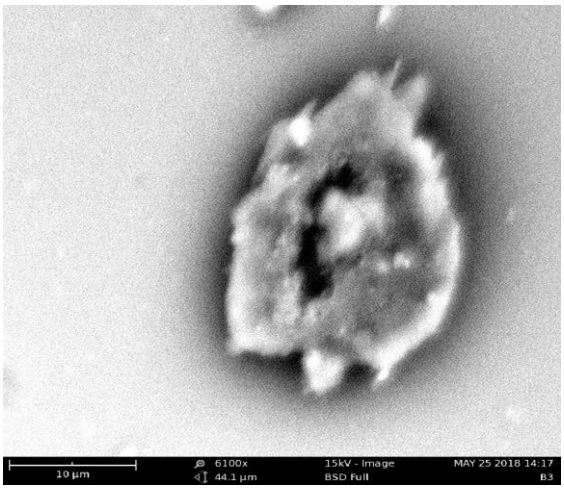

Figure 4.24a: SEM image of ZnSe:Eu at a resolution of 6100x

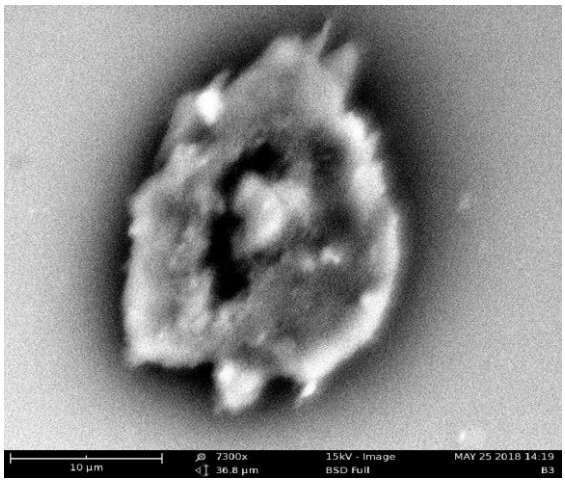

Figure 4.24b: SEM image of ZnSe:Eu at a resolution of 7300x

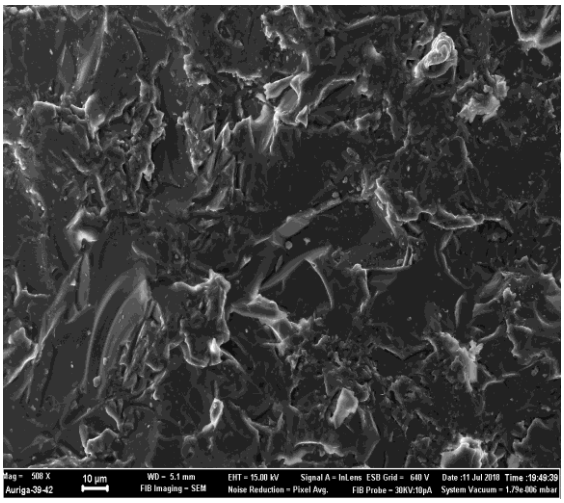

Figure 4.24c: SEM image of ZnSe:Eu film at 375 ºC and 10% dopant concentration

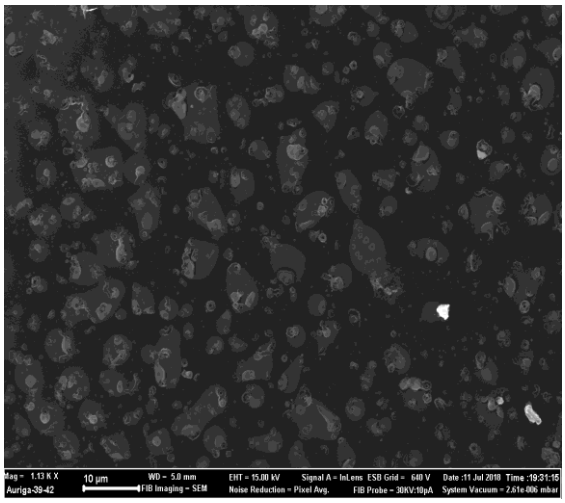

Figure 4.24d: SEM image of ZnSe:Eu film at 375 ºC and 20% dopant concentration

From figures 4.24a and 4.24b, the surface appears smooth and homogeneous, however, cotton-like morphology is observed for the doped films. As the solution containing ZnSe:Eu is sprayed on the hot substrate, the water content present evaporates due to the high deposition temperature. The formation of the cotton-like morphology could be attributed to the

evaporation observed at this high temperature. A similar view on ZnSe films has been reported by Lohar *et al*., (2014).

The SEM image in figure 4.24c agrees with that obtained by Tanvir (2017) for ZnSe films deposited by chemical bath for 30 mins. Tanvir (2017) reports that such morphology indicates fibre type nature. The fibre nature of the ZnSe:Eu film displayed in figure 4.24c suggests the film's appropriateness for utilization in fibre optics communication technology.

The SEM image of ZnSe:Eu film displayed in figure 4.24d indicates the film is not so dense and shows a fine coverage of the glass substrates with small-sized grains on the surface of the films. This is a further confirmation of the grain sizes estimated from XRD results.

4.9 Thickness variation of the CdSe:Eu films

The thicknesses of the films obtained at different deposition temperatures are presented in tables 4.3a and 4.3b respectively.

Table 4.3a: Thickness variation of CdSe:Eu films with temperature

Temperature (ºC)	Thickness (nm)
300	50
320	100
340	150
360	75
380	60

Table 4.3b: Thickness variation of CdSe:Eu films with dopant concentration

Dopant Concentration (%)	Thickness (nm)
10	125
15	75
20	500
25	650
30	710

Table 4.3c: Thickness variation of CdSe:Eu with flow rate

Flow Rate (µL/spray)	Thickness (nm)
400	50
480	60
560	72
640	83
720	92

From table 4.3a, the thickness of the CdSe:Eu films increases with increase in temperature and thereafter decreases as temperature increases.

From table 4.3b, the thickness of the films decreased from 125 nm to 75 nm when dopant concentration increased from 10% to 15%. However, as dopant concentration increases from 15% to 30%, thickness of the films increased from 75 nm to 710 nm.

From table 4.3c, the thickness of the films was observed to increase as the flow-rate increases.

4.10 Optical study of CdSe:Eu films

4.10.1 Absorption measurement of CdSe:Eu films

The absorption curves for all the deposited CdSe:Eu films are presented in figures 4.25a, 4.25b and 4.25c.

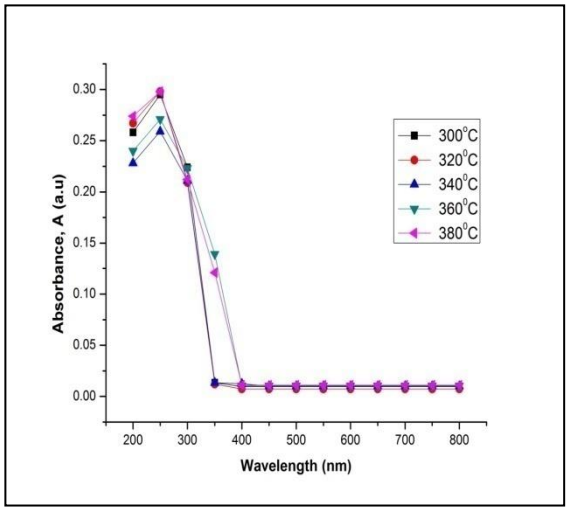

Figure 4.25a: Absorption curves for CdSe:Eu films deposited at different temperatures

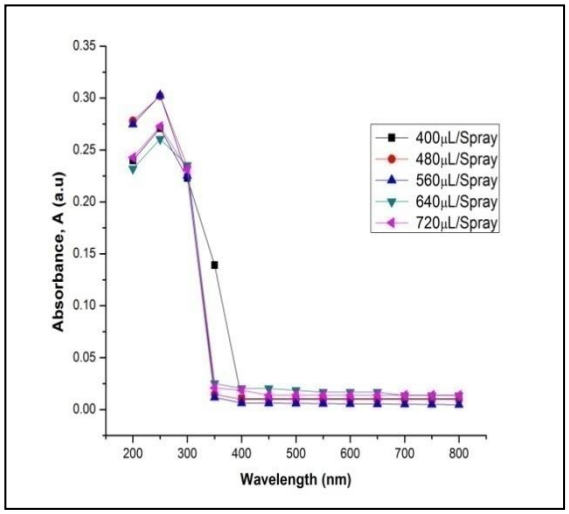

Figure 4.25b: Absorption curves for CdSe:Eu films at different flow rates

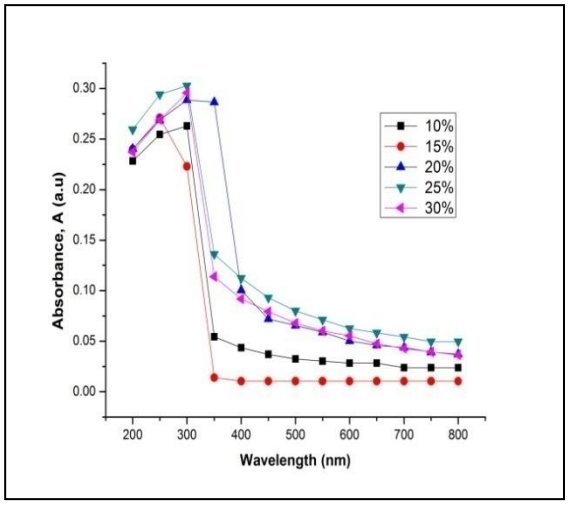

Figure 4.25c: Absorption curves for CdSe:Eu films obtained at different dopant concentration

From figures, 4.25a, 4.25b and 4.25c, it is observed that the absorption curves for all samples exhibit a downward trend (sharp decrease) towards the visible region of the electromagnetic spectrum. The highest absorbance for each of the deposited films was observed in the ultraviolet region of the electromagnetic spectrum. The sharp decrease observed in the absorbance of the films at wavelengths less than 400 nm can be attributed to the onset of interband transitions at the fundamental band edge (Ozutok *et al*., 2012).

The absorbance values of CdSe:Eu for different temperatures, flow rates and dopant concentrations are presented in appendixes C1, C2 and C3 respectively.

4.10.2 Optical transmission of the CdSe:Eu films

Figure 4.26a show the percentage transmission at different temperatures plotted against wavelength, while figures 4.26b and 4.26c represents percentage transmission of CdSe:Eu films at different flow-rates and dopant concentrations respectively.

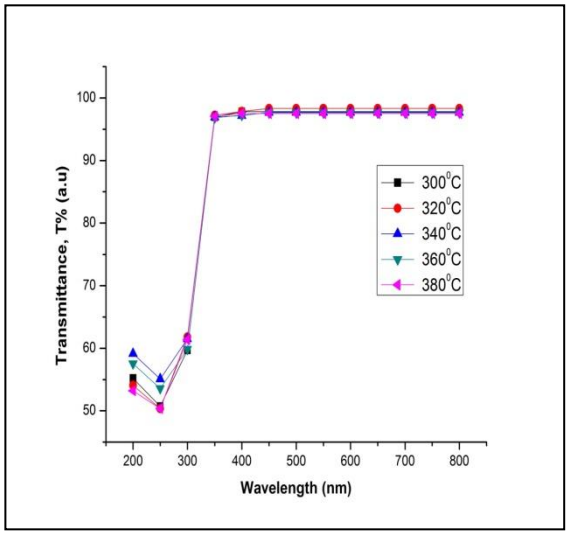

Figure 4.26a: Transmission curves for CdSe:Eu films deposited at different substrate temperatures

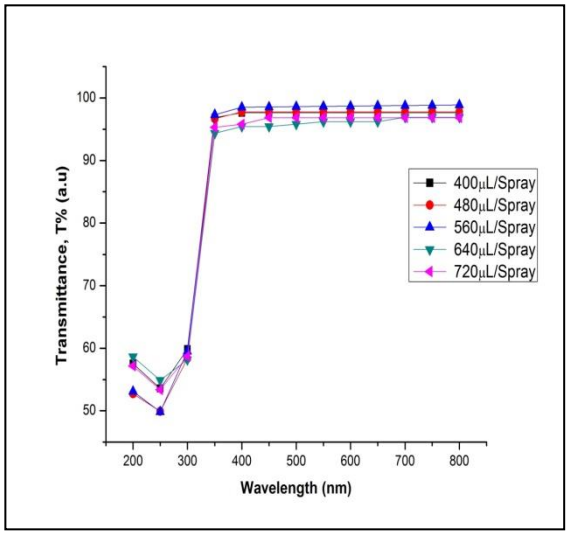

Figure 4.26b: Transmission curves for CdSe:Eu films deposited at different flow rates

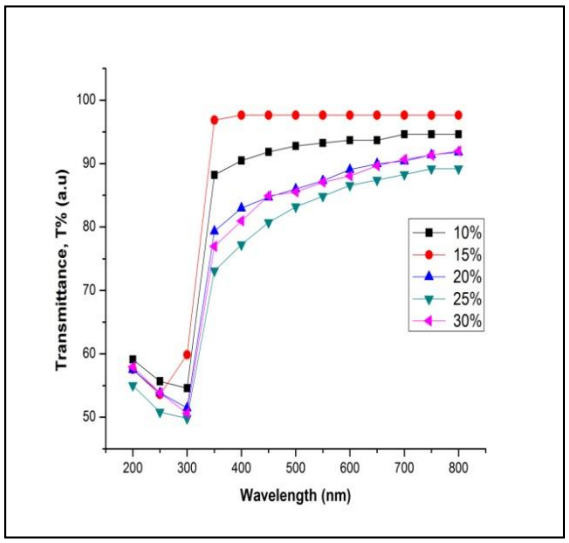

Figure 4.26c: Transmission curves for CdSe:Eu films deposited at different europium concentrations

From figure 4.26a, the optical transmission of CdSe:Eu films deposited at different substrate temperatures indicates that the films have very high transmittance in the visible region of the electromagnetic spectrum. For all the films deposited at different substrate temperatures, the average transmittance in the ultraviolet region was in the range of 50.35% to 61.52%. In the visible region, the deposited films show very high transmittance values within the range of 96.85% to 98.33%.

For the CdSe:Eu films deposited at different flow rates (figure 4.26b), optical transmittance has values between 49.82% and 59.84% in the ultraviolet region while in the visible region to near infra-red region, the films recorded a high transmittance between 94.36% and 98.88%. The CdSe:Eu films deposited at different dopant concentrations recorded a low transmittance within the range of 49.81% to 59.84% in the UV region while the films have high transmittance between 73.08% to 97.63% in the visible region as shown in figure 4.26c.

The very high transmittance exhibited by the CdSe:Eu films in the visible region of the electromagnetic spectrum at different deposition conditions indicates that the material will

prove very useful in the manufacture of glasses, windows, vehicle windscreens, optical lenses and optoelectronic devices. The results obtained in this research follow the same trend as those reported by Meshram and Thombre, (2015) for spray deposited CdSe films. Also, the results show that the CdSe:Eu films are highly transparent in the visible region of the electromagnetic spectrum which agrees with the report of Thirumavalavan *et al*., (2015) for chemical bath deposited CdSe films. However, the transparency of CdSe:Eu films deposited in this work appear to be higher compare to those obtained by Thirumavalavan *et al*., (2015) and the report of Meshram and Thombre, (2015). This observation can be attributed to the addition of rare-earth impurity (europium) to the pure CdSe films in this research.

4.10.3 Reflection spectra of CdSe:Eu films

The reflection spectra of all the deposited CdSe:Eu films for the different deposition conditions are presented in figures 4.27(a-c).

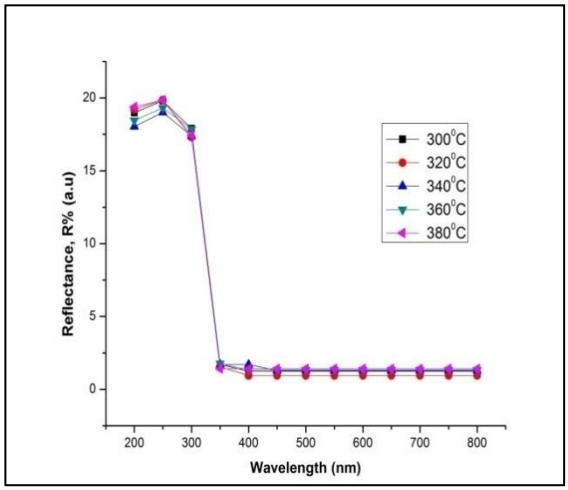

Figure 4.27a: Reflection spectra of CdSe:Eu films deposited at different substrate temperatures

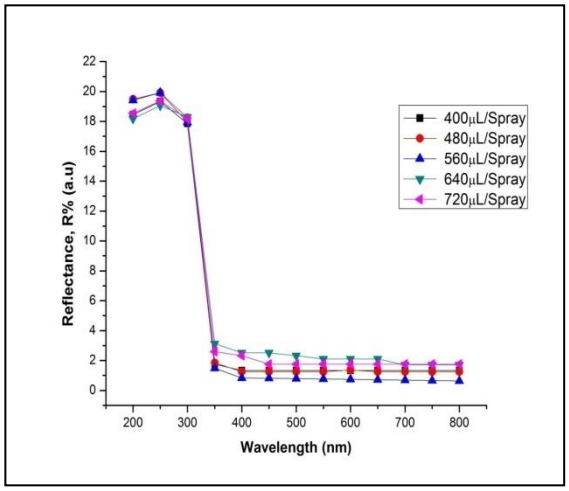

Figure 4.27b: Reflection spectra of CdSe:Eu films deposited at different flow rates

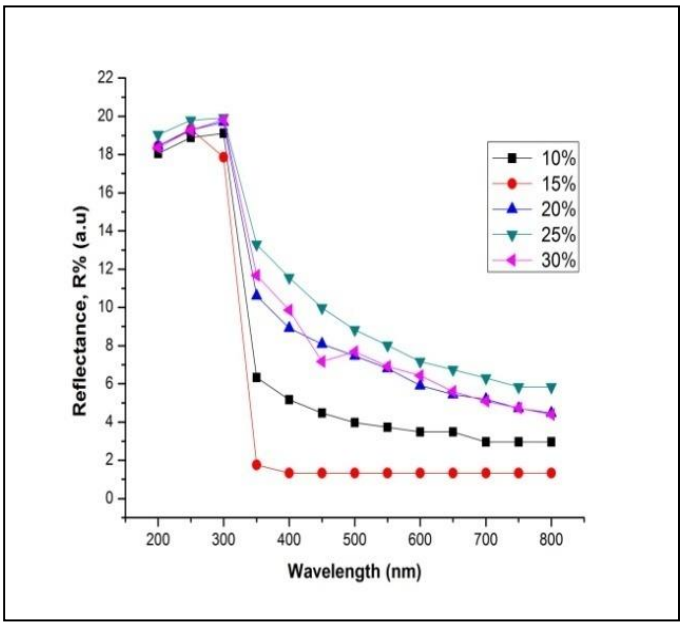

Figure 4.27c: Reflection spectra of CdSe:Eu films deposited at different dopant concentrations

From figure 4.27a, poor reflection of electromagnetic radiation was observed for the films in all cases of temperature variation. The films exhibited reflection within the range of 0.94% to 1.33% in the visible region while 1.4% to 19.85% was observed in the UV region. From figure 4.27a, it is very obvious that all the films exhibited very poor reflection of light throughout the UV-VIS-NIR region of the electromagnetic spectrum.

From figure 4.27b, the reflection spectra of the CdSe:Eu films decreases as wavelength increases in the visible spectrum. However, all the deposited films exhibited similar trend, having very poor reflection values within the range of 0.63% to 2.52% in the visible region while 1.49% to 19.92% was observed in the UV region.

From figure 4.27c, all the reflection spectra exhibited a downward trend in the visible region as wavelength increases. For the films deposited at 10% and 15% dopant concentration, reflection values throughout the UV region were within the range of 6.33% to 19.12% and 1.76% to 19.32% respectively. For the films deposited at 10%, the reflection values were

within the range of 2.96% to 5.18% in the visible region while for the films deposited at 15% dopant concentrations, reflection value was constant at 1.33% in the visible region. For the films deposited at 20% dopant concentration, reflection values recorded in the UV region and visible region were within the range of 10.61% to 19.69% and 4.48% to 8.91% respectively. Films deposited at 25% and 30% dopant concentrations have reflection values within the range of 5.84% to 19.92% and 4.4% to 19.81% throughout the UV-VIS region of the electromagnetic spectrum. It is pertinent to observe that in all cases of variations, all the deposited films of CdSe:Eu exhibited poor reflection of light throughout the entire UV-VIS region of the electromagnetic spectrum. This characteristic of poor reflection exhibited by Eu-doped cadmium selenide films makes the material a very important one for use as an anti-reflective coating on solar cells fabrication in order to achieve high efficiency.

The reflectance values of CdSe:Eu films at different deposition conditions are displayed in appendixes C7, C8 and C9 respectively.

4.10.4 Refractive index of CdSe:Eu films

The refractive index values of the Eu-doped CdSe films obtained at different substrate temperatures plotted against photon energy are shown in figure 4.28.

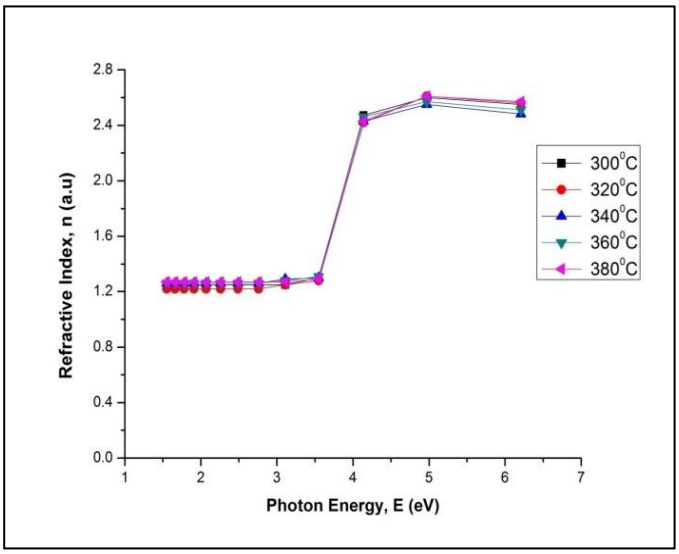

Figure 4.28: Plot of refractive index of CdSe:Eu films at different temperatures against photon energy

The CdSe:Eu films recorded refractive index values between 1.22 to 1.31 at photon energies below 4 eV. However, at photon energies above 4 eV, the CdSe:Eu films recorded high refractive index values between 2.42 and 2.61 with regards to the different substrate temperatures. The high refractive index exhibited by the CdSe:Eu films indicates that the films will prove valuable for fabricating optoelectronic devices. The refractive index values of CdSe:Eu are displayed in appendix C10.

4.10.5 Absorption coefficient of the CdSe:Eu films

The values of absorption coefficient of the CdSe:Eu films at different substrate temperature are plotted against photon energy as shown in figure 4.29 while absorption coefficient values are displayed in appendix C11.

Absorption coefficient within the range of about 1.538 x 10^5 m^{-1} to 6.174 x 10^5 m^{-1} was observed for the films in the temperature range of 300 ^oC to 380 ^oC.

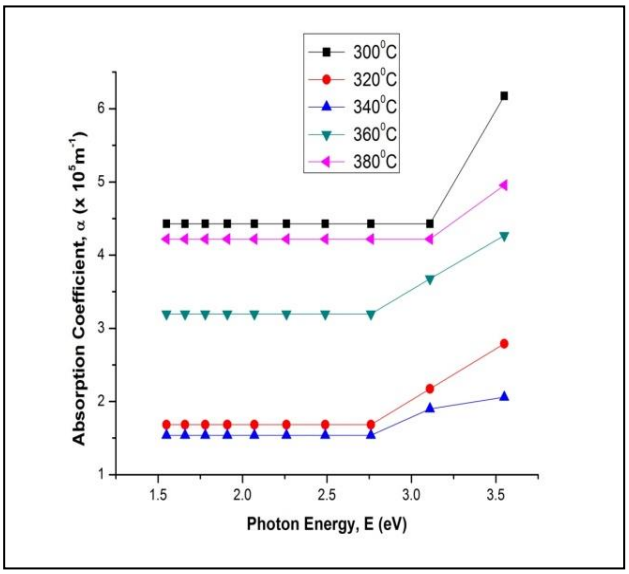

Figure 4.29: Plot of absorption coefficient of CdSe:Eu films at different temperatures against photon energy

4.10.6 Optical conductivity of the CdSe:Eu films

Figure 4.30 displays the plot of optical conductivity of CdSe:Eu versus photon energy for different substrate temperatures.

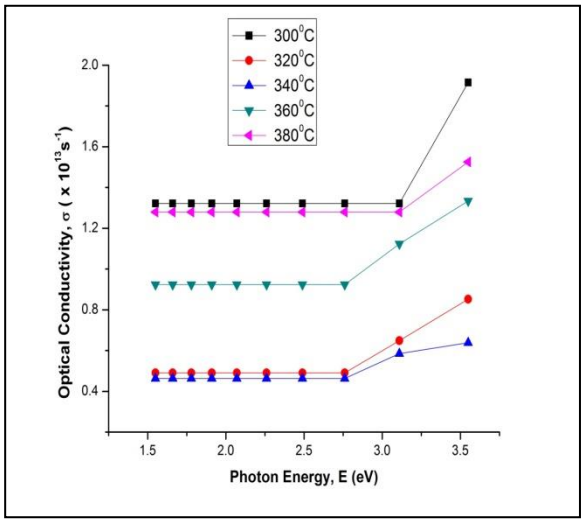

Figure 4.30: Plot of optical conductivity of CdSe:Eu films at different temperatures against photon energy

Optical conductivity values appear constant at lower photon energies but increases sharply at about 2.76 eV (for films deposited at 320 ^{o}C, 340 ^{o}C and 360 ^{o}C) and about 3.11 eV (for films deposited at 300 ^{o}C and 380 ^{o}C).

4.10.7 Extinction coefficient of CdSe:Eu films

Figure 4.31 reveals the plot of extinction coefficient at different substrate temperatures versus photon energy.

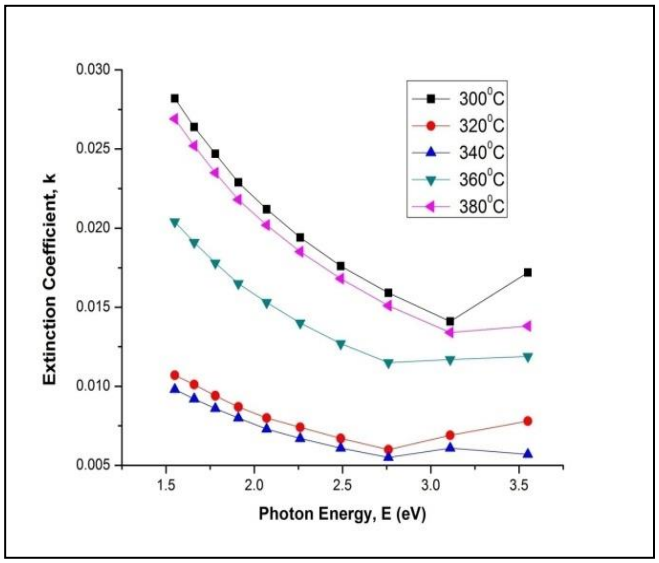

Figure 4.31: Plot of extinction coefficient of CdSe:Eu films at different temperatures against photon energy

From figure 4.31, the extinction coefficient values are observed to decrease steadily as photon energy increases and slightly increased further. The extinction coefficient values of the CdSe:Eu films are very small within the range of 0.0055 to 0.0282 for different substrate temperatures. The low extinction coefficient (k) confirms high transparency of the films (Amatalo, 2014).

Appendix C13 displays the values of extinction coefficient of CdSe:Eu films at different substrate temperatures.

4.10.8 Real dielectric constant of CdSe:Eu films

The plot of real dielectric constant of CdSe:Eu films at different substrate temperatures against photon energy is displayed in figure 4.32.

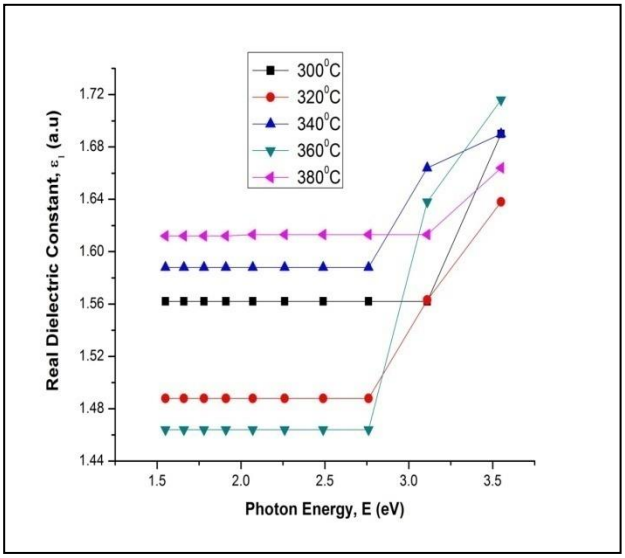

Figure 4.32: Plot of real dielectric constant of CdSe:Eu films at different substrate temperatures against photon energy

The values of real dielectric constant of the CdSe:Eu films are observed to be constant at low photon energies (corresponding to the visible region) and increases sharply at high photon energies as shown in figure 4.32. This is in good agreement with the report of Kariper *et al*., (2014) for CdSe films obtained by chemical bath deposition technique. This behaviour is due to the strong interaction between the highly energetic photons and the charge carriers of the material (Kariper *et al*., 2014).

The values employed in plotting figure 4.32 are displayed in appendix C14.

4.10.9 Imaginary dielectric constant of CdSe:Eu films

The plot of imaginary dielectric constant of CdSe:Eu films at different substrate temperatures against photon energy is displayed in figure 4.33.

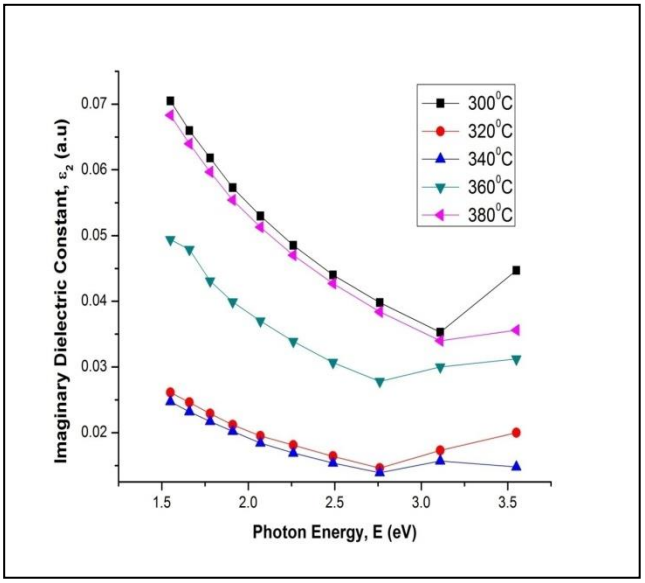

Figure 4.33: Plot of imaginary dielectric constant of CdSe:Eu films at different substrate temperatures against photon energy

From figure 4.33, the values of imaginary dielectric constant of the CdSe:Eu films are observed to decrease as photon energy increases and thereafter exhibited a slight increase in all cases of substrate temperature variation.

The values employed in plotting figure 4.33 are presented in appendix C15.

4.10.10 Band gap energy of CdSe:Eu films

Figure 4.34 shows the plot of $(\alpha h\nu)^2$ versus photon energy for the CdSe:Eu films for different substrate temperatures.

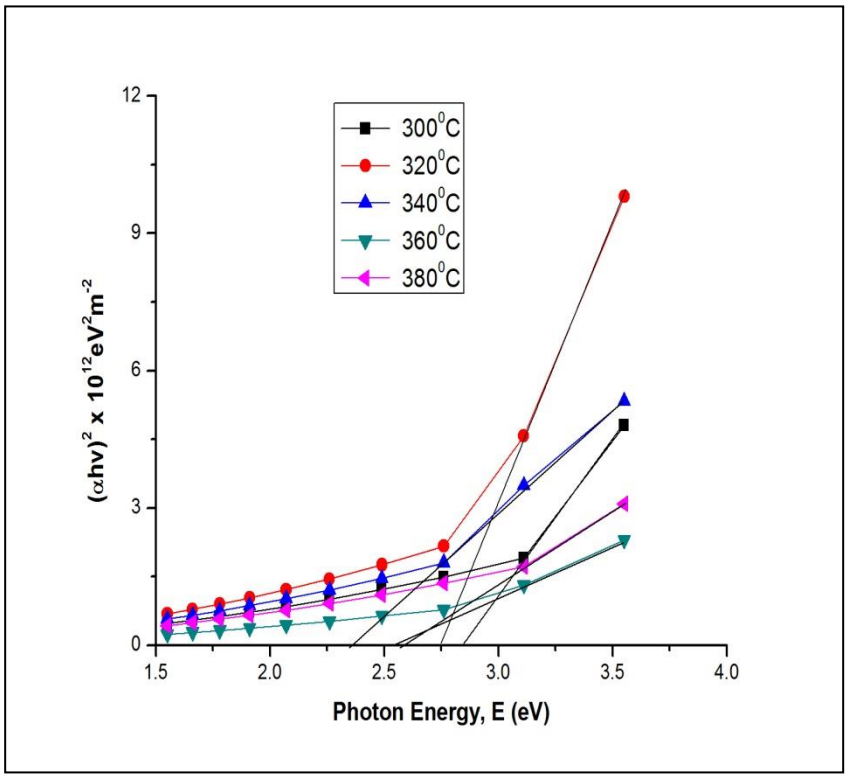

Figure 4.34: Plot of $(\alpha h\nu)^2$ values of CdSe:Eu films at different substrate temperatures against photon energy

The values of $(\alpha h\nu)^2$ versus photon energy were plotted against photon energy for the CdSe:Eu films at different substrate temperature and the direct band gap obtained by extrapolating the linear portion of the curve to the point where $(\alpha h\nu)^2$ equals zero.

From figure 4.34, the band gap of CdSe:Eu films decreases from 2.84 eV to 2.40 eV as temperature increases from 300 ^oC to 340 ^oC. However, as the temperature increases further from 340 ^oC to 380 ^oC, a slight increment in band gap energy (2.4 eV to 2.61 eV) is observed for the CdSe:Eu films. The slight increase in band gap energy at higher temperature may be due to perceived imperfections or defects which may be present in the crystal.

Table 4.4 gives a summary of the band gap energy of CdSe:Eu films obtained in this research at different substrate temperatures. The values of $(\alpha h\nu)^2$ are displayed in appendix C16.

Table 4.4: Band gap energy of CdSe:Eu films at different substrate temperatures

Temperature (°C)	Band Gap Energy (eV)	Thickness (nm)
300	2.84	50
320	2.70	100
340	2.40	150
360	2.52	75
380	2.61	60

From table 4.4, the band gap energy of CdSe:Eu films at different substrate temperatures exhibited a strong blue-shift from the bulk value (1.75 eV). The strong blue-shift of band gap energy observed in this research from the bulk value of CdSe (1.75 eV) indicates quantum confinement effect taking place, which enhances and increases the band gap energy as the thickness approaches the nanoscale range.

4.11 Structural characterization of CdSe:Eu films

4.11.1 X-ray diffraction (XRD) studies

Figure 4.35 displays the XRD pattern of the CdSe:Eu film obtained at a substrate temperature of 360 °C and 10% dopant concentration respectively.

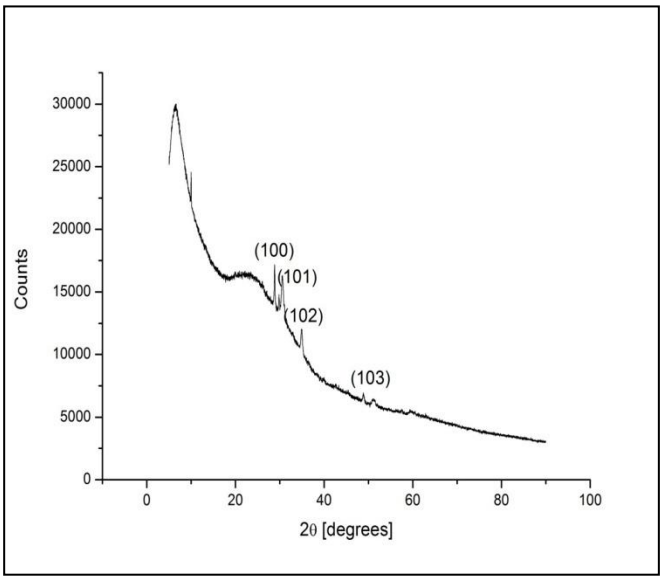

Figure 4.35: XRD pattern of CdSe:Eu films at 360ºC and 10% dopant concentration

From figure 4.35, the observed diffraction peaks obtained at 2θ values of 28.93º, 30.62º, 34.98º and 51.05º are indexed to the diffraction planes; (100), (101), (102) and (103) which is very close to reported standard values in the JCPDS-15-0105 card number.

From the XRD pattern, the films presents crystalline characteristics and the indexed planes (miller indices or hkl values) suggests a hexagonal wurtzite structure for the deposited CdSe:Eu films. The crystallite size corresponding to 2θ values of 28.93º, 30.62º, 34.98º and 51.05º are 38.95 nm, 25.30 nm, 24.16 nm and 21.89 nm respectively.

Other lattice parameters for the CdSe:Eu films have also been calculated from the relevant equations and presented in appendixes C17 and C18 respectively.

4.12 Surface morphology of CdSe:Eu film

4.12.1 Scanning electron microscopy (SEM) studies

The SEM micrographs of CdSe:Eu film at 360 ºC, flow-rate of 400 µL/spray (10% and 15% dopant concentrations) obtained are displayed in figures 4.36 (a-b).

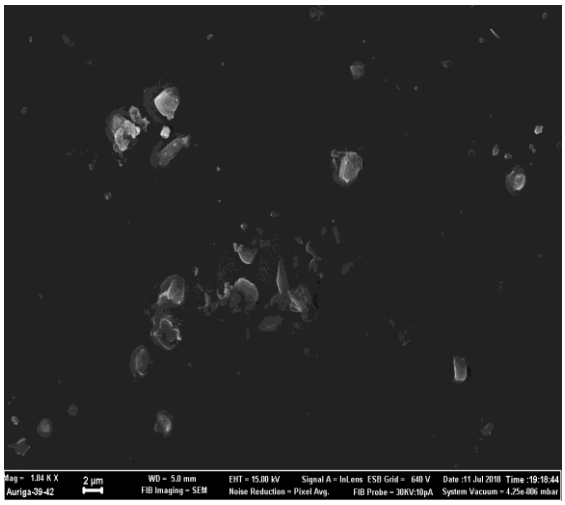

Figure 4.36a: SEM micrograph of CdSe:Eu film at 360 ^{o}C, 10% dopant concentration

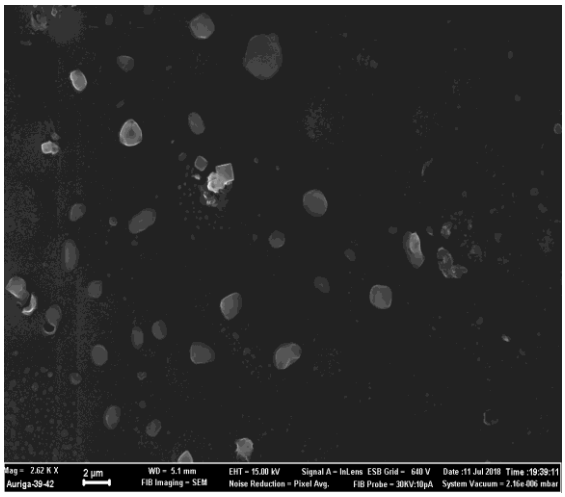

Figure 4.36b: SEM micrograph of CdSe:Eu film at 360 ^{o}C, 15% dopant concentration

From figures 4.36 (a-b), the film appears to have a smooth surface morphology. A very close look at the SEM images reveals the presence of very small spherical shapes (though, not uniformly spread) which indicate the growth of small crystallites on the surface of the film.

4.13 Optical absorption spectra of MgSe:Eu films

The absorption spectra for MgSe:Eu films obtained at different deposition temperatures, flow-rate and dopant concentrations are presented in figures 4.37 (a-c).

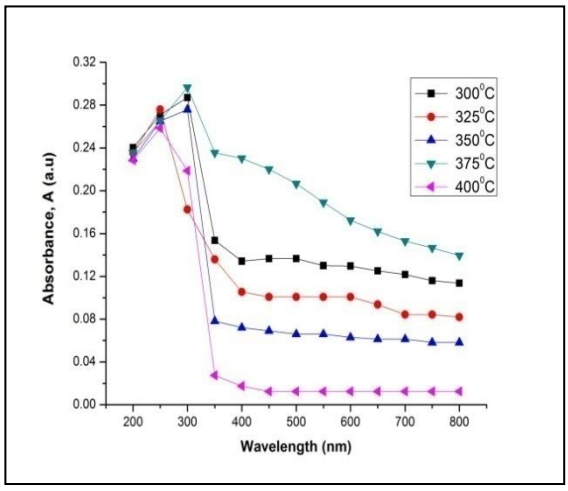

Figure 4.37a: Absorption spectra of sprayed Eu-doped MgSe films at different substrate temperatures

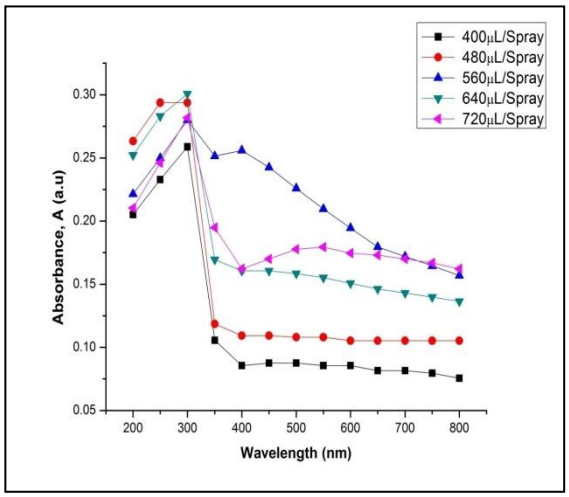

Figure 4.37b: Absorption spectra of sprayed Eu-doped MgSe films at different flow-rates

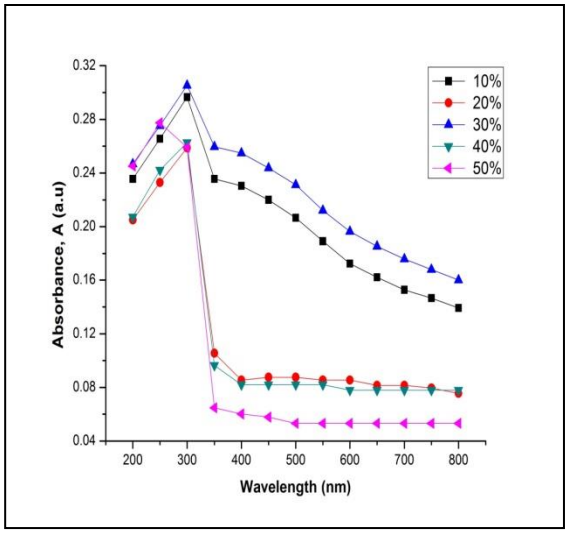

Figure 4.37c: Absorption spectra of sprayed Eu-doped MgSe films at different dopant concentrations

From figure 4.37a, all the films show very poor absorption throughout the visible region of the electromagnetic spectrum. The highest absorbance (29.66%) was observed in the visible region at a deposition temperature of 350 ^{o}C.

For the films deposited at different flow rates (figure 4.37b), minimal absorbance within the range of 10.55% to 25.87% at a flow rate of 400 μL/hr, 11.96% to 29.38% at the rate of 480 μL/hr, 22.15% to 28% at 560 μL/hr, 16.95% to 30.07% 640 μL/hr and 19.48% to 28.19% at a flow rate of 720 μL/hr throughout the UV region was observed. However in the visible region, all the films deposited at different flow rates exhibit very poor absorption of radiation within the range of 7.56% to 24.25%.

From figure 4.37c, the absorbance value lies within 6.47% to 30.53% in the UV region. In the visible region, absorbance values were within the range of 5.32% to 25.47% for all the deposited films. The results however indicate that MgSe:Eu films exhibited very poor absorption of electromagnetic radiation in the visible spectrum. The low absorption of light exhibited by these films in the visible region indicates that more light will be transmitted by the material in this region.

4.14 Optical transmission of the MgSe:Eu films

The percentage transmission curves of MgSe:Eu films deposited at different substrate temperatures are presented in figure 4.38a. The plot of transmission (%) against wavelength for the films deposited at different flow-rates is shown in figure 4.38b. The optical transmission curves for MgSe:Eu films deposited by varying the concentration of the dopant are presented in figure 4.38c.

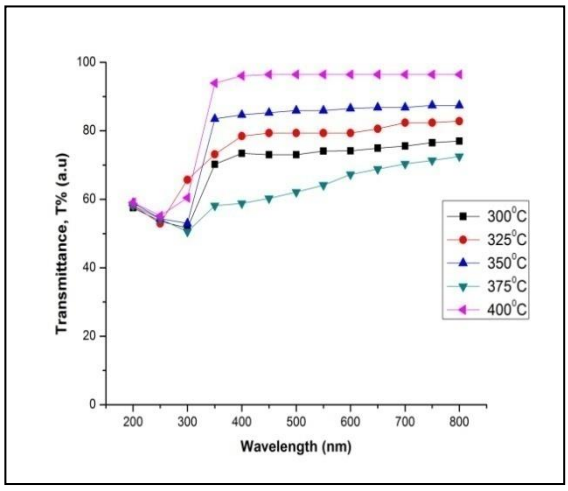

Figure 4.38a: Transmission spectra for MgSe:Eu films deposited at different substrate temperatures

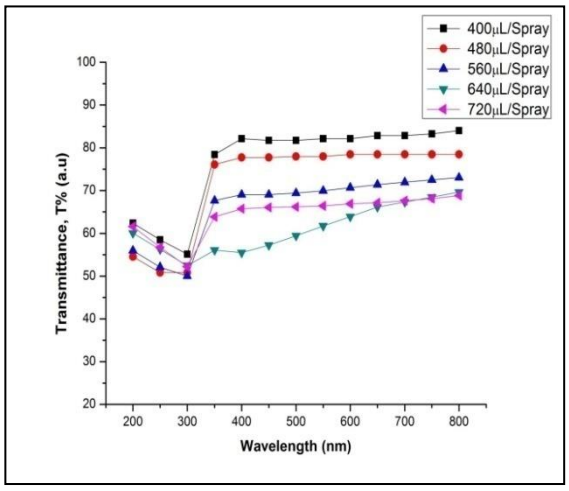

Figure 4.38b: Optical transmission spectra of MgSe:Eu films deposited at different flow rates

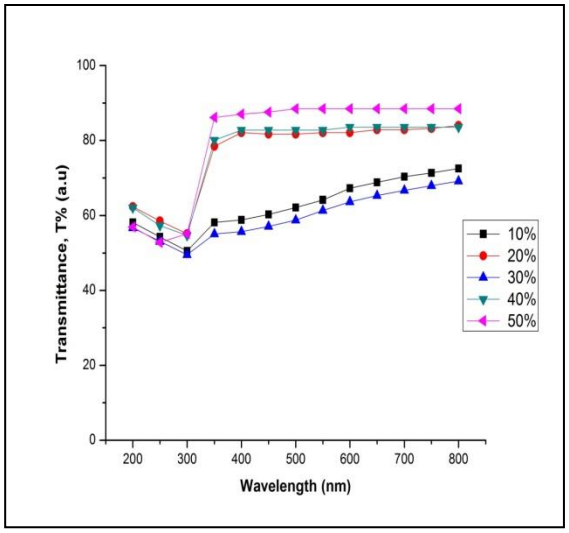

Figure 4.38c: Optical transmittance curves for MgSe:Eu films deposited at different variations of Europium concentrations

From figure 4.38a, for the film deposited at 300 ^{o}C, the optical transmission lies between 51.63% and 70.21% in the UV region while in the visible region, the transmission was in the range of 73.42% to 76.97% respectively. For the films deposited at 325 ^{o}C, the optical transmission varies between 52.97% and 81.94% in the UV region and 91.75% to 95.06% in

the visible region to near infra-red region. For the film deposited at 350 ^{o}C, transmission values were within the range of 50.51% to 58.14% in the UV region while transmission between 58.83% and 72.56% was recorded in the visible region of the electromagnetic spectrum. The film deposited at 375 ^{o}C had transmission in the visible region within the range of 84.72% to 87.46% and 52.98% to 83.52% in the UV region. The film deposited at 400 ^{o}C recorded the highest optical transmission in the visible region in the range of 96.07% to 96.47% while having transmission within the range of 55.16% to about 93.91% in the UV region.

For the films deposited at different flow-rates, figure 4.38b indicates that the optical transmission decreased in the visible region as flow rate increases from 400 μL/spray to 640 μL/spray and slightly increased when the flow rate was 720 μL/spray. A maximum optical transmission of 84.02% was recorded at 800 nm for films deposited at a flow rate of 400 μL/spray and 78.47% at 800 nm for films deposited 480 μL/spray. The films deposited at 560 μL/spray, 640 μL/spray and 720 μL/spray exhibited maximum transmission of 73.05%, 69.66% and 68.83% recorded at 800 nm respectively.

The films deposited at 10% concentration of Eu recorded optical transmission in the range of 50.51% to 58.14% in the UV region while 58.83% to 72.56% was recorded in the visible region of the electromagnetic spectrum. For the films obtained at 20% dopant concentration, transmission in the UV region varied from 55.12% to 78.43% while in the visible region, transmission was in the range of 81.73% to 84.02%. The films deposited at 30% dopant concentration recorded the lowest transmission in the range of 49.51% to 56.65% in the UV region and 55.63% to 69.18% in the visible region. The film deposited at 40% exhibited transmission of 54.63% to 80.09% in the UV region and 82.78% to 83.56% in the visible

region. The films deposited with 50% concentration produced the highest transmission in the range of 52.78% to 86.16% in the ultraviolet region and 87.08% to 88.47% in the visible region.

A careful observation of all the films obtained at different deposition conditions reveals that the films exhibited high transmission in the visible region. The high transmission exhibited by the MgSe:Eu films in the visible region of the electromagnetic spectrum makes the material applicable in manufacturing transparent products.

Another notable observation in figures 4.38a, 4.38b and 4.38c shows that for the films deposited at different substrate temperatures, the highest transmission was observed for the film obtained at 400 ^{o}C. For the films deposited at different flow rates, optimum transmission was observed at a flow rate of 400 μL/spray, while for films deposited by varying dopant concentration, the deposited film with 50% dopant concentration recorded the highest transmission. From the fore-going, it is suggested that for one to achieve the desired property of this material for several applications, the deposition parameters should be studied effectively and optimization done by taking the different deposition parameters into serious consideration. The results presented in this research clearly show that the film quality and properties depend on the deposition process and deposition parameters.

The values of the optical transmission for the MgSe:Eu films at different deposition conditions are presented in appendixes D4, D5 and D6 respectively.

4.15 Reflection spectra of MgSe:Eu films

The reflection spectra of MgSe:Eu films deposited at different substrate temperatures are presented in figure 4.39a. Figure 4.39b shows the reflection spectra of MgSe:Eu films

deposited at different flow rates. The reflection spectra of the MgSe:Eu films deposited at different concentrations of Eu are displayed in figure 4.39c.

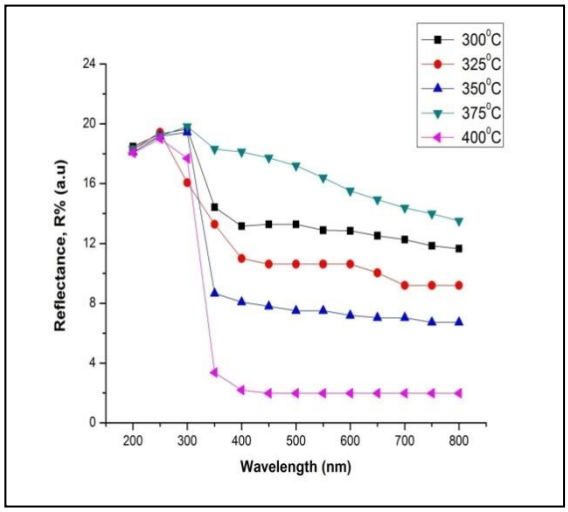

Figure 4.39a: Reflection spectra of MgSe:Eu films deposited at different substrate temperatures

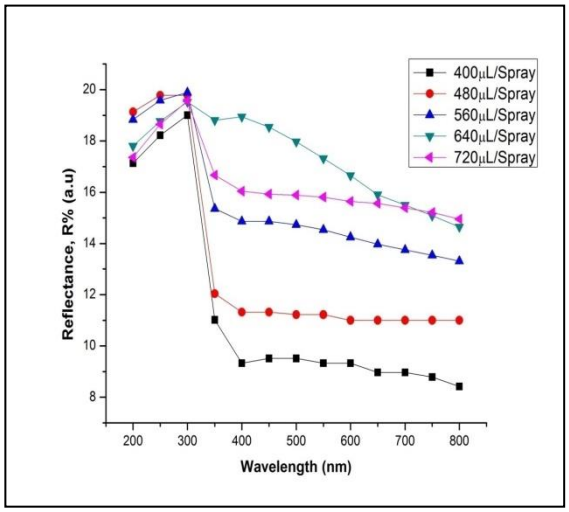

Figure 4.39b: Reflection spectra of MgSe:Eu films deposited at different flow-rates

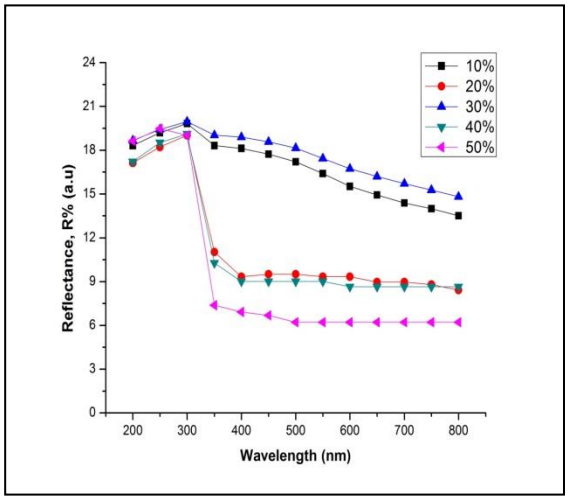

Figure 4.39c: Reflection spectra of MgSe:Eu films deposited at different concentrations of europium

From figure 4.39a, the reflection spectra of the films deposited at different substrate temperatures are observed to decrease with increasing wavelength in the visible region. The

films exhibited poor reflection of light throughout the UV-VIS region of the electromagnetic spectrum. The reflection values of the films were within the range of 1.97% to 19.83% for the range of temperature (300 ^{o}C to 400 ^{o}C) under investigation.

From figure 4.39b, reflection spectra shows that MgSe:Eu films exhibited poor reflection throughout the UV-VIS region with the visible region recording the lowest range of reflection values for all the deposited films. In the visible region, the films are observed to decrease steadily towards higher wavelengths. From figure 4.38b, reflection values for all the films are within the range of 8.42% to 19.89% throughout the UV-VIS region for the range of flow rate (400 μL/spray to 720 μL/spray) under study.

From figure 4.39c, the MgSe:Eu films deposited with different dopant concentrations also exhibited poor reflection of light. Reflectance values within the range of 6.21% to 19.96% were observed for all the deposited films throughout the ultraviolet and visible regions of the electromagnetic spectrum.

Appendixes D7, D8 and D9 contain the reflectance values of MgSe:Eu films at different deposition conditions.

4.16 Refractive index of the MgSe:Eu films

The refractive index values at different substrate temperature of the Eu-doped magnesium selenide films were calculated and plotted against photon energy as illustrated in figure 4.40.

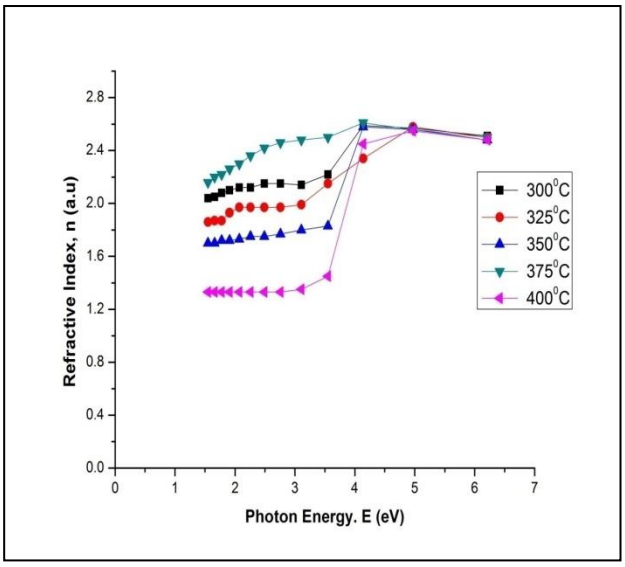

Figure 4.40: Refractive index of MgSe:Eu films plotted against photon energy at different substrate temperatures

From figure 4.40, the MgSe:Eu films deposited at 300 ^{o}C and 325 ^{o}C recorded refractive index within the range of 2.04 to 2.59 and 1.86 to 2.58 respectively. For the films deposited at 350 ^{o}C, 375 ^{o}C and 400 ^{o}C, refractive index is within the ranges of 1.70 to 2.68, 2.16 to 2.61 and 1.33 to 2.55 respectively. However, the MgSe:Eu films deposited at 300 ^{o}C to 375 ^{o}C show relatively high refractive index which suggests that MgSe:Eu would be a viable raw material for the fabrication of optoelectronic devices.

Appendix D10 displays the calculated refractive index values of MgSe:Eu films at different substrate temperatures.

4.17 Absorption coefficient of the MgSe:Eu films

The values of absorption coefficient of the MgSe:Eu films at different substrate temperatures are plotted against photon energy as shown in figure 4.41.

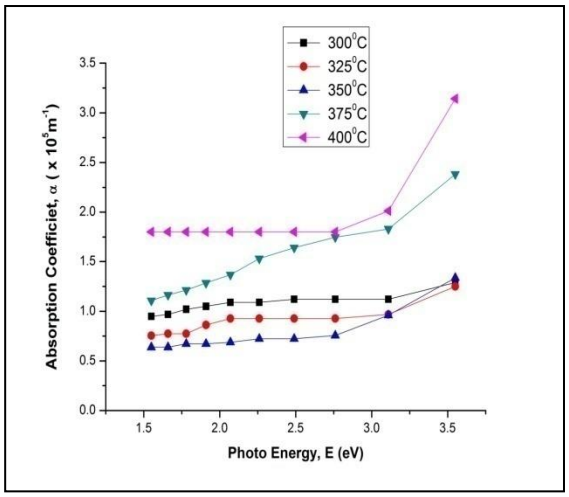

Figure 4.41: Absorption coefficient of MgSe:Eu films versus photon energy at different substrate temperatures

From figure 4.41, absorption coefficient within the range of about 0.950 x 10^5 m^{-1} to 1.29 x 10^5 m^{-1} was observed for the film deposited at 300 ^oC. For the films deposited at 325 ^oC and 350 ^oC, absorption coefficient values were within 0.755 x 10^5 m^{-1} to 1.25 x 10^5 m^{-1} and 0.638 x 10^5 m^{-1} to 1.337 x 10^5 m^{-1} while absorption coefficient between 1.106 x 10^5 m^{-1} and 2.381 x 10^5 m^{-1} was observed for the films obtained at substrate temperature of 375 ^oC. For the films obtained at 400 ^oC, absorption coefficient ranged between 1.8 x 10^5 m^{-1} to 3.142 x 10^5 m^{-1}.

The absorption coefficient values of MgSe:Eu films are displayed in appendix D11.

4.18 Optical conductivity of MgSe:Eu films

The optical conductivity values of MgSe:Eu films were obtained for different substrate temperatures and plotted against photon energy as shown in figure 4.42.

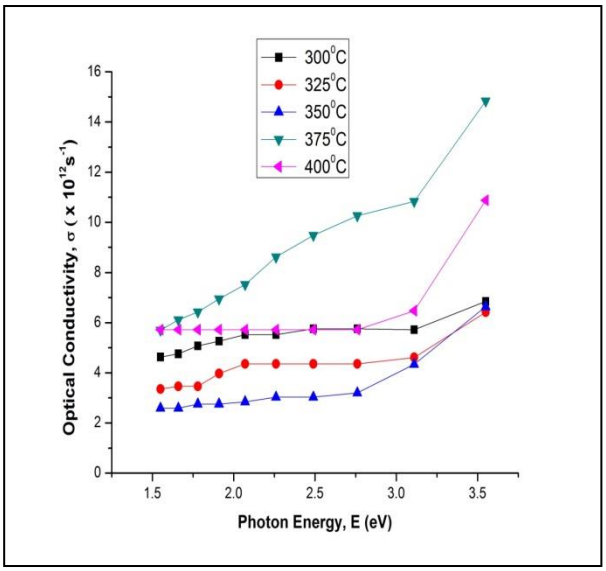

Figure 4.42: Optical conductivity of MgSe:Eu films versus photon energy at different substrate temperatures

Optical conductivity in all cases of temperature variation increases sharply at high photon energies and are between 2.589 x 10^{12} s^{-1} and 14.84 x 10^{12} s^{-1} for deposition temperature between 300 ^{o}C and 400 ^{o}C respectively.

The values of optical conductivity for MgSe:Eu films at different substrate temperatures are given in appendix D12.

4.19 Extinction coefficient of MgSe:Eu films

Figure 4.43 reveals the plot of extinction coefficient at different substrate temperature versus photon energy.

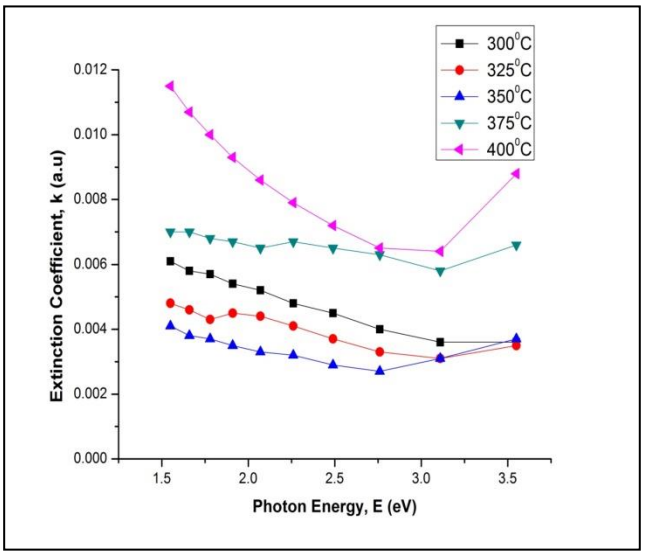

Figure 4.43: Extinction coefficient of MgSe:Eu films versus photon energy at different substrate temperatures

From figure 4.42, the extinction coefficient values in all cases were observed to decrease steadily as photon energy increases and slightly increased further. The extinction coefficient values of the MgSe:Eu films are very small within the range of 0.0027 to 0.0115 for all deposition conditions. The low extinction coefficient (k) confirms high transparency of the films (Amatalo, 2014).

Appendix D13 displays the values of extinction coefficient of MgSe:Eu films at different substrate temperatures.

4.20 Real dielectric constant of MgSe:Eu films

Figure 4.44 displays the plot of real dielectric constant of MgSe:Eu films at different substrate temperature against photon energy.

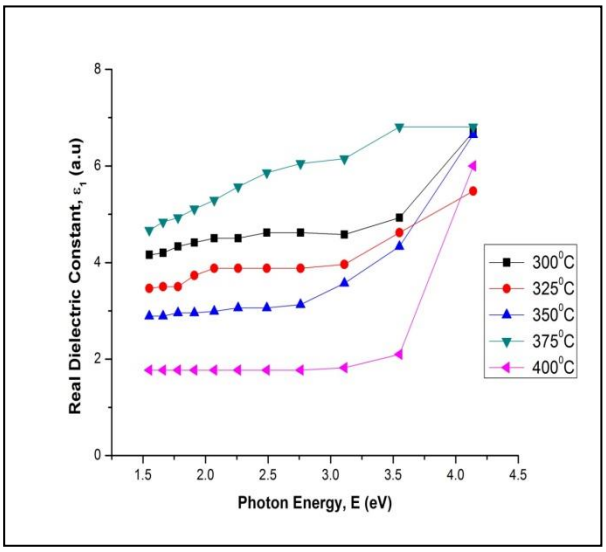

Figure 4.44: Real dielectric constant of MgSe:Eu films versus photon energy at different substrate temperatures

For the films deposited between 300 ^{o}C and 375 ^{o}C, real dielectric constant increases steadily with photon energy. However, for the MgSe:Eu film deposited at 400 ^{o}C, real dielectric constant values were observed to be constant at low photon energies (corresponding to the visible region) and increases very sharply at high photon energy (corresponding to the near ultra-violet region).

The values employed in plotting figure 4.44 are displayed in appendix D14.

4.21 Imaginary dielectric constant of MgSe:Eu films

The plot of imaginary dielectric constant of MgSe:Eu films at different substrate temperatures against photon energy is displayed in figure 4.45.

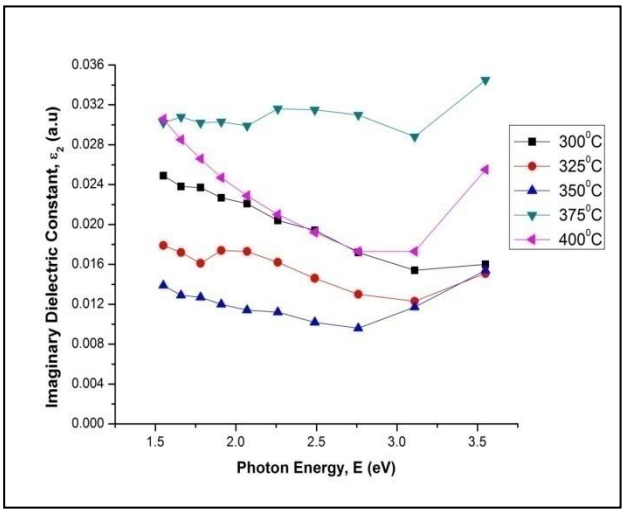

Figure 4.45: Imaginary dielectric constant of MgSe:Eu films versus photon energy at different substrate temperatures

From figure 4.45, the values of imaginary dielectric constant of the MgSe:Eu films decreases as photon energy increases and thereafter increases slightly as photon energy increases.

The values employed in plotting the graph are presented in appendix D15.

4.22 Band gap energy of MgSe:Eu films

Figure 4.46 shows the plot of $(\alpha h\nu)^2$ versus photon energy for the MgSe:Eu films for different deposition temperatures.

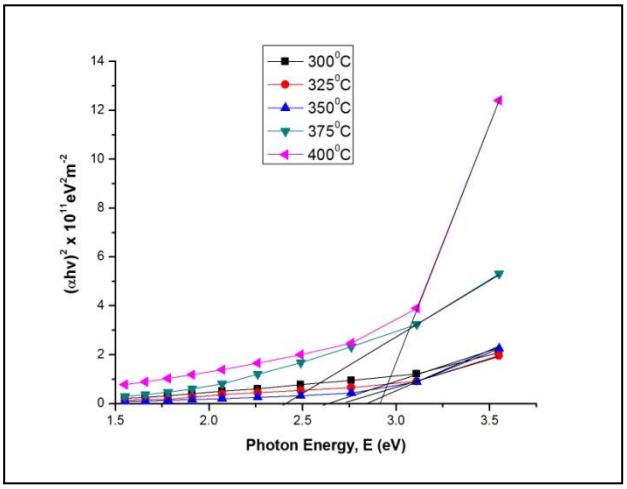

Figure 4.46: Plot of $(\alpha h\nu)^2$ versus photon energy for MgSe:Eu films at different substrate temperatures

From figure 4.46, the band gaps of the films are within the range of 2.49 eV to 2.95 eV depending on the substrate temperature. The band gap energy is observed to increase slightly with temperature between 300 ^{o}C and 350 ^{o}C, reduces at 375 ^{o}C and further increased at 400 ^{o}C. However, a clear observation shows that the band gaps of MgSe:Eu films are thickness dependent such that the obtained band gaps decreased with increasing thickness (band gap increases with thickness reduction).

Appendix D16 shows the values of $(\alpha hv)^2$ for MgSe:Eu films at different substrate temperatures.

Table 4.5 displays the band gap energies at different substrate temperatures for the MgSe:Eu films.

Table 4.5: Band gap energies of MgSe:Eu films at different substrate temperatures

Temperature (^{o}C)	Band Gap Energy, E (eV)
300	2.65
325	2.75
350	2.85
375	2.49
400	2.95

From table 4.5, the band gap energy increases with increase in temperature up to 350 ^{o}C, decreased at 375 ^{o}C and further increased at 400 ^{o}C. The distortion in trend could be as a result of the strain and cracks observed in the structure of the films.

4.23 Structural characterization of MgSe:Eu films

4.23.1 X-ray diffraction (XRD) analysis

The x-ray diffractogram of the Eu-doped MgSe films obtained at a deposition temperature of 350 ^{o}C, flow-rate of 480 μL/spray and 10% dopant concentration is displayed in figure 4.47a. The diffractogram of Eu-doped MgSe films obtained at 350 ^{o}C, flow-rate of 480 μL/spray and 40% dopant concentration is displayed in figure 4.47b.

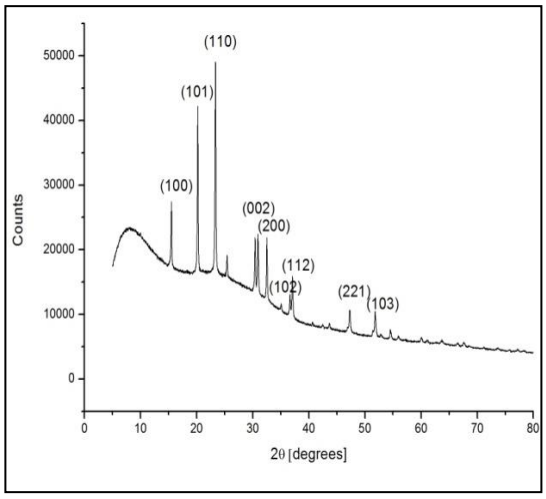

Figure 4.47a: X-ray diffractogram of MgSe:Eu films at 350 ^{o}C and 10% dopant concentration

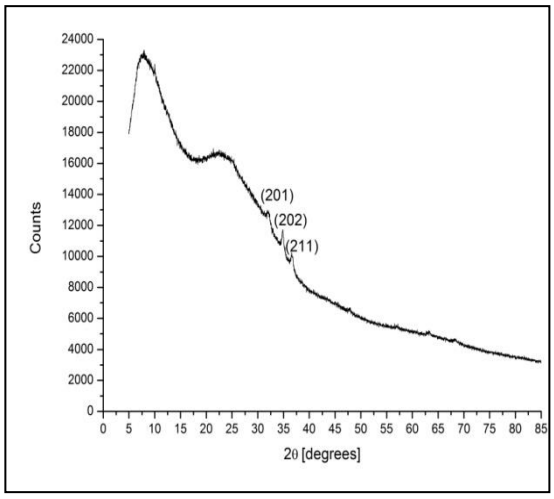

Figure 4.47b: X-ray diffractogram of MgSe:Eu films at 350 ^{o}C and 40% dopant concentration

From figure 4.47a, multiple planes of reflection are observed from the XRD pattern of the grown MgSe:Eu films. The x-ray diffractogram indicates the films are polycrystalline. The diffraction patterns are indexed to the (100), (101), (110), (002), (200), (102), (112), (221) and

(103) planes with corresponding 2θ values: 15.68º, 20.37º, 23.53º, 30.67º, 32.68º, 36.77º, 37.21º, 47.43º and 51.97º respectively. The most prominent reflection planes; (100), (101), (110), (002), (200), (102), (112) and (103) clearly suggests a hexagonal structure.

The peak at 2θ equals 23.53º recorded the highest intensity indicating the preferred growth angle which has been indexed to the (110) plane. The lattice constant for the (110) plane was calculated to be about 5.3427 Å which is lower than the reported standard value (5.462 Å) published by National Bureau of Standards, (1967) for MgSe films.

From figure 4.47b, the reflections are indexed to (101), (110), (002) and (200) planes which clearly indicates a hexagonal structure for the film. The reflection angles corresponding to the indexed planes have 2θ values at 15.58º, 20.26º, 23.43º, 30.46º and 32.57º respectively.

By comparison of figures 4.47a and 4.47b, it is observed that the number of prominent peaks decreased substantially when the dopant concentration was increased to 40%. This is an indication that as the dopant levels increases, a distortion in the crystallinity of the material occurs, thus resulting in decrease in intensity of the peaks.

Other structural parameters have been estimated from the relevant equations and are tabulated in appendixes D18 and D19 respectively.

4.24 Surface morphology studies

4.24.1 Scanning electron microscopy (SEM)

The SEM image of MgSe:Eu film at 350ºC, doping concentration of 10% and flow rate of 480 μL/spray was obtained at different resolutions and displayed in figures 4.48 (a-b). The SEM image of the MgSe:Eu film obtained at 350 ºC, 480 μL/spray and 40% dopant concentration is displayed in figure 4.48c.

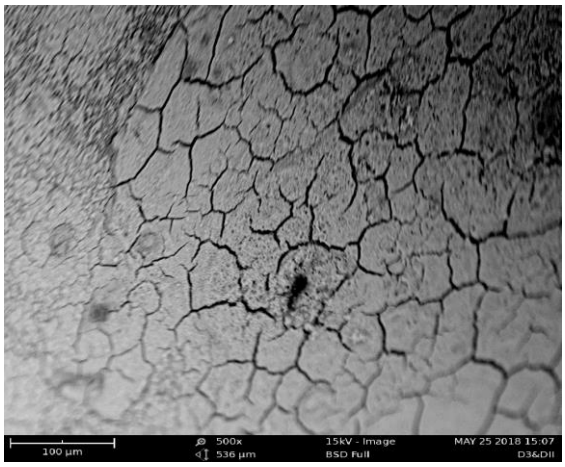

Figure 4.48a: SEM micrograph of MgSe:Eu film at a resolution of 500x

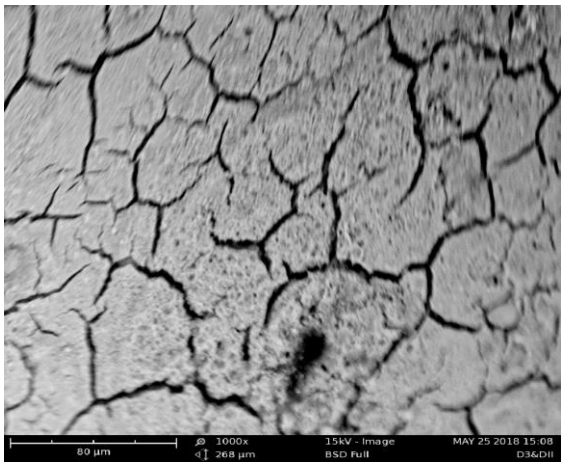

Figure 4.48b: SEM micrograph of MgSe:Eu film at a resolution of 1000x

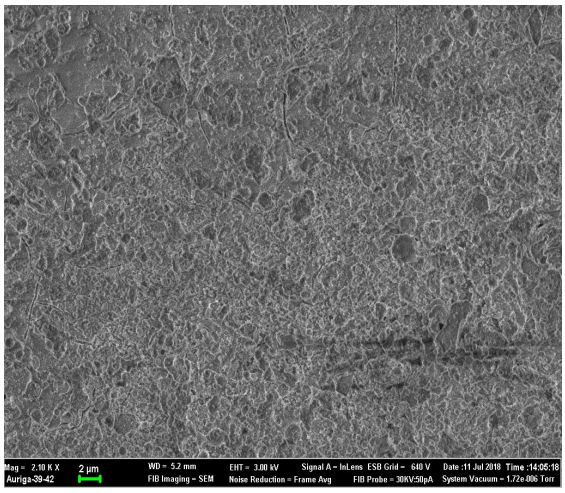

Figure 4.48c: SEM micrograph of MgSe:Eu film at 350 ºC, 480 µL/spray and 40% dopant concentration

From figures 4.48a and 4.48b, the SEM image indicates the agglomerate of small grains. However, cracks are visible on the surface of the film which indicates the grown film is rough and highly strained.

From figure 4.48c, the SEM image shows the formation and agglomeration of many small grains resulting from increased dopant concentration.

4.25 Elemental composition of all the films

The elemental compositions of all the films were obtained by Energy Dispersive X-ray Analysis (EDX) and are displayed in figures 4.49a to figure 4.49f.

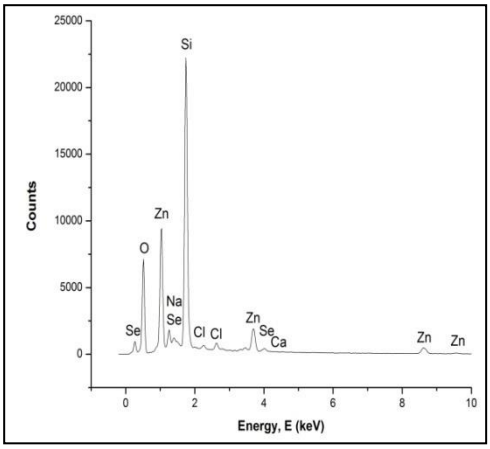

Figure 4.49a: EDX spectra of ZnSe film deposited at 300 ^{o}C

Peaks corresponding to zinc and selenium are obvious from the EDX spectra which indicate the growth of ZnSe film. Other peaks corresponding to silicon (Si), sodium (Na) and calcium (Ca) are due to the glass substrate used for the deposition process while the oxygen peak observed may be as a result of atmospheric exposure. The presence of chlorine (Cl) peak is from the hydrochloric acid used for the stabilization process.

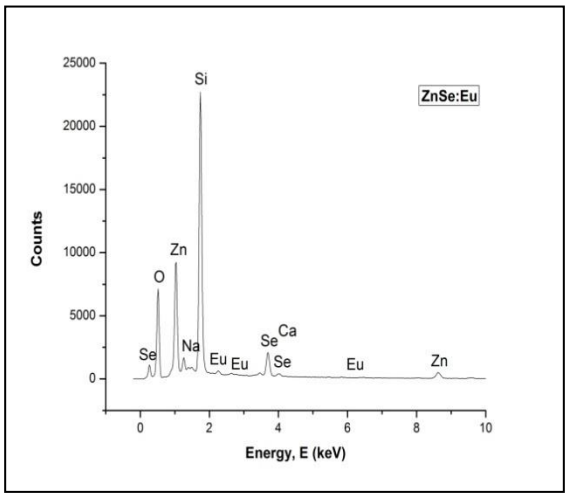

Figure 4.49b: EDX spectra of ZnSe:Eu film obtained at 375 ^{o}C

From figure 4.49b, peaks corresponding to zinc, selenium and europium are obvious from the EDX spectra which indicate the growth of ZnSe:Eu film. The peaks corresponding to silicon (Si), sodium (Na) and calcium (Ca) are due to the silicon substrate used for the deposition process while the presence of oxygen (O) peak may be due to atmospheric exposure.

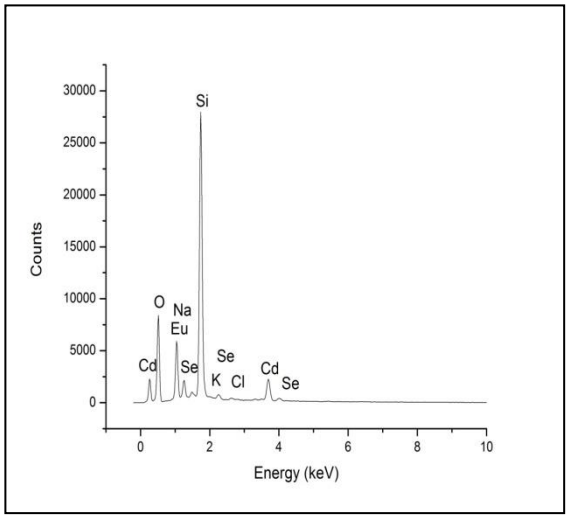

Figure 4.49c: EDX spectra of CdSe:Eu film obtained at 360 ºC, 10% dopant concentration

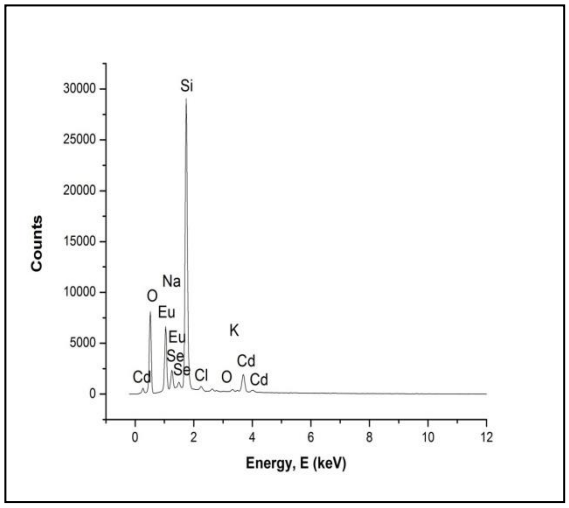

Figure 4.49d: EDX spectra of CdSe:Eu film obtained at 360 ºC, 15% dopant concentration

Peaks corresponding to cadmium (Cd), selenium (Se) and europium (Eu) are obvious from the EDX spectra (figures 4.49c and 4.49d) which indicate the growth of CdSe:Eu film. The peaks corresponding to Si, Na, and K are due to the glass substrate used for the deposition process. The chlorine (Cl) peak is as a result of the HCl used in the deposition process while the oxygen (O) peak is possibly due to atmospheric exposure.

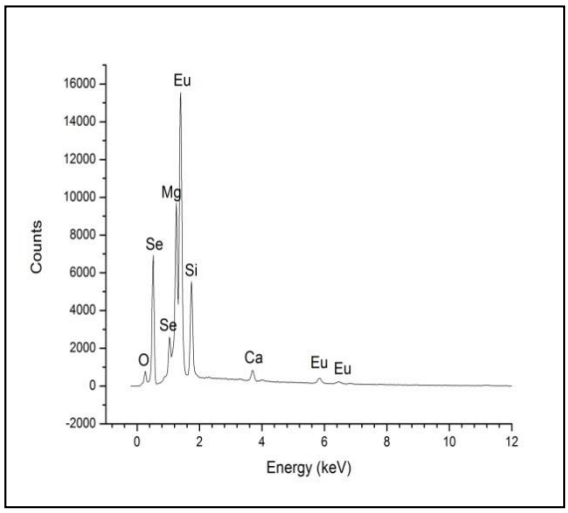

Figure 4.49e: EDX spectra of MgSe:Eu film obtained at 350 ºC and 10% dopant concentration

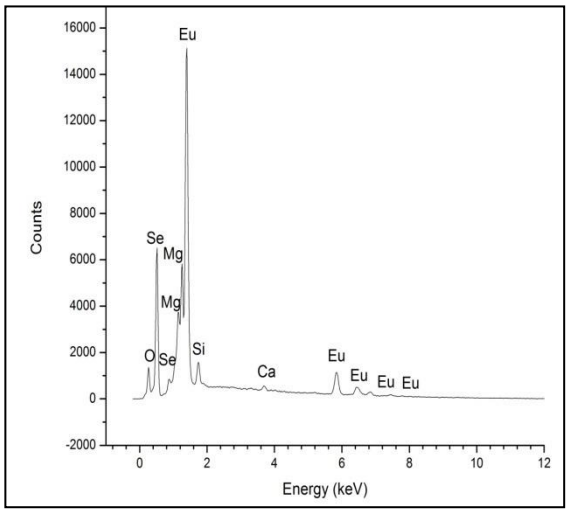

Figure 4.49f: EDX spectra of MgSe:Eu film obtained at 350 ºC and 40% dopant concentration

Peaks corresponding to magnesium, selenium and europium are obvious from the EDX spectra which indicate the growth of MgSe:Eu film. The peaks corresponding to silicon (Si) and Calcium (Ca) are due to the silicon substrate used for the deposition process while the oxygen (O) peak may be as a result of atmospheric exposure.

CHAPTER FIVE

SUMMARY, CONCLUSION AND RECOMMENDATIONS

5.1 Summary

This research is centered on the deposition of ZnSe, ZnSe:Eu, CdSe:Eu and MgSe:Eu films onto glass substrates by electrostatic spray pyrolysis technique. In the course of growing the films, three spray parameters (temperature, flow rate and dopant concentration) were varied at steps of five percent (5%) apart. After growth of the films, the thickness was obtained by surface profile analysis. The optical, structural, surface morphology properties and the elemental composition of the films were obtained by the appropriate techniques.

Optical studies conducted on ZnSe indicate the films show poor absorption and reflection of light in the visible region of the electromagnetic spectrum and moderate absorbance in the ultraviolet region. However, due to low absorption of light, transmission of the ZnSe films in the visible region was high. The diffraction pattern for the ZnSe film obtained at 300 ^{o}C indicates the film is amorphous which can be attributed to the low deposition temperature. At low deposition temperature for ZnSe film, the film was observed to be a bit rich in solvent thus resulting in amorphous nature. However, for the film deposited at 350 ^{o}C, crystalline film possessing the hexagonal phase structure was obtained. The SEM image obtained indicates that the films are smooth with some small spots observed on the surface which may be a collection of some smaller grains.

For the ZnSe:Eu films, optical studies show very poor absorption and reflection of light in the visible region of the electromagnetic spectrum. When compared with the pure ZnSe films, the ZnSe:Eu films possess a higher transmission of visible light. Due to the very high transmittance exhibited by Eu-doped ZnSe films, it is concluded that the material will prove

absolutely useful in coating airplane windows in order to help maintain transparency at all weather conditions. XRD results indicated that the ZnSe:Eu film obtained at 350 ^{o}C (10% dopant concentration) is polycrystalline in nature having the hexagonal phase. The ZnSe:Eu film obtained at 350 ^{o}C (20% dopant concentration) also possess the hexagonal structure but was observed to have reduced sharp peaks as a result of the increased dopant concentration. SEM images obtained revealed the formation of cotton-like morphology for the films. This is as a result of the fact that as the solution containing ZnSe:Eu is sprayed on the hot substrate, the water content present evaporates due to the high deposition temperature resulting in the formation of the cotton-like morphology.

Extremely low absorption and reflection of visible light was observed for the CdSe:Eu films at different deposition conditions. The films possess very high transmission of light (96.85% to 98.33%) for different temperature variation in the visible region of the electromagnetic spectrum. These optical properties exhibited by CdSe:Eu films clearly suggests that the material will be of immense use in the manufacture of optoelectronic devices and coating of airplane windows respectively. XRD analysis suggests polycrystalline nature having the hexagonal phase of CdSe. SEM micrograph shows the CdSe:Eu films possess a smooth surface morphology with the presence of very small spherical spots which is an indication that the films were slightly strained.

Optical analysis of the MgSe:Eu films reveals that in all deposition conditions and variations, the films exhibited low absorption and reflection of visible light while transmission of visible light was a bit high. The XRD diffractograms of the Eu-doped MgSe films obtained at a deposition temperature of 350 ^{o}C, deposition time of 10mins and 10% and 40% dopant concentrations were studied. The X-ray Diffractogram indicates the films in both cases are

polycrystalline with the film deposited at 10% showing more sharp peaks than the film deposited at a higher dopant concentration. SEM image obtained indicates the MgSe:Eu film contains some small grains with cracks visible all over the surface of the films. The cracks observed help one to conclude that the film is rough and highly strained.

In all cases of deposition of the films reported in this research, band gap energy calculated reveals a strong blue shift from the bulk value of each of the materials. This observation is as a result of strong quantum confinement occurring within the crystals which explains the fact that the electrons are in a bound state. Such is expected when the dimensions of a semiconductor material approaches the nanoscale range where the properties of the material are size dependent.

5.2 Conclusion

Electrostatic spray pyrolysis was successfully used to grow ZnSe, ZnSe:Eu, CdSe:Eu and MgSe:Eu films at different variations respectively. Optical studies on ZnSe films show the films are highly transparent in the visible region of the electromagnetic spectrum. However, optical transparency was improved for the ZnSe:Eu films which can be attributed to the inclusion of europium ion to the ZnSe crystal. The CdSe:Eu and MgSe:Eu films equally exhibited high transparency in the visible region. The optical results obtained help draw the conclusion that all the deposited films in this research will be very useful for manufacturing optoelectronic devices, optical lenses, coating of transparent materials and can also be used as a window layer in solar cells. Interference pattern observed for the films suggests the films are specula (smooth).

5.3 Contributions to knowledge

This research has contributed to knowledge in the following ways:

The technique (Electrostatic spray pyrolysis) employed for growing the films is a novel technique for the growth of ZnSe, ZnSe:Eu, CdSe:Eu and MgSe:Eu films. Report in the literature either electronically or in print on the growth of these films using this technique is missing.

Very few reports are available on the detailed analysis of the optical properties of ZnSe and ZnSe:Eu films. In this research, a detailed analysis of the optical properties at different temperature variations is presented. Also, analysis of the optical properties of ZnSe and ZnSe:Eu films at different volumes of spray solution is reported in this research which is unavailable in reported literatures.

In this research, a detailed report on the optical properties for CdSe:Eu is reported. To the best of my knowledge, the parameters varied and the range considered for depositing CdSe:Eu films has not been found in previous literatures.

Some few reports on the deposition of MgSe films are evident in reported literatures. However, for the first time, MgSe:Eu films have been deposited and characterized for its optical, structural and surface morphological properties by a novel technique.

It has been further established in this research that the properties and characteristics of nanomaterials are quite different from their bulk counterparts.

5.4 Recommendations

To further suggest suitable applications and a better understanding of the ZnSe, ZnSe:Eu, CdSe:Eu and MgSe:Eu films, the following studies may be carried out on the stated materials:

Optimization of deposition conditions for the films. Transmission Electron Microscopy (TEM) and Atomic Force Microscopy (AFM) studies should be performed to get a proper understanding of the surface morphology. Photoluminescence studies should be performed on the materials. Magnetic characterization of the films should be performed in order to effectively explain the magnetic properties.

REFERENCES

Abdolmadjid N. (2010). Ferromagnetism and transport in diluted magnetic semiconductors. *An unpublished Ph.D dissertation submitted to the graduate faculty of the Louisiana State University and Agricultural and Mechanical College, U.S.A.*

Alagarasi, A. (2011). Introduction to nanomaterials. *Retrieved from https://nccr.iitm.ac.in/2011.pdf on 17/09/2016 at 10:56pm.*

Al-Mashhadany, A.N. and Sadeq, N.S. (2007). The effect of annealing temperatures on optical and electrical properties of PbTe thin films. *Engineering and Technology, 25(10), 1171-1183.*

Aly, S., Akl, A.A.S. and Howari, H. (2015): Effect of pulsed laser power annealing on structural and optical characteristics of ZnSe Thin films. *Acta Physica Polonica A, 128(2), 414-418.*

Amatalo, I. (2014). Fabrication and characterization of Al/ZnSe thin film schottky diode. *Unpublished M.Sc project, Kenyatta University, Kenya.*

Amiri, G.R., Fatahian, S. and Mahmoudi, S. (2013). Preparation and optical properties assessment of CdSe quantum dots. *Materials Science and Applications, 4, 134-137.*

Anuar, K., Tan, W.T., Ho, S.M., Shanthi, M. and Saravanan, N. (2010). Effect of bath temperature on the chemical bath deposition of PbSe thin films. *Kathmandu University Journal of Science, Engineering and Technology, 6(2), 126-132.*

Atsuya, T. Manickam, S., Kyuichi, Y., Toru, T. Teruyuki, K. and Yasuo, I. (2008). Synthesis of europium-doped yttrium hydroxide and yttrium oxide nanosheets. *Journal of Materials Science 43: 1214–1219.*

Avadhanulu, M.N. and Kshirsagar, P.G. (2008). *A Textbook on Engineering Physics.* New Delhi, India: Chand and Company Publishers.

Barron, A.R. (2009): Chemical vapour Deposition. *Retrieved from http://cnx.org/content/m25495/latest/ on 7/7/2011 at 11:29am.*

Bhuiyan, M.R.A., Miah, M.A.H. and Begum, J. (2012). Substrate temperature effect on the structural and optical properties of ZnSe thin films. *Journal of Bangladesh Academy of Sciences, 36(2), 233-240.*

Buba, A.D.A. (2016): Optoelectronic properties of zinc selenide (ZnSe) thin films deposited using chemical bath deposition (CBD) technique. *British Journal of Applied Science & Technology, 14(3), 1-7.*

Carlsson, J.O. and Martin, P.M. (2010). Chemical vapour deposition. In P.M. Martin (Ed.), *Handbook of Deposition Technologies for Films and Coatings: Science, Applications and Technology.* (pp. 314-363).

Chen, C.Y., Tseng, T.K., Tsai, S.C., Lin, C.K., Lin, H.M. (2006). Effect of precursor characteristics on zirconia and ceria particle morphology in spray pyrolysis. *Ceramics International, doi:10.1016/j.ceramint.2006.10.013.*

Creighton, J.R. and Ho, P. (2001). Introduction to chemical vapour deposition. *ASM International Publishers, Materials Park, Ohio, USA. www.asminternational.org*

Dawood, Y.Z., Hassoni, M.H. and Mohamad, M.S. (2014): Effect of solution concentration on some optical properties of indium oxide doped with SnO_2 thin films prepared by chemical spray pyrolysis technique. *International Journal of Pure and Applied Physics, 2(1), 1-8.*

Desai, H.N., Dhimmar, J.M. and Modi, B.P. (2015). Study of linear and non-linear optical parameters of zinc selenide thin film. *International Journal of Engineering Research and Applications, 5(6), 117-122.*

Deshpande, M.P., Chaki, S.H., Patel, N.H., Bhatt, S.V. and Soni, B.H. (2011). Study on nanoparticles of ZnSe synthesized by chemical method and their characterization. *Journal of Nano- and Electron Physics, 3(1), 193-202.*

Dietl, T. (1994). Diluted Magnetic Semiconductors. In T.S. Moss (Ed.), *Handbook on Semiconductors* (pp. 1251-1324). Elsevier Science Publishers.

Dongsheng, L., Zang, X., Jin, L., Yang, D. (2010). Structure and Luminescence Evolution of Annealed Europium-doped Silicon Oxides Films. *Optics Express, 18(26), 27191-27196.*

Fakhururrazi, A., Josephine, L.Y.C., Zainal, A.T., Wahmood, W.W.Y., Leong, Y.J., Lee, H.K., Chang, F.D. and Burhanuddin, Y.M. (2016). Optical characterization of colloidal zinc selenide quantum dots prepared through hydrothermal method. *Sains Malaysiana, 45(8), 1191–1196.*

Feymann, R.P. (1959): Plenty of Room at the Bottom. *Retrieved from www.pa.msu.edu/~yang/RFeymann_plentySpace.pdf on 23/7/2015 at 1.03 pm.*

Filipponi, L. and Sutherland, D. (2013). Nanotechnologies: Principles, applications, implications and hands-on activities. *Published by European Commission, Luxembourg.*

Fox, M. (2001): Optical properties of solids, first ed., pp. 9, Oxford University Press, New York.

Ghaffarian, H. R., Saiedi, M.S., Mohammad, A. and Rashidi, A.M. (2011). Synthesis of ZnO nanoparticles by spray pyrolysis method. *Iranian Journal of Chemistry and Chemical Engineering, 30(1), 1-6.*

Ghosh (2009). Introduction to Nanomaterials and Nanotechnology. *Retrieved from www.nptel.ac.in on 4/04/2017 at 11.08pm.*

Girija, K., Thirumalairajan, S., Mohan, S.M., Chandrasekaran, J. (2009). Structural and optical characteristics of CdSe thin films prepared by chemical bath deposition technique. *Iraqi Journal of Applied Physics Letters, 2(4).*

Gnanamuthu, S.J., Jeyakumar, S.J., Balu, A.R., Usharani, K., Nagarethinam, V.S. (2015). characteristic analysis on the physical properties of nanostructured MgSe thin films – substrate temperature effect. *International Journal of Thin Films Science and Technology, 4(2), 121-123.*

Gorer, S.A., Albu, Y. and Hodes, G. (1995). Quantum size effects in chemically deposited nanocrystalline lead selenide films. *Journal of Physical Chemistry, 16442.*

Howari, H. (2012). Influence of pulsed laser annealing on the optical properties of thermally evaporated ZnSe thin films. *Journal of Natural Science and Mathematics, 5, 139-154.*

Igwebuike, H.N. and Okoli, D.N. (2017). Optical, electrical and structural properties of zinc selenide semiconductor nanofilms deposited by electrodeposition technique. *IOSR Journal of Applied Physics, 9(3), 40-44.*

Islam, A., Das, C., Choudhury, S., Sharmin, M. and Begum, T. (2014). Structural and optical characterization of vacuum evaporated zinc selenide thin films. *European Scientific Journal, 10(15), 241-253.*

Ivashchenko, M.M., Opanasyuk, A.S., Buryk, I.P., Lutsenko, V.A. and Shevchenko, A.V. (2017). Optical properties of pure and Eu-doped ZnSe films deposited by CSVS technique. *Journal of Nano- and Electronic Physics, 9(1), 1-5.*

Jensen, K., Weldon, J., Garcia, H. and Zettl, A. (2007). Nanotube radio. *Nano Letters, American Chemical Society, 7(11), 3508-3511.*

Jeroh, M.D. (2012). Growth and characterization of antimony sulphide and copper-antimony thin films fabricated by solution growth technique. *An M.Sc Thesis Submitted to the Department of Physics/Industrial Physics, Faculty of Physical Sciences, Nnamdi Azikiwe University, Awka, Nigeria.*

Kalyana, C.P., Shuguang, D. and Rockstraw, D.A. (2009). Synthesis of nanowires by spray pyrolysis. *Journal of Sensors, Article ID 683280, 1-6. doi:10.1155/2009/683280*

Kariper, I.A., Baglayan, O. and Gode, F. (2014). Fabrication and optical characterization of CdSe thin films grown by chemical bath deposition. *Acta Physica Polonica A, 128(2B), 219-221.*

Kathalingam, A., Mahalingam, T. and Sanjeeviraja, C. (2007). Optical and structural study of electrodeposited zinc selenide thin films. *Materials Chemistry and Physics, 106, 215–221.*

Khan, T.M. and Bibi, T. (2012). Compatibility and optoelectronic of ZnSe nano crystalline thin film. *Chinese Physical Society B, 21(9), 097303-1 – 097303-6.*

Khairnar, U., Behere, S. and Pawar, P. (2012). Optical properties of polycrystalline zinc selenide thin films. *Materials Sciences and Applications, 3, 36-40.*

Kissinger, N.J.S., Velmurugan, N. and Perumal, K. (2009). Substrate-temperature-dependent structural and optical properties of ZnSe thin films fabricated by using an electron beam evaporation technique. *Journal of the Korean Physical Society, 55(4), 1577-1581.*

Kumar, P., Singh, J., Ramam, K. and Pandey, A.C. (2012). ZnSe/ZnSe:Ag nanoparticles: Synthesis, characterizations, optical and Raman studies. *Journal of Nanoscience and Nanotechnology, 12, 1-7.*

Kumar, M. (2015). Optical study of zinc selenide. *Indian Journal of Applied Research, 5(10), 511-512.*

Kumar, T.R., Prabukanthan, P., Harichandran, G., Theerthagiri, J., Moydeen, A.M., Durai, G., Kuppusami, P. and Tatarchuk, T. (2018). Comparative study of structural, optical and electrical properties of electrochemically deposited Eu, Sm and Gd doped ZnSe thin films. *Journal of Materials Science: Materials in Electronics.*

Lohar, G.M., Shinde, S.K. and Fulari, V.J. (2014). Structural, morphological, optical and photoluminescent properties of spray-deposited ZnSe thin film. *Journal of Semiconductors, 35(11), 1-5.*

Luo, L., Gong, L., Liu, Y.F., Chen, J., Ding, C.R., Tang, X.G., Li, X.L., Qiu, Z.R., Wang, H.Z., Chen, X.M., Li, K.F., Fan, H.H. and Cheah, K.W. (2010). Enhanced ultraviolet lasing from europium-doped zinc oxide nanocrystals. *Optical Materials, 32, 1066-1070.*

Lupan, O., Pauporte, T., Viana, B., Aschehoug, P., Ahmadi, M., Cuenya, B.R., Rudzevich, Y., Linc, Y., Chow, L. (2013). Eu-doped ZnO nanowire arrays grown by electrodeposition. *Applied Surface Science, 282, 782– 788.*

Mammadov, M.N., Aliyev, A.S. and Elrouby, M. (2012). Electrodeposition of cadmium sulfide. *International Journal of Thin Film Science and Technology, 1(2), 43-53.*

Mendelson, A. (2010). Identification and control of deposition processes. *An unpublished doctoral dissertation submitted to the faculty of electronics, communications and automation at the Aalto University School of Science and Technology, Espoo, Finland.*

Meshram, R.S. and Thombre, R.M. (2015). Structural and optical properties of CdSe thin films prepared by spray pyrolysis technique. *International Journal of Advances in Science Engineering and Technology, Special Issue (1), 167-170.*

Meshram, R.S. and Thombre, R.M. (2016). Structural and optical properties of ZnSe thin films prepared by spray pyrolysis technique. *International Journal of Recent Scientific Research, 7(3), 9579-9582.*

Minelli, C. (2004). Bottom-up approaches for organizing nanoparticles with polymers. *An unpublished Ph.D thesis submitted to the École Polytechnique Fédérale De Lausanne, Università degli Studi di Firenze, Italie.*

Minoru, I. and Jifeng, W. (2017). Wide-band gap II-VI semiconductors: Growth and properties. In S. Kasap, P. Capper (Eds.), *Handbook of Electronic and Photonic Materials* (pp. 365-383). USA: Springer International Publishing.

Mitra, P. and Mondal, S. (2013). Structural and morphological characterization of ZnO thin films synthesized by SILAR. *Progress in Theoretical and Applied Physics, 1, 17-31.*

Mote, V.D., Dargad, J.S. and Dole, B.N. (2013): Effect of Mn doping concentration on structural, morphological and optical studies of ZnO nano-particles. *Nanoscience and Nanoengineering, 1(2), 116-122.*

Murali, K.R., Dhanemozhi, A.C. and John, R. (2008). Structural, optical and electrical properties of brush plated ZnSe films. *Chalcogenide Letters, 5(11), 277-280.*

Muthumari, S., Devi, G., Revathi, P., Vijayalakshmi, R. and Sanjeeviraja, C. (2012). Structural investigation of zinc selenide thin films. *Journal of Applied sciences, 12(16), 1722-1725.*

Nai-Chang, Y. (2008). A perspective of frontiers in modern condensed matter physics. *AAPPS Bulletin, 18(2), 11-29.*

National Bureau of Standards (NBS) Monograph 25-Section 5 (1967), Card No: 53-61386.

Nweze, C.I. (2012). Electrodeposition and characterization of zinc selenide (ZnSe) nano and thin films. *An M.Sc thesis submitted to the department of physics/industrial physics, faculty of physical sciences, Nnamdi Azikiwe University, Awka, Nigeria.*

Okereke, N.A. and Ekpunobi, A.J. (2011). ZnSe buffer layer deposition for solar cell application. *Journal of Non-Oxide Glasses, 3(1), 31-36.*

Ompong, D. (2010). Investigating the optical properties of $Cd_{1-x}Zn_xS$ thin films deposited by the dip technique. *An M.Sc thesis submitted to the department of physics, faculty of the physical sciences, Kwame Nkrumah University of Science and Technology, Kumasi, Ghana.*

Ozutok, F., Erturk, K. and Bilgin, V. (2012). Growth, electrical and optical study of ZnS:Mn thin films. *Acta Physica Polonica A, 1 (121), 221-223.*

Pal, M., Pal, U., Jimenez, J.M.G.Y. and Rodriguez, F.P. (2012). Effects of crystallization and dopant concentration on the emission behaviour of TiO_2:Eu nanophosphors. *Nanoscale Research Letters, 7(1), 1-12.*

Paritosh, M., Bongsoo, K. and Jeunghee, P. (2007). Synthesis of single crystalline europium-doped ZnO nanowires. *Materials Science and Engineering B 138, 224–227.*

Park, J.H., Back, N.G., Hong, K.S., Kims, C.S., Yoo, D.H., Kwak, M.G., Han, J.I., Sung, J.H., Moon, B.K., Seo, H.J. and Choi, B.C. (2005). Annealing effect on photoluminescence intensity of Eu-doped Y_2O_3 nanocrystals. *Journal of the Korean Physical Society, 47, S368-S371.*

Pathan, H.M. and Lokhande, C.D. (2004). Deposition of metal chalcogenide thin films by successive ionic layer adsorption and reaction (SILAR) method. *Bulletin of Materials Science, 27(2), 85-111.*

Popa, M.E. and Rusu, G.I. (2011). Structural characteristics and optical properties of zinc selenide thin films. *Optoelectronics and Advanced Materials – Rapid Communications, 5(8), 842 – 845.*

Popkin, G. (2016). Physicist makes thin films for tough conditions. *American Physical Society Bulletin, 25, 1.*

Putut, M. Sugianto, S. and Wibowo, E. (2012). Growth of europium-doped gallium oxide (Ga_2O_3:Eu) thin films deposited by homemade DC magnetron sputtering. *Journal of Theoretical and Applied Physics, 6(17), 1-8.*

Raidou, A., Aggour, M., Qachaou, A., Laanab, L. and Fahoume, M. (2010). Preparation and characterization of ZnO thin films deposited by SILAR method. *Moroccan Journal of Condensed Matter, 12(2), 125-130.*

Shinde, S.S., Patil, P.S., Gaikwad, R.S., Mane, R.S., Pawar, B.N. and Rajpure, K.Y. (2010). Influences in high quality zinc oxide films and their photoelectrochemical performance. *Journal of Alloys and Compound, 503, 416-421.*

Singh, R.P., Tiwari, A., Choi, J.W. and Pandey, A.C. (2012). Smart nanomaterials for biosensors, biochips and molecular bioelectronics. In S. Li, Y.Ge, H. Li (Eds.), *Smart Nanomaterials for Sensor Application* (pp. 3-12). United Arab Emirates: Bentham Science Publishers.

Sulabha, K.K. (2015). *Nanotechnology: Principles and Practice.* Switzerland: Springer International Publishing.

Swapp, S. (2011). Scanning electron microscopy. *Retrieved from http://serc.carleton.edu/research_education/geochemsheets/techniques/ on 9/4/2011 at 2:15am.*

Sze, S.M. and Kwok, K.N. (2007). *Physics of semiconductor devices*. New Jersey, USA: John Wiley and Sons.

Tang, P.T. (2008). Utilising electrochemical deposition for micro manufacturing. In S. Dimov, W. Menz (Eds.) *Multi-Material Micro Manufacture* (pp. 1-10). United Kingdom: Whittles Publishing Ltd.

Tanvil, A. (2017). Investigation of structural, optical and electrical properties of zinc selenide thin films prepared by chemical bath deposition technique. *An M.Sc dissertation submitted to the department of physics, Bangladesh University of Engineering and Technology (BUET).*

Thirumavalavan, S., Mani, K. and Suresh, S. (2015). Structural, surface morphology, optical and electrical investigation of CdSe thin films. *Chalcogenide Letters 12(5), 237-246.*

Tsao, J.Y. (2004). The world of compound semiconductors: A guidebook to the core science and technology. Retrieved from https://www.sandia.gov on 15/09/2018 at 02:50am

Venkatachalam, S., Jeyachandran, Y.L. and Sureshkumar, P., Dhayalraj, A., Mangalaraj, D., Narayandas, S.K. and Velumani, S. (2007). Characterization of vacuum-evaporated ZnSe thin films. *Materials Characterization, 58, 794-799.*

Wei, C. Dongchen, Q., Xingyu, G. and Andrew T.S.W. (2009). Surface transfer doping of semiconductors. *Progress in Surface Science, 84, 279–321.*

Yadev, R.S., Pandey, A.C. and Sanjay, S.S. (2009). Optical properties of europium doped bunches of ZnO nanowires synthesized by co-precipitation method. *Chalcogenide Letters, 6(6), 233-239.*

APPENDIXES

Appendix A1: Absorption values of pure ZnSe films at different substrate temperatures

Wavelength (nm)	ZnSe A (300 °C)	ZnSe A (325 °C)	ZnSe A (350 °C)	ZnSe A (375 °C)	ZnSe A (400 °C)
200	0.3851	0.4414	0.3750	0.4128	0.3825
250	0.4628	0.5517	0.4563	0.4709	0.4488
300	0.5275	0.1241	0.5188	0.1715	0.1416
350	0.1073	0.0792	0.1469	0.1494	0.1298
400	0.0860	0.0609	0.1125	0.1171	0.0975
450	0.0552	0.0609	0.0625	0.0865	0.0711
500	0.0552	0.0609	0.0625	0.0865	0.0711
550	0.0552	0.0609	0.0625	0.0865	0.0711
600	0.0552	0.0609	0.0625	0.0865	0.0711
650	0.0552	0.0609	0.0625	0.0865	0.0711
700	0.0552	0.0609	0.0625	0.0865	0.0711
750	0.0552	0.0609	0.0625	0.0865	0.0711
800	0.0552	0.0609	0.0625	0.0865	0.0711

Appendix A2: Absorption values of pure ZnSe films at different flow rates

Wavelength (nm)	ZnSe A (400 µL)	ZnSe A (480 µL)	ZnSe A (560 µL)	ZnSe A (640 µL)	ZnSe A (720 µL)
200	0.3750	0.3940	0.3901	0.3818	0.3791
250	0.4563	0.4687	0.4613	0.4606	0.4567
300	0.5188	0.1642	0.1424	0.1485	0.1552
350	0.1469	0.1418	0.1217	0.1475	0.0469
400	0.0625	0.0558	0.0517	0.0412	0.0460
450	0.0625	0.0558	0.0517	0.0412	0.0449
500	0.0625	0.0558	0.0517	0.0412	0.0437
550	0.0625	0.0558	0.0517	0.0412	0.0424
600	0.0625	0.0558	0.0517	0.0412	0.0409
650	0.0625	0.0558	0.0517	0.0412	0.0409
700	0.0625	0.0558	0.0517	0.0473	0.0409
750	0.0625	0.0558	0.0517	0.0473	0.0409
800	0.0625	0.0558	0.0517	0.0473	0.0409

Appendix A3: Transmission values of un-doped ZnSe films at different substrate

temperatures

Wavelength (nm)	ZnSe T% (300 ºC)	ZnSe T% (325 ºC)	ZnSe T% (350 ºC)	ZnSe T% (375 ºC)	ZnSe T% (400 ºC)
200	41.20	36.19	42.17	38.66	41.45
250	34.45	28.07	34.97	33.81	35.58
300	70.45	75.15	71.30	67.38	72.18
350	78.11	75.34	72.11	70.89	74.17
400	82.03	83.34	77.18	76.37	79.90
450	88.06	86.92	86.60	83.04	84.89
500	88.06	86.92	86.60	83.04	84.89
550	88.06	86.92	86.60	83.04	84.89
600	88.06	86.92	86.60	83.04	84.89
650	88.06	86.92	86.60	83.04	84.89
700	88.06	86.92	86.60	83.04	84.89
750	88.06	86.92	86.60	83.04	84.89
800	88.06	86.92	86.60	83.04	84.89

Appendix A4: Transmission values of un-doped ZnSe films at different flow rates

Wavelength (nm)	ZnSe T% (400 µL/Spray)	ZnSe T% (480 µL/Spray)	ZnSe T% (560 µL/Spray)	ZnSe T% (640 µL/Spray)	ZnSe T% (720 µL/Spray)
200	42.17	40.37	40.73	41.52	41.77
250	34.97	33.99	34.57	34.63	34.94
300	71.30	68.52	72.04	71.04	69.95
350	72.11	72.14	74.10	71.20	74.66
400	86.60	87.94	88.78	90.95	89.95
450	86.60	87.94	88.78	90.95	90.18
500	86.60	87.94	88.78	90.95	90.43
550	86.60	87.94	88.78	90.95	90.70
600	86.60	87.94	88.78	90.95	91.01
650	86.60	87.94	88.78	90.95	91.01
700	86.60	87.94	88.78	90.95	91.01
750	86.60	87.94	88.78	90.95	91.01
800	86.60	87.94	88.78	90.95	91.01

Appendix A5: Reflection values (in percentage) of un-doped ZnSe films for different substrate temperatures

Wavelength (nm)	ZnSe R% (300 ºC)	ZnSe R% (325 ºC)	ZnSe R% (350 ºC)	ZnSe R% (375 ºC)	ZnSe R% (400 ºC)
200	20.29	19.67	20.33	20.06	20.30
250	19.27	16.76	19.4	19.10	19.54
300	14.34	12.44	14.01	15.47	13.66
350	11.16	8.74	13.69	14.17	12.85
400	9.37	6.99	11.57	11.92	10.35
450	5.88	6.99	7.15	8.31	8.00
500	5.88	6.99	7.15	8.31	8.00
550	5.88	6.99	7.15	8.31	8.00
600	5.88	6.99	7.15	8.31	8.00
650	5.88	6.99	7.15	8.31	8.00
700	5.88	6.99	7.15	8.31	8.00
750	5.88	6.99	7.15	8.31	8.00
800	5.88	6.99	7.15	8.31	8.00

Appendix A6: Reflection values (percentage) of un-doped ZnSe films for different flow rates

Wavelength (nm)	ZnSe R (400 µL)	ZnSe R (480 µL)	ZnSe R (560 µL)	ZnSe R (640 µL)	ZnSe R (720µL)
200	20.33	20.23	20.26	20.3	20.32
250	19.4	19.14	19.3	19.31	19.39
300	14.01	15.06	13.72	14.11	14.53
350	13.69	13.68	12.88	14.05	12.65
400	7.15	6.48	6.05	4.93	5.45
450	7.15	6.48	6.05	4.93	5.33
500	7.15	6.48	6.05	4.93	5.20
550	7.15	6.48	6.05	4.93	5.06
600	7.15	6.48	6.05	4.93	4.90
650	7.15	6.48	6.05	4.93	4.90
700	7.15	6.48	6.05	5.59	4.90
750	7.15	6.48	6.05	5.59	4.90
800	7.15	6.48	6.05	5.59	4.90

Appendix A7: Refractive index values for pure ZnSe films at different substrate temperatures and photon energies

Photon Energy, E (eV)	n (300 ºC)	n (325 ºC)	n (350 ºC)	n (375 ºC)	n (400 ºC)
1.55	1.64	1.72	1.73	1.81	1.79
1.66	1.64	1.72	1.73	1.81	1.79
1.78	1.64	1.72	1.73	1.81	1.79
1.91	1.64	1.72	1.73	1.81	1.79
2.07	1.64	1.72	1.73	1.81	1.79
2.26	1.64	1.72	1.73	1.81	1.79
2.49	1.64	1.72	1.73	1.81	1.79
2.76	1.64	1.72	1.73	1.81	1.79
3.11	1.88	1.72	2.03	2.06	1.95
3.55	2.00	1.84	2.18	2.21	2.12
4.14	2.22	2.09	2.20	2.30	2.17
4.97	2.57	2.39	2.58	2.55	2.58
6.21	2.64	2.59	2.64	2.62	2.64

Appendix A8: Absorption coefficient values of ZnSe films at different substrate temperatures

Photon Energy, E (eV)	ZnSe α (300ºC)	ZnSe α (325 ºC)	ZnSe α (350 ºC)	ZnSe α (375 ºC)	ZnSe α (400 ºC)
4.14	3.5	2.72	2.45	1.97	2.17
3.55	2.48	1.74	2.37	1.72	1.99
3.11	1.98	1.34	1.88	1.35	1.50
2.76	1.27	1.34	1.04	0.93	1.09
2.49	1.27	1.34	1.04	0.93	1.09
2.26	1.27	1.34	1.04	0.93	1.09
2.07	1.27	1.34	1.04	0.93	1.09
1.91	1.27	1.34	1.04	0.93	1.09
1.78	1.27	1.34	1.04	0.93	1.09
1.66	1.27	1.34	1.04	0.93	1.09
1.55	1.27	1.34	1.04	0.93	1.09

Appendix A9: Optical conductivity values of ZnSe films at different substrate temperatures

Photon Energy (eV)	ZnSe σ (300 ºC)	ZnSe σ (325 ºC)	ZnSe σ (350 ºC)	ZnSe σ (375 ºC)	ZnSe σ (400 ºC)
4.14	18.50	13.60	12.90	10.80	11.20
3.55	11.80	7.64	12.30	9.08	10.10
3.11	8.90	5.50	9.11	6.64	6.98
2.76	5.00	5.50	4.30	4.02	4.66
2.49	5.00	5.50	4.30	4.02	4.66
2.26	5.00	5.50	4.30	4.02	4.66
2.07	5.00	5.50	4.30	4.02	4.66
1.91	5.00	5.50	4.30	4.02	4.66
1.78	5.00	5.50	4.30	4.02	4.66
1.66	5.00	5.50	4.30	4.02	4.66
1.55	5.00	5.50	4.30	4.02	4.66

Appendix A10: Extinction coefficient values of ZnSe films at different substrate temperatures

Photon Energy, E (eV)	ZnSe k (300ºC)	ZnSe k (325 ºC)	ZnSe k (350 ºC)	ZnSe k (375 ºC)	ZnSe k (400 ºC)
3.55	0.0691	0.0485	0.0660	0.0479	0.0554
3.11	0.0630	0.0427	0.0598	0.0430	0.0478
2.76	0.0455	0.048	0.0372	0.0333	0.0390
2.49	0.0505	0.0533	0.0414	0.0370	0.0434
2.26	0.0556	0.0587	0.0455	0.0407	0.0477
2.07	0.0606	0.0640	0.0497	0.0445	0.0520
1.91	0.0657	0.0693	0.0538	0.0481	0.0564
1.78	0.0707	0.0746	0.0579	0.0518	0.0607
1.66	0.0758	0.0800	0.0621	0.0556	0.0651
1.55	0.0809	0.0853	0.0662	0.0592	0.0694

Appendix 11: Real dielectric constant values of ZnSe films at different substrate temperatures

Photon Energy, E (eV)	ZnSe ε_1 (300 °C)	ZnSe ε_1 (325 °C)	ZnSe ε_1 (350 °C)	ZnSe ε_1 (375 °C)	ZnSe ε_1 (400 °C)
4.14	4.88	4.36	4.84	5.29	4.71
3.55	4.00	3.38	4.75	4.88	4.49
3.11	3.53	2.96	4.12	4.24	3.80
2.76	2.69	2.96	2.99	3.28	3.20
2.49	2.69	2.96	2.99	3.28	3.20
2.26	2.69	2.96	2.99	3.27	3.20
2.07	2.69	2.95	2.99	3.27	3.20
1.91	2.69	2.95	2.99	3.27	3.20
1.78	2.69	2.95	2.99	3.27	3.20
1.66	2.68	2.95	2.99	3.27	3.20
1.55	2.68	2.95	2.99	3.27	3.20

Appendix A12: Imaginary dielectric constant values of ZnSe films at different substrate temperatures

Photon Energy, E (eV)	ZnSe ε_2 (300 ºC)	ZnSe ε_2 (325 ºC)	ZnSe ε_2 (350 ºC)	ZnSe ε_2 (375 ºC)	ZnSe ε_2 (400 ºC)
4.14	0.37	0.27	0.26	0.22	0.23
3.55	0.28	0.18	0.29	0.21	0.24
3.11	0.24	0.15	0.24	0.18	0.19
2.76	0.15	0.17	0.13	0.12	0.14
2.49	0.17	0.18	0.14	0.13	0.16
2.26	0.18	0.20	0.16	0.15	0.17
2.07	0.20	0.22	0.17	0.16	0.19
1.91	0.22	0.24	0.19	0.17	0.20
1.78	0.23	0.26	0.20	0.19	0.22
1.66	0.25	0.28	0.22	0.20	0.23
1.55	0.27	0.29	0.23	0.21	0.25

Appendix A13: $(\alpha h\nu)^2$ values for ZnSe films at different substrate temperatures

Photon Energy, E (eV)	ZnSe (300) $(\alpha h\nu)^2$ x $10^{13}eV^2m^{-2}$	ZnSe (325) $(\alpha h\nu)^2$ x $10^{13}eV^2m^{-2}$	ZnSe (350) $(\alpha h\nu)^2$ x $10^{13}eV^2m^{-2}$	ZnSe (375) $(\alpha h\nu)^2$ x $10^{13}eV^2m^{-2}$	ZnSe (400) $(\alpha h\nu)^2$ x $10^{13}eV^2m^{-2}$
3.55	7.75	3.8	7.08	3.73	4.99
3.11	3.79	1.74	3.42	1.76	2.18
2.76	1.23	1.37	0.82	0.659	0.91
2.49	1	1.11	0.67	0.536	0.74
2.26	0.82	0.92	0.55	0.442	0.61
2.07	0.69	0.77	0.46	0.371	0.51
1.91	0.59	0.66	0.4	0.316	0.43
1.78	0.51	0.57	0.34	0.274	0.38
1.66	0.45	0.5	0.3	0.238	0.34
1.55	0.39	0.43	0.26	0.208	0.29

Appendix A14: Diffraction angles and FWHM values for ZnSe films deposited at 350 ^oC

2θ	θ	Cos θ	FWHM β^o	FWHM (Radians)	βCosθ
21.04	10.52	0.9832	0.2000	0.003491	0.003432
32.06	16.03	0.9611	0.1200	0.002094	0.002013
34.77	17.39	0.9543	0.2800	0.004887	0.004664
36.50	18.25	0.9497	0.3400	0.005934	0.005636
45.78	22.89	0.9213	0.0800	0.001396	0.001286
57.05	28.53	0.8786	0.1000	0.001745	0.001533

Appendix A15: Lattice parameters for ZnSe Nanocrystals deposited at 350 ^{o}C

D (nm)	d (Å)	ε (x 10^{-4})	δ (x 10^{14} lines/m^2)	N (x 10^{14})	hkl
42.20	4.2190	8.58	5.62	24.35	101
71.94	2.7895	5.03	1.93	4.92	201
31.05	2.5773	11.66	10.37	61.13	202
25.69	2.4597	14.09	15.15	107.93	211
112.61	1.9804	3.22	0.79	1.28	221
94.47	1.6128	3.83	1.12	2.17	321

Appendix B1: Absorption values of Eu-doped ZnSe films at different deposition

temperatures

Wavelength (nm)	ZnSe:Eu A (300 ºC)	ZnSe:Eu A (325 ºC)	ZnSe:Eu A (350 ºC)	ZnSe:Eu A (375 ºC)	ZnSe:Eu A (400 ºC)
200	0.3880	0.4550	0.4640	0.3819	0.3740
250	0.4720	0.5680	0.6812	0.4585	0.4530
300	0.1580	0.0338	0.2290	0.1369	0.1400
350	0.0864	0.0227	0.0200	0.0185	0.0853
400	0.0433	0.0227	0.0070	0.0185	0.0234
450	0.0303	0.0227	0.0070	0.0185	0.0234
500	0.0303	0.0227	0.0070	0.0185	0.0234
550	0.0303	0.0227	0.0070	0.0185	0.0234
600	0.0303	0.0227	0.0070	0.0185	0.0234
650	0.0303	0.0227	0.0070	0.0185	0.0234
700	0.0303	0.0227	0.0070	0.0185	0.0327
750	0.0303	0.0227	0.0070	0.0185	0.0327
800	0.0303	0.0227	0.0070	0.0185	0.0327

Appendix B2: Absorption values of Eu-doped ZnSe films at different flow rates

Wavelength (nm)	ZnSe:Eu A (400 µL)	ZnSe:Eu A (480 µL)	ZnSe:Eu A (560 µL)	ZnSe:Eu A (640 µL)	ZnSe:Eu A (720 µL)
200	0.3850	0.4770	0.4810	0.2148	0.4740
250	0.4550	0.5480	0.6010	0.2110	0.5020
300	0.1440	0.2260	0.2400	0.2870	0.2630
350	0.0224	0.1821	0.1192	0.0867	0.0226
400	0.0096	0.0129	0.0380	0.0602	0.0075
450	0.0096	0.0129	0.0380	0.0457	0.0075
500	0.0096	0.0129	0.0380	0.0386	0.0075
550	0.0096	0.0129	0.0380	0.0361	0.0075
600	0.0096	0.0129	0.0380	0.0313	0.0075
650	0.0096	0.0129	0.0380	0.0313	0.0075
700	0.0096	0.0129	0.0380	0.0313	0.0075
750	0.0096	0.0129	0.0380	0.0313	0.0075
800	0.0096	0.0129	0.0380	0.0289	0.0075

Appendix B3: Absorption values of Eu-doped ZnSe films at different dopant concentrations

Wavelength (nm)	ZnSe:Eu A (10%)	ZnSe:Eu A (15%)	ZnSe:Eu A (20%)	ZnSe:Eu A (25%)	ZnSe:Eu A (30%)
200	0.3819	0.4710	0.3850	0.4830	0.4810
250	0.4585	0.5000	0.4550	0.6010	0.5200
300	0.1369	0.2580	0.1440	0.2520	0.1490
350	0.0185	0.1872	0.0224	0.1157	0.1045
400	0.0185	0.0194	0.0096	0.0067	0.0065
450	0.0185	0.0194	0.0096	0.0067	0.0065
500	0.0185	0.0194	0.0096	0.0067	0.0065
550	0.0185	0.0194	0.0096	0.0067	0.0065
600	0.0185	0.0194	0.0096	0.0067	0.0065
650	0.0185	0.0194	0.0096	0.0067	0.0065
700	0.0185	0.0194	0.0096	0.0067	0.0065
750	0.0185	0.0194	0.0096	0.0067	0.0065
800	0.0185	0.0194	0.0096	0.0067	0.0065

Appendix B4: Transmission values of ZnSe:Eu films deposited at different substrate temperatures

Wavelength (nm)	ZnSe:Eu T% (300 ºC)	ZnSe:Eu T% (325 ºC)	ZnSe:Eu T% (350 ºC)	ZnSe:Eu T% (375 ºC)	ZnSe:Eu T% (400 ºC)
200	40.93	35.08	34.36	41.51	42.27
250	33.73	27.04	20.84	34.79	35.24
300	69.50	68.08	59.02	72.96	72.44
350	81.96	88.51	95.50	95.83	92.44
400	90.52	94.91	98.40	95.83	94.76
450	93.26	94.91	98.40	95.83	94.76
500	93.26	94.91	98.40	95.83	94.76
550	93.26	94.91	98.40	95.83	94.76
600	93.26	94.91	98.40	95.83	94.76
650	93.26	94.91	98.40	95.83	94.76
700	93.26	94.91	98.40	95.83	94.76
750	93.26	94.91	98.40	95.83	94.76
800	93.26	94.91	98.40	95.83	94.76

Appendix B5: Transmission values of ZnSe:Eu films deposited at different flow rates

Wavelength (nm)	ZnSe:Eu T% (400 µL)	ZnSe:Eu T% (480 µL)	ZnSe:Eu T% (560 µL)	ZnSe:Eu T% (640 µL)	ZnSe:Eu T% (720 µL)
200	41.21	33.34	33.04	60.98	33.57
250	35.08	28.31	25.06	61.52	31.48
300	71.78	59.43	57.74	51.64	54.58
350	94.98	65.75	76.00	81.90	94.93
400	97.81	97.07	91.62	87.06	98.29
450	97.81	97.07	91.62	90.01	98.29
500	97.81	97.07	91.62	91.50	98.29
550	97.81	97.07	91.62	92.02	98.29
600	97.81	97.07	91.62	93.05	98.29
650	97.81	97.07	91.62	93.05	98.29
700	97.81	97.07	91.62	93.05	98.29
750	97.81	97.07	91.62	93.05	98.29
800	97.81	97.07	91.62	93.56	98.29

Appendix B6: Transmission values of ZnSe:Eu films deposited at different europium concentrations

Wavelength (nm)	ZnSe:Eu T% (10%)	ZnSe:Eu T% (15%)	ZnSe:Eu T% (20%)	ZnSe:Eu T% (25%)	ZnSe:Eu T% (30%)
200	41.51	33.81	41.21	32.89	33.07
250	34.79	31.62	35.08	25.06	30.20
300	72.96	55.21	71.78	55.98	70.96
350	95.83	64.98	94.98	76.61	78.61
400	95.83	95.63	97.81	98.47	98.52
450	95.83	95.63	97.81	98.47	98.52
500	95.83	95.63	97.81	98.47	98.52
550	95.83	95.63	97.81	98.47	95.52
600	95.83	95.63	97.81	98.47	98.52
650	95.83	95.63	97.81	98.47	98.52
700	95.83	95.63	97.81	98.47	98.52
750	95.83	95.63	97.81	98.47	98.52
800	95.83	95.63	97.81	98.47	98.52

Appendix B7: Reflection values (percentage) of Eu-doped ZnSe films for different substrate temperatures

Wavelength (nm)	ZnSe:Eu R% (300 ºC)	ZnSe:Eu R% (325 ºC)	ZnSe:Eu R% (350 ºC)	ZnSe:Eu R% (375 ºC)	ZnSe:Eu R% (400 ºC)
200	20.27	19.42	19.24	20.3	20.33
250	19.07	16.16	11.04	19.36	19.46
300	14.70	15.22	18.08	13.35	13.56
350	6.44	6.19	0.38	2.32	9.30
400	4.40	2.82	0.90	2.32	1.97
450	4.40	2.82	0.90	2.32	1.97
500	4.40	2.82	0.90	2.32	1.97
550	4.40	2.82	0.90	2.32	1.97
600	4.40	2.82	0.90	2.32	1.97
650	4.40	2.82	0.90	2.32	1.97
700	4.73	2.82	0.90	2.32	1.97
750	4.73	2.82	0.90	2.32	1.97
800	4.73	2.82	0.90	2.32	1.97

Appendix B8: Reflection values (percentage) of Eu-doped ZnSe films for different flow rates

Wavelength (nm)	ZnSe:Eu R (400 µL)	ZnSe:Eu R (480 µL)	ZnSe:Eu R (560 µL)	ZnSe:Eu R (640 µL)	ZnSe:Eu R (720 µL)
200	20.26	18.96	18.86	17.54	19.03
250	19.42	16.89	14.84	17.38	18.32
300	13.82	17.97	18.46	19.66	19.12
350	2.78	16.04	12.08	9.43	2.81
400	1.23	1.64	4.58	6.92	0.96
450	1.23	1.64	4.58	5.42	0.96
500	1.23	1.64	4.58	4.64	0.96
550	1.23	1.64	4.58	4.37	0.96
600	1.23	1.64	4.58	3.82	0.96
650	1.23	1.64	4.58	3.82	0.96
700	1.23	1.64	4.58	3.82	0.96
750	1.23	1.64	4.58	3.82	0.96
800	1.23	1.64	4.58	3.55	0.96

Appendix B9: Reflection values (percentage) of Eu-doped ZnSe films for different concentrations of europium

Wavelength (nm)	ZnSe:Eu R% (10%)	ZnSe:Eu R% (15%)	ZnSe:Eu R% (20%)	ZnSe:Eu R% (25%)	ZnSe:Eu R% (30%)
200	20.30	19.09	20.26	18.81	18.83
250	19.36	18.38	19.42	14.84	17.80
300	13.35	18.99	13.82	18.82	14.14
350	2.32	16.30	2.78	11.82	10.94
400	2.32	2.43	1.23	0.86	0.83
450	2.32	2.43	1.23	0.86	0.83
500	2.32	2.43	1.23	0.86	0.83
550	2.32	2.43	1.23	0.86	0.83
600	2.32	2.43	1.23	0.86	0.83
650	2.32	2.43	1.23	0.86	0.83
700	2.32	2.43	1.23	0.86	0.83
750	2.32	2.43	1.23	0.86	0.83
800	2.32	2.43	1.23	0.86	0.83

Appendix B10: Refractive index values for ZnSe:Eu films at different photon energies and substrate temperatures

Photon Energy, E (eV)	n (300 ºC)	n (325 ºC)	n (350 ºC)	n (375 ºC)	n (400 ºC)
1.55	1.41	1.06	1.21	1.36	1.33
1.66	1.41	1.06	1.21	1.36	1.33
1.78	1.41	1.06	1.21	1.36	1.33
1.91	1.41	1.06	1.21	1.36	1.33
2.07	1.41	1.06	1.21	1.36	1.33
2.26	1.41	1.06	1.21	1.36	1.33
2.49	1.41	1.06	1.21	1.36	1.33
2.76	1.41	1.06	1.21	1.36	1.33
3.11	1.50	1.06	1.21	1.43	1.33
3.55	1.88	1.66	1.26	1.46	1.51
4.14	2.24	1.51	2.48	2.15	2.17
4.97	2.55	2.35	2.68	2.57	2.58
6.21	2.64	2.58	2.56	2.64	2.64

Appendix B11: Absorption coefficient values for ZnSe:Eu films at different photon energies and substrate temperatures

Photon Energy, E(eV)	α(x $10^6 m^{-1}$) (300°C)	α(x $10^6 m^{-1}$) (325 °C)	α(x $10^6 m^{-1}$) (350 °C)	α(x $10^6 m^{-1}$) (375 °C)	α(x $10^6 m^{-1}$) (400 °C)
4.14	7.28	4.81	5.27	1.720	2.690
3.55	3.98	1.526	0.46	0.356	1.637
3.11	1.95	0.653	0.16	0.321	0.449
2.76	1.36	0.653	0.16	0.233	0.449
2.49	1.36	0.653	0.16	0.233	0.449
2.26	1.36	0.653	0.16	0.233	0.449
2.07	1.36	0.653	0.16	0.233	0.449
1.91	1.36	0.653	0.16	0.233	0.449
1.78	1.36	0.653	0.16	0.233	0.449
1.66	1.36	0.653	0.16	0.233	0.449
1.55	1.36	0.653	0.16	0.223	0.449

Appendix B12: Optical conductivity values for ZnSe:Eu films at different photon energies and substrate temperatures

Photon Energy, E (eV)	σ (x $10^{13}s^{-1}$) (300 ºC)	σ (x $10^{13}s^{-1}$) (325 ºC)	σ (x $10^{13}s^{-1}$) (350 ºC)	σ (x $10^{13}s^{-1}$) (375 ºC)	σ (x $10^{13}s^{-1}$) (400 ºC)
4.14	38.9	26.2	31.2	8.828	13.94
3.55	21.09	3.51	0.722	1.241	2.36
3.11	7.31	1.652	0.462	1.096	1.43
2.76	4.58	1.652	0.462	0.757	1.43
2.49	4.58	1.652	0.462	0.757	1.43
2.26	4.58	1.652	0.462	0.757	1.43
2.07	4.58	1.652	0.462	0.757	1.43
1.91	4.58	1.652	0.462	0.757	1.43
1.78	4.58	1.652	0.462	0.757	1.43
1.66	4.58	1.652	0.462	0.757	1.43
1.55	4.58	1.652	0.462	0.757	1.43

Appendix B13: Extinction coefficient values for ZnSe:Eu films at different substrate temperatures

Photon Energy, E (eV)	k (300 ºC)	k (325 ºC)	k (350 ºC)	k (375 ºC)	k (400 ºC)
4.14	0.1700	0.1200	0.1300	0.0410	0.0642
3.55	0.1100	0.0271	0.0067	0.0027	0.0182
3.11	0.0620	0.0208	0.0051	0.0074	0.0143
2.76	0.0490	0.0234	0.0057	0.0083	0.0161
2.49	0.0540	0.026	0.0064	0.0093	0.0179
2.26	0.0600	0.0286	0.0070	0.0102	0.0197
2.07	0.0650	0.0312	0.0076	0.0111	0.0214
1.91	0.0700	0.0338	0.0083	0.0121	0.0232
1.78	0.0760	0.0364	0.0089	0.0130	0.0250
1.66	0.0810	0.0390	0.0096	0.0139	0.0268
1.55	0.0870	0.0416	0.0101	0.0148	0.0286

Appendix B14: Values of real dielectric constant for ZnSe:Eu Films at different substrate temperatures

Photon Energy, E (eV)	ε_1 (300 °C)	ε_1 (325 °C)	ε_1 (350 °C)	ε_1 (375 °C)	ε_1 (400 °C)
4.14	4.99	5.18	6.13	4.62	4.71
3.55	4.92	2.28	1.59	2.13	2.28
3.11	2.46	1.12	1.46	2.05	1.77
2.76	1.99	1.12	1.46	1.85	1.77
2.49	1.99	1.12	1.46	1.85	1.77
2.26	1.99	1.12	1.46	1.85	1.77
2.07	1.99	1.12	1.46	1.85	1.77
1.91	1.99	1.12	1.46	1.85	1.77
1.78	1.99	1.12	1.46	1.85	1.77
1.66	1.98	1.12	1.46	1.85	1.77
1.55	1.98	1.12	1.46	1.85	1.77

Appendix B15: Values of imaginary dielectric constant for ZnSe:Eu films at different substrate temperature

Photon Energy, E (eV)	ε_2 (300 °C)	ε_2 (325 °C)	ε_2 (350 °C)	ε_2 (375 °C)	ε_2 (400 °C)
4.14	0.760	0.550	0.650	0.180	0.280
3.55	0.490	0.080	0.017	0.029	0.060
3.11	0.200	0.040	0.012	0.029	0.040
2.76	0.140	0.050	0.014	0.023	0.040
2.49	0.150	0.060	0.016	0.025	0.050
2.26	0.170	0.060	0.017	0.028	0.050
2.07	0.180	0.070	0.018	0.030	0.060
1.91	0.200	0.070	0.020	0.033	0.060
1.78	0.210	0.080	0.022	0.035	0.070
1.66	0.230	0.080	0.023	0.038	0.070
1.55	0.250	0.090	0.024	0.040	0.080

Appendix B16: $(\alpha h\nu)^2$ values for ZnSe:Eu films at different substrate temperatures

Photon Energy, E (eV)	$(\alpha h\nu)^2$ x $10^{12}eV^2m^{-2}$ (300 ^oC)	$(\alpha h\nu)^2$ x $10^{12}eV^2m^{-2}$ (325 ^oC)	$(\alpha h\nu)^2$ x $10^{12}eV^2m^{-2}$ (350 ^oC)	$(\alpha h\nu)^2$ x $10^{12}eV^2m^{-2}$ (375 ^oC)	$(\alpha h\nu)^2$ x $10^{12}eV^2m^{-2}$ (400 ^oC)
3.55	19.55	29.94	26.7	11.5	33.75
3.11	1.86	4.12	2.52	0.997	1.95
2.76	1.35	3.25	1.95	0.414	1.54
2.49	1.21	2.64	1.59	0.337	1.25
2.26	0.95	2.18	1.31	0.277	1.03
2.07	0.75	1.83	1.10	0.233	0.864
1.91	0.68	1.56	0.93	0.198	0.736
1.78	0.57	1.35	0.81	0.172	0.639
1.66	0.51	1.18	0.71	0.15	0.556
1.55	0.44	1.03	0.62	0.13	0.484

Appendix B17: Diffraction angles and FWHM values for ZnSe:Eu nanocrystals deposited at 350^{o}C and 10% dopant concentration

2θ	θ	Cos θ	FWHM β^o	FWHM (Radians)	βCosθ
12.99	6.50	0.9936	0.0800	0.001396	0.001387
32.12	16.06	0.9610	0.0800	0.001396	0.001342
34.82	17.41	0.9542	0.2400	0.004189	0.003997
36.63	18.32	0.9493	0.2200	0.003840	0.003645

Appendix B18: Lattice parameters for ZnSe:Eu nanocrystals deposited at 350ºC and 10% dopant concentration

D (nm)	d (Å)	ε (x 10^{-4})	δ (x 10^{14} lines/m^2)	N (x 10^{14})	hkl
104.41	6.3963	3.47	0.92	1.61	100
107.91	2.6174	3.36	0.86	1.46	201
36.23	2.4200	9.99	7.62	38.48	202
39.73	2.3036	9.11	6.34	29.18	211

Appendix B19: Diffraction angles and FWHM values for ZnSe:Eu nanocrystals deposited at 350ºC and 20% dopant concentration

2θ	θ	Cos θ	FWHM β^o	FWHM (Radians)	βCosθ
31.99	15.995	0.9613	0.3400	0.005934	0.005704
34.75	17.375	0.9544	0.2800	0.004887	0.004664
36.55	18.275	0.9496	0.1800	0.003142	0.002984

Appendix B20: Lattice parameters for ZnSe:Eu nanocrystals deposited at 350ºC and 20% dopant concentration

D (nm)	d (Å)	ε (x 10^{-4})	δ (x 10^{14} lines/m^2)	N (x 10^{15})	hkl
25.39	2.796	14.26	1.55	12.22	201
31.05	2.580	11.66	1.04	6.68	202
48.53	2.457	7.46	0.425	1.75	211

Appendix C1: Absorption values of CdSe:Eu films at different deposition temperatures

Wavelength (nm)	A (300 ºC)	A (320 ºC)	A (340 ºC)	A (360 ºC)	A (380 ºC)
200	0.2580	0.2670	0.2280	0.2400	0.2740
250	0.2950	0.2980	0.2590	0.2710	0.2980
300	0.2240	0.2090	0.2110	0.2230	0.2120
350	0.0134	0.0121	0.0134	0.1390	0.0121
400	0.0096	0.0073	0.0124	0.0104	0.0110
450	0.0096	0.0073	0.0100	0.0104	0.0110
500	0.0096	0.0073	0.0100	0.0104	0.0110
550	0.0096	0.0073	0.0100	0.0104	0.0110
600	0.0096	0.0073	0.0100	0.0104	0.0110
650	0.0096	0.0073	0.0100	0.0104	0.0110
700	0.0096	0.0073	0.0100	0.0104	0.0110
750	0.0096	0.0073	0.0100	0.0104	0.0110
800	0.0096	0.0073	0.0100	0.0104	0.0110

Appendix C2: Absorption values of CdSe:Eu films obtained at different flow rates

Wavelength (nm)	CdSe:Eu (400 µL)	CdSe:Eu (480 µL)	CdSe:Eu (560 µL)	CdSe:Eu (640 µL)	CdSe:Eu (720 µL)
200	0.2400	0.2780	0.2749	0.2319	0.2428
250	0.2710	0.3020	0.3026	0.2605	0.2728
300	0.2230	0.2340	0.2254	0.2353	0.2312
350	0.1390	0.0146	0.0117	0.0252	0.0208
400	0.0104	0.0098	0.0065	0.0202	0.0185
450	0.0104	0.0098	0.0063	0.0202	0.0139
500	0.0104	0.0098	0.0061	0.0185	0.0139
550	0.0104	0.0098	0.0059	0.0168	0.0139
600	0.0104	0.0098	0.0057	0.0168	0.0139
650	0.0104	0.0098	0.0055	0.0168	0.0139
700	0.0104	0.0098	0.0053	0.0135	0.0139
750	0.0104	0.0098	0.0051	0.0135	0.0139
800	0.0104	0.0098	0.0049	0.0135	0.0139

Appendix C3: Absorption values of CdSe:Eu films for different dopant concentrations

Wavelength (nm)	CdSe:Eu (10%)	CdSe:Eu (15%)	CdSe:Eu (20%)	CdSe:Eu (25%)	CdSe:Eu (30%)
200	0.2283	0.2400	0.2404	0.2595	0.2372
250	0.2544	0.2710	0.2689	0.2941	0.2688
300	0.2630	0.2230	0.2885	0.3027	0.2957
350	0.0544	0.0139	0.2863	0.1362	0.1138
400	0.0435	0.0140	0.1005	0.1124	0.0917
450	0.0370	0.0140	0.0721	0.0093	0.0791
500	0.0326	0.0140	0.0656	0.0800	0.0680
550	0.0304	0.0140	0.0590	0.0714	0.0601
600	0.0283	0.0140	0.0503	0.0627	0.0553
650	0.0283	0.0140	0.0459	0.0584	0.0474
700	0.0239	0.0140	0.0437	0.0541	0.0427
750	0.0239	0.0140	0.0393	0.0497	0.0395
800	0.0239	0.0140	0.0372	0.0497	0.0364

Appendix C4: Transmission values of CdSe:Eu films deposited at different substrate

temperatures

Wavelength (nm)	CdSe:Eu T% (300 ºC)	CdSe:Eu T% (320 ºC)	CdSe:Eu T% (340 ºC)	CdSe:Eu T% (360 ºC)	CdSe:Eu T% (380 ºC)
200	55.21	54.08	59.16	57.54	53.21
250	50.70	50.35	55.08	53.58	50.35
300	59.70	61.80	61.52	59.84	61.38
350	96.96	97.25	96.96	96.85	97.07
400	97.81	97.85	97.19	97.28	97.50
450	97.81	98.33	97.72	97.63	97.50
500	97.81	98.33	97.72	97.63	97.50
550	97.81	98.33	97.72	97.63	97.50
600	97.81	98.33	97.72	97.63	97.50
650	97.81	98.33	97.72	97.63	97.50
700	97.81	98.33	97.72	97.63	97.50
750	97.81	98.33	97.72	97.63	97.50
800	97.81	98.33	97.72	97.63	97.50

Appendix C5: Percentage transmission values of CdSe:Eu films at different flow

rates

Wavelength (nm)	CdSe:Eu T% (400 µL)	CdSe:Eu T% (480 µL)	CdSe:Eu T% (560 µL)	CdSe:Eu T% (640 µL)	CdSe:Eu T% (720 µL)
200	57.54	52.72	53.1	58.63	57.17
250	53.58	49.89	49.82	54.89	53.36
300	59.84	58.35	59.51	58.17	58.72
350	96.85	96.69	97.34	94.36	95.32
400	97.63	97.77	98.52	95.46	95.83
450	97.63	97.77	98.56	95.46	96.85
500	97.63	97.77	98.61	95.83	96.85
550	97.63	97.77	98.65	96.21	96.85
600	97.63	97.77	98.7	96.21	96.85
650	97.63	97.77	98.74	96.21	96.85
700	97.63	97.77	98.79	96.94	96.85
750	97.63	97.77	98.83	96.94	96.85
800	97.63	97.77	98.88	96.94	96.85

Appendix C6: Percentage transmission values of CdSe:Eu films at different dopant

concentrations

Wavelength (nm)	CdSe:Eu T% (10%)	CdSe:Eu T% (15%)	CdSe:Eu T% (20%)	CdSe:Eu T% (25%)	CdSe:Eu T% (30%)
200	59.12	57.54	57.49	55.02	57.92
250	55.67	53.58	53.84	50.80	53.85
300	54.58	59.84	51.46	49.81	50.62
350	88.23	96.85	79.34	73.08	76.95
400	90.47	97.63	83.00	77.20	80.97
450	91.83	97.63	84.70	80.72	84.92
500	92.77	97.63	85.98	83.18	85.51
550	93.24	97.63	87.30	84.84	87.08
600	93.69	97.63	89.06	86.56	88.04
650	93.69	97.63	89.97	87.42	89.66
700	94.65	97.63	90.43	88.29	90.64
750	94.65	97.63	91.35	89.19	91.31
800	94.65	97.63	91.80	89.19	91.96

Appendix C7: Percentage reflection values of CdSe:Eu films obtained at different substrate temperatures

Wavelength (nm)	CdSe:Eu R% (300 ºC)	CdSe:Eu R% (320 ºC)	CdSe:Eu R% (340 ºC)	CdSe:Eu R% (360 ºC)	CdSe:Eu R% (380 ºC)
200	18.99	19.22	18.04	18.46	19.39
250	19.8	19.85	19.02	19.32	19.85
300	17.90	17.30	17.38	17.86	17.42
350	1.70	1.54	1.70	1.76	1.40
400	1.23	0.94	1.70	1.33	1.40
450	1.23	0.94	1.28	1.33	1.40
500	1.23	0.94	1.28	1.33	1.40
550	1.23	0.94	1.28	1.33	1.40
600	1.23	0.94	1.28	1.33	1.40
650	1.23	0.94	1.28	1.33	1.40
700	1.23	0.94	1.28	1.33	1.40
750	1.23	0.94	1.28	1.33	1.40
800	1.23	0.94	1.28	1.33	1.40

Appendix C8: Percentage reflection values of CdSe:Eu films obtained at different flow rates

Wavelength (nm)	CdSe:Eu R% (400 µL)	CdSe:Eu R% (480 µL)	CdSe:Eu R% (560 µL)	CdSe:Eu R% (640 µL)	CdSe:Eu R% (720 µL)
200	18.46	19.48	19.41	18.18	18.55
250	19.32	19.91	19.92	19.06	19.36
300	17.86	18.25	17.95	18.3	18.16
350	1.76	1.85	1.49	3.12	2.60
400	1.33	1.25	0.83	2.52	2.32
450	1.33	1.25	0.81	2.52	1.76
500	1.33	1.25	0.78	2.32	1.76
550	1.33	1.25	0.76	2.11	1.76
600	1.33	1.35	0.73	2.11	1.76
650	1.33	1.25	0.71	2.11	1.76
700	1.33	1.25	0.68	1.71	1.76
750	1.33	1.25	0.66	1.71	1.76
800	1.33	1.25	0.63	1.71	1.76

Appendix C9: Percentage reflection values of CdSe:Eu films obtained at different concentrations of europium

Wavelength (nm)	CdSe:Eu R% (10%)	CdSe:Eu R% (15%)	CdSe:Eu R% (20%)	CdSe:Eu R% (25%)	CdSe:Eu R% (30%)
200	18.05	18.46	18.47	19.03	18.36
250	18.89	19.32	19.27	19.79	19.27
300	19.12	17.86	19.69	19.92	19.81
350	6.33	1.76	10.61	13.30	11.67
400	5.18	1.33	8.91	11.56	9.86
450	4.47	1.33	8.09	9.98	7.17
500	3.97	1.33	7.46	8.82	7.69
550	3.72	1.33	6.80	8.02	6.91
600	3.48	1.33	5.91	7.17	6.43
650	3.48	1.33	5.44	6.74	5.60
700	2.96	1.33	5.20	6.30	5.09
750	2.96	1.33	4.72	5.84	4.74
800	2.96	1.33	4.48	5.84	4.40

Appendix C10: Refractive index values for CdSe:Eu films at different substrate temperatures and photon energies

Photon Energy, E (eV)	n (300°C)	n (320°C)	n (340°C)	n (360°C)	n (380°C)
1.55	1.25	1.22	1.26	1.26	1.27
1.66	1.25	1.22	1.26	1.26	1.27
1.78	1.25	1.22	1.26	1.26	1.27
1.91	1.25	1.22	1.26	1.26	1.27
2.07	1.25	1.22	1.26	1.26	1.27
2.26	1.25	1.22	1.26	1.26	1.27
2.49	1.25	1.22	1.26	1.26	1.27
2.76	1.25	1.22	1.26	1.26	1.27
3.11	1.25	1.25	1.29	1.28	1.27
3.55	1.30	1.28	1.30	1.31	1.29
4.14	2.47	2.42	2.43	2.46	2.43
4.97	2.60	2.61	2.55	2.57	2.61
6.21	2.55	2.56	2.48	2.51	2.57

Appendix C11: Absorption coefficient values for CdSe:Eu films at different substrate temperatures

Photon Energy, E (eV)	α (x $10^5 m^{-1}$) 300°C	α (x $10^5 m^{-1}$) 320°C	α (x $10^5 m^{-1}$) 340°C	α (x $10^5 m^{-1}$) 360°C	α (x $10^5 m^{-1}$) 380°C
3.55	6.174	2.789	2.058	4.268	4.956
3.11	4.429	2.173	1.900	3.677	4.220
2.76	4.429	1.684	1.538	3.198	4.220
2.49	4.429	1.684	1.538	3.198	4.220
2.26	4.429	1.684	1.538	3.198	4.220
2.07	4.429	1.684	1.538	3.198	4.220
1.91	4.429	1.684	1.538	3.198	4.220
1.78	4.429	1.684	1.538	3.198	4.220
1.66	4.429	1.684	1.538	3.198	4.220
1.55	4.429	1.684	1.538	3.198	4.220

Appendix C12: Optical conductivity values for CdSe:Eu films at different substrate temperatures

Photon Energy, E (eV)	σ (x $10^{13}s^{-1}$) 300°C	σ (x $10^{13}s^{-1}$) 320°C	σ (x $10^{13}s^{-1}$) 340°C	σ (x $10^{13}s^{-1}$) 360°C	σ (x $10^{13}s^{-1}$) 380°C
3.55	1.916	0.852	0.639	1.335	1.526
3.11	1.322	0.649	0.585	1.124	1.280
2.76	1.322	0.491	0.463	0.924	1.280
2.49	1.322	0.491	0.463	0.924	1.280
2.26	1.322	0.491	0.463	0.924	1.280
2.07	1.322	0.491	0.463	0.924	1.280
1.91	1.322	0.491	0.463	0.924	1.280
1.78	1.322	0.491	0.463	0.924	1.280
1.66	1.322	0.491	0.463	0.924	1.280
1.55	1.322	0.491	0.463	0.924	1.280

Appendix C13: Extinction coefficient values for CdSe:Eu films at different substrate temperatures

Photon Energy, E (eV)	k 300°C	k 320°C	k 340°C	k 360°C	k 380°C
3.55	0.0172	0.0078	0.0057	0.0119	0.0138
3.11	0.0141	0.0069	0.0061	0.0117	0.0134
2.76	0.0159	0.0060	0.0055	0.0115	0.0151
2.49	0.0176	0.0067	0.0061	0.0127	0.0168
2.26	0.0194	0.0074	0.0067	0.0140	0.0185
2.07	0.0212	0.0080	0.0073	0.0153	0.0202
1.91	0.0229	0.0087	0.0080	0.0165	0.0218
1.78	0.0247	0.0094	0.0086	0.0178	0.0235
1.66	0.0264	0.0101	0.0092	0.0191	0.0252
1.55	0.0282	0.0107	0.0098	0.0204	0.0269

Appendix C14: Real dielectric constant values for CdSe:Eu films at different substrate temperatures

Photon Energy, E (eV)	ε_1 (300°C)	ε_1 (320°C)	ε_1 (340°C)	ε_1 (360°C)	ε_1 (380°C)
3.55	1.690	1.638	1.690	1.716	1.664
3.11	1.562	1.563	1.664	1.638	1.613
2.76	1.562	1.488	1.588	1.464	1.613
2.49	1.562	1.488	1.588	1.464	1.613
2.26	1.562	1.488	1.588	1.464	1.613
2.07	1.562	1.488	1.588	1.464	1.613
1.91	1.562	1.488	1.588	1.464	1.612
1.78	1.562	1.488	1.588	1.464	1.612
1.66	1.562	1.488	1.588	1.464	1.612
1.55	1.562	1.488	1.588	1.464	1.612

Appendix C15: Imaginary dielectric constant values for CdSe:Eu films at different substrate temperatures

Photon Energy, E (eV)	ε_2 (300°C)	ε_2 (320°C)	ε_2 (340°C)	ε_2 (360°C)	ε_2 (380°C)
3.55	0.0447	0.0200	0.0148	0.0312	0.0356
3.11	0.0353	0.0173	0.0157	0.0300	0.0340
2.76	0.0398	0.0146	0.0139	0.0278	0.0384
2.49	0.0440	0.0164	0.0154	0.0307	0.0427
2.26	0.0485	0.0181	0.0169	0.0339	0.0470
2.07	0.0530	0.0195	0.0184	0.0370	0.0513
1.91	0.0573	0.0212	0.0202	0.0399	0.0554
1.78	0.0618	0.0229	0.0217	0.0431	0.0597
1.66	0.0660	0.0246	0.0232	0.0479	0.0640
1.55	0.0705	0.0261	0.0247	0.0494	0.0683

Appendix C16: $(\alpha h\nu)^2$ values of CdSe:Eu films at different substrate temperatures

Photon Energy, E (eV)	$(\alpha h\nu)^2$ x $10^{12}eV^2m^{-2}$ (300°C)	$(\alpha h\nu)^2$ x $10^{12}eV^2m^{-2}$ (320°C)	$(\alpha h\nu)^2$ x $10^{12}eV^2m^{-2}$ (340°C)	$(\alpha h\nu)^2$ x $10^{12}eV^2m^{-2}$ (360°C)	$(\alpha h\nu)^2$ x $10^{12}eV^2m^{-2}$ (380°C)
3.55	4.804	9.800	5.338	2.295	3.096
3.11	1.897	4.569	3.492	1.308	1.723
2.76	1.494	2.160	1.801	0.779	1.357
2.49	1.216	1.758	1.467	0.634	1.104
2.26	1.002	1.448	1.208	0.522	0.910
2.07	0.841	1.215	1.014	0.438	0.763
1.91	0.716	1.035	0.863	0.373	0.650
1.78	0.622	0.899	0.750	0.324	0.564
1.66	0.541	0.782	0.652	0.282	0.491
1.55	0.471	0.681	0.568	0.246	0.428

Appendix C17: Diffraction Angles and FWHM Values for CdSe:Eu Nanocrystals Deposited at 360ºC and 10% Dopant Concentration.

2θº	θº	Cos θ	FWHM βº	FWHM (Radians)	βCosθ
28.93	14.47	0.9683	0.2200	0.003840	0.003718
30.62	15.31	0.9645	0.3400	0.005934	0.005723
34.98	17.49	0.9538	0.3600	0.006283	0.005993
51.05	25.53	0.9024	0.4200	0.007330	0.006615

Appendix C18: Lattice Parameters for CdSe:Eu Nanocrystals Deposited at 360°C and 10% Dopant Concentration.

D (nm)	d (Å)	ε (x 10^{-4})	δ (x 10^{14} lines/m^2)	N (x 10^{15})	hkl
38.95	3.08	9.30	6.59	1.69	001
25.30	2.92	14.31	15.62	6.18	100
24.16	2.56	14.98	17.13	7.09	101
21.89	1.79	16.54	20.87	9.53	103

Appendix D1: Absorption data of MgSe:Eu films deposited at different temperatures

Wavelength (nm)	MgSe:Eu (300 ºC)	MgSe:Eu (325 ºC)	MgSe:Eu (350 ºC)	MgSe:Eu (375 ºC)	MgSe:Eu (400 ºC)
200	0.2403	0.2530	0.2355	0.2299	0.2286
250	0.2711	0.2760	0.2655	0.2651	0.2584
300	0.2871	0.1825	0.2966	0.2759	0.2186
350	0.1536	0.0889	0.2355	0.0782	0.0273
400	0.1342	0.0374	0.2304	0.0720	0.0174
450	0.1365	0.0187	0.2200	0.0690	0.0124
500	0.1365	0.0187	0.2066	0.0659	0.0124
550	0.1301	0.0187	0.1890	0.0659	0.0124
600	0.1297	0.0140	0.1724	0.0628	0.0124
650	0.1251	0.0070	0.1621	0.0613	0.0124
700	0.1217	0.0070	0.1528	0.0613	0.0124
750	0.1160	0.0070	0.1466	0.0582	0.0124
800	0.1137	0.0023	0.1393	0.0582	0.0124

Appendix D2: Absorption values of MgSe:Eu films deposited at different flow rates

Wavelength (nm)	MgSe:Eu A (400 µL)	MgSe:Eu A (480 µL)	MgSe:Eu A (560 µL)	MgSe:Eu A (640 µL)	MgSe:Eu A (720 µL)
200	0.2050	0.2633	0.2215	0.2522	0.2104
250	0.2328	0.2938	0.2500	0.2831	0.2461
300	0.2587	0.2938	0.2800	0.3007	0.2819
350	0.1055	0.1186	0.2515	0.1695	0.1948
400	0.0856	0.1093	0.2560	0.1607	0.1622
450	0.0876	0.1093	0.2425	0.1607	0.1700
500	0.0876	0.1080	0.2260	0.1585	0.1777
550	0.0856	0.1080	0.2095	0.1552	0.1793
600	0.0856	0.1053	0.1945	0.1507	0.1746
650	0.0816	0.1053	0.1795	0.1463	0.1731
700	0.0816	0.1053	0.1720	0.1430	0.1700
750	0.0796	0.1053	0.1645	0.1397	0.1688
800	0.0756	0.1053	0.1570	0.1364	0.1622

Appendix D3: Absorption values of MgSe:Eu films at different dopant concentrations

Wavelength (nm)	MgSe:Eu (10%)	MgSe:Eu (20%)	MgSe:Eu (30%)	MgSe:Eu (40%)	MgSe:Eu (50%)
200	0.2355	0.2050	0.2468	0.2072	0.2451
250	0.2655	0.2328	0.2753	0.2421	0.2775
300	0.2966	0.2587	0.3053	0.2626	0.2590
350	0.2355	0.1055	0.2595	0.0964	0.0647
400	0.2304	0.0856	0.2547	0.0821	0.0601
450	0.2200	0.0876	0.2437	0.0821	0.0578
500	0.2066	0.0876	0.2311	0.0821	0.0532
550	0.1890	0.0856	0.2121	0.0821	0.0532
600	0.1724	0.0856	0.1963	0.0780	0.0532
650	0.1621	0.0816	0.1853	0.0780	0.0532
700	0.1528	0.0816	0.1758	0.0780	0.0532
750	0.1466	0.0796	0.1679	0.0780	0.0532
800	0.1393	0.0756	0.1600	0.0780	0.0532

Appendix D4: Transmittance values of MgSe:Eu films at different substrate temperatures

Wavelength (nm)	MgSe:Eu T% (300ºC)	MgSe:Eu T% (325ºC)	MgSe:Eu T% (350ºC)	MgSe:Eu T% (375ºC)	MgSe:Eu T% (400ºC)
200	57.50	55.85	58.14	58.90	59.08
250	53.57	52.97	54.26	54.31	55.16
300	51.63	65.69	50.51	52.98	60.45
350	70.21	81.94	58.14	83.52	93.91
400	73.42	91.75	58.83	84.72	96.07
450	73.03	93.61	60.26	85.31	96.47
500	73.03	93.61	62.14	85.92	96.47
550	74.11	93.61	64.17	85.92	96.47
600	74.18	94.62	67.24	86.54	96.47
650	74.97	94.82	68.85	86.84	96.47
700	75.56	94.82	70.34	86.84	96.47
750	76.56	94.82	71.35	87.46	96.47
800	76.97	95.06	72.56	87.46	96.47

Appendix D5: Transmittance values of MgSe:Eu films at different flow rates

Wavelength (nm)	MgSe:Eu T% (400µL)	MgSe:Eu T% (480µL)	MgSe:Eu T% (560µL)	MgSe:Eu T% (640µL)	MgSe:Eu T% (720µL)
200	62.37	54.54	55.95	60.05	61.60
250	58.50	50.84	52.11	56.23	56.74
300	55.12	50.84	50.04	52.48	52.25
350	78.43	76.10	67.69	56.04	63.84
400	82.11	77.75	69.07	55.46	65.74
450	81.73	77.75	69.07	57.21	66.07
500	81.73	77.98	69.42	59.43	66.18
550	82.11	77.98	69.95	61.73	66.42
600	82.11	78.47	70.68	63.90	66.90
650	82.87	78.47	71.40	66.15	67.13
700	82.87	78.47	71.95	67.30	67.61
750	83.25	78.47	72.49	68.47	68.11
800	84.02	78.47	73.05	69.66	68.83

Appendix D6: Transmittance values of MgSe:Eu films at different concentrations of europium

Wavelength (nm)	MgSe:Eu T% (10%)	MgSe:Eu T% (20%)	MgSe:Eu T% (30%)	MgSe:Eu T% (40%)	MgSe:Eu T% (50%)
200	58.14	62.37	56.65	62.06	56.87
250	54.26	58.5	53.05	57.27	52.78
300	50.51	55.12	49.51	54.63	55.08
350	58.14	78.43	55.02	80.09	86.16
400	58.83	82.11	55.63	82.78	87.08
450	60.26	81.73	57.06	82.78	87.54
500	62.14	81.73	58.74	82.78	88.47
550	64.17	82.11	61.36	82.78	88.47
600	67.24	82.11	63.64	83.56	88.47
650	68.85	82.87	65.27	83.56	88.47
700	70.34	82.87	66.71	83.56	88.47
750	71.35	83.25	67.94	83.56	88.47
800	72.56	84.02	69.18	83.56	88.47

Appendix D7: Percentage reflectance values of MgSe:Eu films obtained at different substrate temperatures

Wavelength (nm)	MgSe:Eu R% (300ºC)	MgSe:Eu R% (325ºC)	MgSe:Eu R% (350ºC)	MgSe:Eu R% (375ºC)	MgSe:Eu R% (400ºC)
200	18.47	18.85	18.31	18.11	18.06
250	19.32	19.43	19.19	19.18	19.00
300	19.66	16.06	19.83	19.43	17.69
350	14.43	9.62	18.31	8.66	3.36
400	13.16	4.51	18.13	8.08	2.19
450	13.28	3.52	17.74	7.79	1.97
500	13.28	3.52	17.2	7.49	1.97
550	12.88	3.52	16.39	7.49	1.97
600	12.85	2.98	15.52	7.18	1.97
650	12.52	2.87	14.94	7.03	1.97
700	12.27	2.87	14.38	7.03	1.97
750	11.84	2.87	13.99	6.72	1.97
800	11.66	2.74	13.51	6.72	1.97

Appendix D8: Percentage reflectance values of MgSe:Eu films obtained at different flow rates

Wavelength (nm)	MgSe:Eu R% (400µL)	MgSe:Eu R% (480µL)	MgSe:Eu R% (560µL)	MgSe:Eu R% (640µL)	MgSe:Eu R% (720µL)
200	17.13	19.13	18.83	17.80	17.36
250	18.22	19.78	19.58	18.77	18.65
300	19.01	19.78	19.89	19.52	19.56
350	11.02	12.04	15.36	18.81	16.67
400	9.33	11.32	14.86	18.94	16.04
450	9.51	11.32	14.86	18.54	15.93
500	9.51	11.22	14.73	17.97	15.89
550	9.33	11.22	14.53	17.32	15.81
600	9.33	11.00	14.25	16.65	15.64
650	8.97	11.00	13.97	15.90	15.56
700	8.97	11.00	13.75	15.50	15.39
750	8.79	11.00	13.54	15.08	15.21
800	8.42	11.00	13.31	14.64	14.95

Appendix D9: Percentage reflectance values of MgSe:Eu films obtained at different dopant concentrations

Wavelength (nm)	MgSe:Eu R% (10%)	MgSe:Eu R% (20%)	MgSe:Eu R% (30%)	MgSe:Eu R% (40%)	MgSe:Eu R% (50%)
200	18.31	17.13	18.67	17.22	18.62
250	19.19	18.22	19.42	18.52	19.47
300	19.83	19.01	19.96	19.11	19.02
350	18.31	11.02	19.03	10.27	7.37
400	18.13	9.33	18.90	9.01	6.91
450	17.74	9.51	18.57	9.01	6.68
500	17.20	9.51	18.15	9.01	6.21
550	16.39	9.33	17.43	9.01	6.21
600	15.52	9.33	16.73	8.64	6.21
650	14.94	8.97	16.2	8.64	6.21
700	14.38	8.97	15.71	8.64	6.21
750	13.99	8.79	15.27	8.64	6.21
800	13.51	8.42	14.82	8.64	6.21

Appendix D10: Refractive index values of MgSe:Eu films at different temperatures

Photon Energy, E (eV)	n (300ºC)	n (325 ºC)	n (350 ºC)	n (375 ºC)	n (400 ºC)
6.21	2.51	2.50	2.48	2.50	2.48
4.97	2.57	2.58	2.56	2.56	2.55
4.14	2.59	2.34	2.58	2.61	2.45
3.55	2.22	2.15	1.83	2.50	1.45
3.11	2.14	1.99	1.80	2.48	1.35
2.76	2.15	1.97	1.77	2.46	1.33
2.49	2.15	1.97	1.75	2.42	1.33
2.26	2.12	1.97	1.75	2.36	1.33
2.07	2.12	1.97	1.73	2.30	1.33
1.91	2.10	1.93	1.72	2.26	1.33
1.78	2.08	1.87	1.72	2.22	1.33
1.66	2.05	1.87	1.70	2.20	1.33
1.55	2.04	1.86	1.70	2.16	1.33

Appendix D11: Absorption coefficient values of MgSe:Eu films at different substrate temperatures

Photon Energy, E (eV)	α (x $10^5 m^{-1}$) (300°C)	α (x $10^5 m^{-1}$) (325°C)	α (x $10^5 m^{-1}$) (350°)	α (x $10^5 m^{-1}$) (375°C)	α (x $10^5 m^{-1}$) (400°C)
3.55	1.290	1.250	1.337	2.381	3.142
3.11	1.120	0.970	0.961	1.829	2.010
2.76	1.120	0.927	0.757	1.747	1.800
2.49	1.120	0.927	0.723	1.641	1.800
2.26	1.090	0.927	0.723	1.530	1.800
2.07	1.090	0.927	0.688	1.369	1.800
1.91	1.050	0.862	0.672	1.287	1.800
1.78	1.020	0.775	0.672	1.213	1.800
1.66	0.970	0.775	0.638	1.164	1.800
1.55	0.950	0.755	0.638	1.106	1.800

Appendix D12: Optical conductivity values of MgSe:Eu films at different substrate temperature

Photon Energy, E (eV)	σ (x $10^{12}s^{-1}$) (300°C)	σ (x $10^{12}s^{-1}$) (325°C)	σ (x $10^{12}s^{-1}$) (350°C)	σ (x $10^{12}s^{-1}$) (375°C)	σ (x $10^{12}s^{-1}$) (400°C)
3.55	6.84	6.42	6.639	14.84	10.876
3.11	5.72	4.61	4.336	10.83	6.478
2.76	5.75	4.36	3.199	10.26	5.715
2.49	5.75	4.36	3.021	9.48	5.715
2.26	5.52	4.36	3.021	8.62	5.715
2.07	5.52	4.36	2.842	7.52	5.715
1.91	5.26	3.97	2.759	6.94	5.715
1.78	5.07	3.46	2.759	6.43	5.715
1.66	4.75	3.46	2.589	6.11	5.715
1.55	4.63	3.35	2.589	5.70	5.715

Appendix D13: Extinction coefficient values of MgSe:Eu films at different substrate temperatures

Photon Energy, E (eV)	k (300°C)	k (325°C)	k (350°C)	k (375°C)	k (400°C)
3.55	0.0036	0.0035	0.0037	0.0066	0.0088
3.11	0.0036	0.0031	0.0031	0.0058	0.0064
2.76	0.0040	0.0033	0.0027	0.0063	0.0065
2.49	0.0045	0.0037	0.0029	0.0065	0.0072
2.26	0.0048	0.0041	0.0032	0.0067	0.0079
2.07	0.0052	0.0044	0.0033	0.0065	0.0086
1.91	0.0054	0.0045	0.0035	0.0067	0.0093
1.78	0.0057	0.0043	0.0037	0.0068	0.0100
1.66	0.0058	0.0046	0.0038	0.0070	0.0107
1.55	0.0061	0.0048	0.0041	0.0070	0.0115

Appendix D14: Real dielectric constant values of MgSe:Eu films at different substrate temperatures

Photon Energy, E (eV)	ε_1 (300°C)	ε_1 (325°C)	ε_1 (350°C)	ε_1 (375°C)	ε_1 (400°C)
4.14	6.71	5.48	6.65	6.81	6.00
3.55	4.93	4.62	4.33	6.81	2.10
3.11	4.58	3.96	3.57	6.15	1.82
2.76	4.62	3.88	3.13	6.05	1.77
2.49	4.62	3.88	3.06	5.86	1.77
2.26	4.50	3.88	3.06	5.57	1.77
2.07	4.50	3.88	2.99	5.29	1.77
1.91	4.41	3.73	2.96	5.11	1.77
1.78	4.33	3.50	2.96	4.93	1.77
1.66	4.20	3.50	2.89	4.84	1.77
1.55	4.16	3.46	2.89	4.67	1.77

Appendix D15: Imaginary dielectric constant values of MgSe:Eu films at different substrate temperatures

Photon Energy, E (eV)	ε_2 (300°C)	ε_2 (325°C)	ε_2 (350°C)	ε_2 (375°C)	ε_2 (400°C)
3.55	0.0160	0.0151	0.0154	0.0345	0.0255
3.11	0.0154	0.0123	0.0117	0.0288	0.0173
2.76	0.0172	0.0130	0.0096	0.0310	0.0173
2.49	0.0194	0.0146	0.0102	0.0315	0.0192
2.26	0.0204	0.0162	0.0112	0.0316	0.0210
2.07	0.0221	0.0173	0.0114	0.0299	0.0229
1.91	0.0227	0.0174	0.0120	0.0303	0.0247
1.78	0.0237	0.0161	0.0127	0.0302	0.0266
1.66	0.0238	0.0172	0.0129	0.0308	0.0285
1.55	0.0249	0.0179	0.0139	0.0302	0.0306

Appendix D16: $(\alpha h\nu)^2$ values of MgSe:Eu films at different substrate temperatures

Photon Energy, E (eV)	$(\alpha h\nu)^2$ x $10^{11}eV^2m^{-2}$ (300°C)	$(\alpha h\nu)^2$ x $10^{11}eV^2m^{-2}$ (325°C)	$(\alpha h\nu)^2$ x $10^{11}eV^2m^{-2}$ (350°C)	$(\alpha h\nu)^2$ x $10^{11}eV^2m^{-2}$ (375°C)	$(\alpha h\nu)^2$ x $10^{11}eV^2m^{-2}$ (400°C)
3.55	2.1	1.969	2.25	5.31	12.41
3.11	1.21	0.91	0.894	3.236	3.91
2.76	0.956	0.655	0.437	2.325	2.47
2.49	0.778	0.533	0.324	1.67	2.01
2.26	0.607	0.439	0.267	1.196	1.66
2.07	0.509	0.368	0.203	0.803	1.39
1.91	0.402	0.271	0.165	0.604	1.18
1.78	0.330	0.19	0.143	0.466	1.03
1.66	0.259	0.166	0.112	0.373	0.89
1.55	0.217	0.137	0.098	0.294	0.78

Appendix D17: Band gap energies of MgSe:Eu films at different thicknesses

Band Gap Energy, E (eV)	Thickness (nm)
2.95	200
2.85	2100
2.75	2500
2.65	2750
2.49	2900

Appendix D18: Diffraction angles and FWHM values for MgSe:Eu nanocrystals deposited at 350ºC and 10% dopant concentration

2θ	θ	Cos θ	FWHM βº	FWHM (Radians)	βCosθ
15.68	7.84	0.9907	0.1200	0.002094	0.002075
20.37	10.19	0.9842	0.1600	0.002793	0.002042
23.53	11.77	0.9790	0.1600	0.002793	0.002734
30.67	15.34	0.9644	0.1800	0.003142	0.003030
32.68	16.34	0.9596	0.1400	0.002444	0.002345
36.77	18.39	0.9490	0.1800	0.003142	0.002982
37.21	18.61	0.9477	0.1600	0.002793	0.002647
47.43	23.72	0.9156	0.2200	0.003840	0.003516
51.97	25.99	0.8989	0.2000	0.003491	0.003138

Appendix D19: Lattice parameters for MgSe:Eu film deposited at 350°C and 10% dopant concentration

D (nm)	d (Å)	ε (x 10^{-4})	δ (x 10^{14} lines/m^2)	N (x 10^{15})	hkl
69.79	5.6470	5.1875	2.0531	8.09	100
70.92	4.3562	5.1050	1.9882	7.71	101
52.97	3.7779	6.8350	3.5640	18.50	110
47.79	2.9127	7.5750	4.3785	25.20	002
61.76	2.7380	5.8625	2.6217	11.67	200
48.56	2.4423	7.4550	4.2408	24.02	102
54.81	2.4144	6.6175	3.3287	16.70	112
41.19	1.9153	8.7900	5.8941	39.35	221
46.15	1.7581	7.8450	4.6952	27.98	103

Appendix D20: Diffraction angles and FWHM values for MgSe:Eu nanocrystals deposited at 350ºC and 40% dopant concentration

2θ	θ	Cos θ	FWHM β^o	FWHM (Radians)	βCosθ
15.58	7.79	0.9908	0.1200	0.002094	0.002075
20.26	10.13	0.9844	0.1200	0.002094	0.002061
23.43	11.72	0.9792	0.1200	0.002094	0.002051
30.46	15.23	0.9649	0.1600	0.002793	0.002695
32.57	16.29	0.9599	0.1400	0.002444	0.002346

Appendix D21: Lattice parameters for MgSe:Eu film deposited at 350°C and 40% dopant concentration

D (nm)	d (Å)	ε (x 10^{-4})	δ (x 10^{14} lines/m^2)	N (x 10^{15})	hkl
69.79	5.6831	5.1875	2.0531	8.826	100
70.26	4.3796	5.1525	2.0257	8.650	101
70.61	3.7938	5.1275	2.0057	8.522	110
53.73	2.9323	6.7375	3.4639	19.341	002
61.73	2.7500	5.8650	2.6243	12.754	200

Appendix E1: Ethanol (C_2H_5OH)

This was already a prepared solution and needed no further method for its preparation.

Appendix E2: Dilute nitric acid (HNO_3)

20ml of this solution was prepared by diluting 3ml of concentrated nitric acid in 17ml of ethanol.

Appendix E3: Preparation of europium trioxide (Eu_2O_3)

A 0.1M solution of Eu_2O_3 was prepared by dissolving 0.70g of it in 20ml of dilute nitric acid.

The mass of Eu_2O_3 needed to form the required solution was calculated as follows:

Molar mass of Eu_2O_3 = 351.962g/mol

$$\text{Molarity} = \frac{\text{Mass of 0.1M of Europium Trioxide}}{\text{Molar Mass of Europium Trioxide}}$$

But a 20ml measuring cylinder was used in place of $1000cm^3$ ($1dm^3$).

Thus, the mass for 0.1M of the solution = Molarity x molar mass

$$= 0.1 \times \frac{20}{1000} \times 351.962g$$

$$= 0.1 \times 0.02 \times 351.962g$$

$$= 0.70385g$$

$$\approx 0.70g.$$

Thereafter, volume percentage of Eu_2O_3 was considered for the doping process. Different volume percentages in the range of 10% to 50% were used for doping the required films.

Appendix E4: Preparation of zinc acetate dehydrate {$Zn(CH_3COO)_2.2H_2O$}

0.4M solution of zinc acetate dehydrate was prepared by dissolving 8.78g of the crystals in 100ml of ethanol.

The mass of {$Zn(CH_3COO)_2.2H_2O$} needed to form the required solution was calculated as follows:

Molar mass of {$Zn(CH_3COO)_2.2H_2O$} = 219.50g/mol

$$\text{Molarity} = \frac{\text{Mass 0.4M of Zinc Acetate Dehydrate}}{\text{Molar Mass of Zinc Acetate Dehydrate}}$$

But a 100ml measuring cylinder was used in place of $1000cm^3$ ($1dm^3$).

Thus, the mass for 0.4M of the solution = Molarity x molar mass

$$= 0.4 \text{ x. } \frac{100}{1000} \text{ x } 219.50g$$

$$= 0.4 \text{ x } 0.1 \text{ x } 219.50g$$

$$= 8.78g$$

Appendix E5: Preparation of cadmium acetate dehydrate {$Cd(CH_3COO)_2.2H_2O$}

0.4M solution of cadmium acetate was prepared by dissolving 10.66g in 100ml of ethanol.

The mass of $Cd(CH_3COO)_2.2H_2O$ needed to form the required solution was calculated thus:

Molar mass of $Cd(NO_3)_2.4H_2O$ = 266.529g/mol

$$\text{Molarity} = \frac{\text{Mass of 0.4M of Cadmium Acetate Dehydrate}}{\text{Molar Mass of Cadmium Acetate Dehydrate}}$$

But a 100ml measuring cylinder was used in place of $1000cm^3$ ($1dm^3$).

Thus, the mass for 0.4M of the solution = Molarity x molar mass

$$= 0.4 \text{ x } \frac{100}{1000} \text{ x } 266.529g$$

$$= 0.4 \text{ x } 0.1 \text{ x } 266.529g$$

$$= 10.66g$$

Appendix E6: Preparation of magnesium acetate tetrahydrate {$Mg(CH_3COO)_2.4H_2O$}

0.2M of $Mg(CH_3COO)_2.4H_2O$ was prepared by dissolving 4.29g of the salt in 100ml of absolute ethanol.

The mass of $Mg(CH_3COO)_2.4H_2O$ needed to form the required solution was calculated thus:

Molar mass of $Mg(CH_3COO)_2.4H_2O$ = 214.455g/mol

$$\text{Molarity} = \frac{\text{Mass of 0.2M of Magnesium Acetate Tetrahydrate}}{\text{Molar Mass of Magnesium Acetate Tetrahydrate}}$$

But a 100ml measuring cylinder was used in place of $1000cm^3$ ($1dm^3$).

Thus, the mass for 0.2M of the solution = Molarity x molar mass

$$= 0.2 \times \frac{100}{1000} \times 214.455g$$

$$= 0.2 \times 0.1 \times 214.455g$$

$$= 4.2891g$$

$$\approx 4.29g.$$

Appendix E7: Preparation of selenium dioxide (SeO_2)

0.4M solution of selenium dioxide was prepared by dissolving 4.44g in 100ml of ethanol.

The mass of SeO_2 needed to form the required solution was calculated thus:

Molar mass of SeO_2 = 110.96g/mol

$$\text{Molarity} = \frac{\text{Mass of 0.4M of Selenium Dioxide}}{\text{Molar Mass of Selenium Dioxide}}$$

But a 100ml measuring cylinder was used in place of $1000cm^3$ ($1dm^3$).

Thus, the mass for 0.4M of the solution = Molarity x molar mass

$$= 0.4 \times \frac{100}{1000} \times 110.96g$$

$$= 0.4 \times 0.1 \times 110.96g$$

$$= 4.4384g$$

$$\approx 4.44g.$$

LIST OF PUBLICATIONS

1. **JEROH, D.M.,** EKPUNOBI, A.J. and OKOLI, D.N. (2018): "Growth of Europium-Doped Magnesium Selenide Films by Electric Field-Assisted Spray Pyrolysis: Optical and Structural Analysis." ***East European Journal of Physics, 5(4), 13-21. Published by Kharkiv National University, Ukraine.***

2. **JEROH, M.D.,** EKPUNOBI, A.J. and OKOLI, D.N. (2018): "Optical Analytical Studies of Electrostatic-Sprayed Eu-doped Cadmium Selenide Nanofilms at Different Temperatures." ***Journal of Nano- and Electronic Physics, 10(3), 03006-1 – 03006-5. Published by Sumy State University, Ukraine. Indexed in SCOPUS.***